Thesis for Master's degree in chemistry

Hadgu Gebreslasie

Structural determination of a series of synthetic peptide analogues to the 3_{10}-helical (Pro138-Gly144) segment of aquaporin-4 by X- ray crystallography

60 study points

Department of Chemistry
Faculty of mathematics and natural sciences
UNIVERSITY OF OSLO 05/2011

Acknowledgements

This master thesis has been carried out at the Department of Chemistry, University of Oslo, since autumn 2009.

First of all, I would like to thank my supervisor, Prof. Carl Henrik Görbitz, for giving me the opportunity to conduct my research in his group. In addition, I appreciate his kind guidance, encouragement, and support from the very begging of this research to the final stage. I would also like to record my gratitude to my co-advisor, Øyvind Jacobsen, who has given me motivation and critical comments. Above all and the most needed, he provided me unflinching encouragement and support all the time. This thesis would not have been possible or written without their kind help. I am also thankful to them for writing publications about my results.

I would also like to thank to Vitthal Narayan, for being there and support me in several ways.

To my friend, Alem Tadesse, I say thank you for given me help and guidance. My appreciation also goes to all my friends and families who have encouraged me and stood by my side during these years.

Last but not least, I would like to thank the Norwegian quota scheme for accepting my application and for the financial support.

Table of Contents

List of Figures

List of Tables

List of Abbreviations and Symbols

2D	Two Dimensional
3D	Three Dimensional
α_R	Right-handed alpha-helix
α_L	Left-handed alpha-helix
AcN	Acetonitril
Aib	alpha-Aminoisobutyric acid
AQPs	Aquaporins
AQP0-AQP12	Aquaporins (0-12)
β-sheet	Beta-sheet
Boc	*tert*-Butoxycarbonyl
CCD	Charge-Coupled Device
CCDC	Cambridge Crystallographic Data Center
CIF	Crystallographic Information File
CHIP28	Channel-like Integral Protein of 28 kDa
CNS	Central Nervous System
CSD	Cambridge Structural Database
Et_2O	Diethyl ether
Gly	Glycine
GooF	Goodness of Fit
hAQP4	human Aquaporin-4
IP	Image Plate area detector
MeOH	Methanol
NMR	Nuclear Magnetic Resonance
NPA	One letter codes for: Asparagine (N)-Proline (P)-Alanine (A)
ORTEP	Oak Ridge Thermal Ellipsoids Plot
O-allylSer	allylated L-Serine
L-Pro, D-Pro	L-Proline, D-Proline
PPI and PPII	PolyProline I and PloyProline II
rAQP4	rat Aquaporin-4

Refcodes	Reference codes
R_{int}	Internal Reliability Index
RCM	Ring-Closing Metathesis reaction
r.m.s.d or RMS	root mean square deviations
TFE	Trifluroethanol
SADABS	Siemens Area Detector Absorption Correction
SAINT	SAX Area-detector Integration (SAX-Siemens Analytical X-ray)
Ser	L-Serine
SMART	Siemens Molecular Analysis Research Tool
Val	L-Valine
wR	weighted Reliability Index

Abstract

In order to understand the single crystal X-ray structures of a series of synthetic peptides mimicking the Pro138-Gly144 segment of human AQP4 [1] , we have crystallized and determined the X-ray structures of some of these peptides. The crystal structure of the peptides Boc-Pro-Pro-OH (**1**), Boc-Aib-Aib-OMe in two polymorphs (**2** and **3**), Boc-Val-Val-OMe (**4**), and the tripeptide Boc-allylSer-Aib-Val-OMe (**5**), were elucidated.

Peptide **1**, $C_{15}H_{24}N_2O_5$, was designed and synthesized to the corresponding N-terminal Pro138-Pro139 segment of the 3_{10}-helix loop C (Pro138-Pro139-Ser140-Val141-Val142-Gly143-Gly144) of the AQP4. The compound crystallized in the orthorhombic space group $P2_12_12_1$ with one molecule in the asymmetric unit. tBoc-Pro bond and Pro-Pro along the peptide bond show *cis*- and *trans*-conformations (*cis*-*trans*), approximately with $\omega = -8.2°$ and $\omega = -174.35°$, respectively. Proline residues in **1** adopt incipient Poly-L-proline type I (PPI) and type II (PPII) backbone conformations. Orthorhombic and monoclinic form of the same compound has been determined so far by different authors. Finally, the backbone conformation of **1** is compared with these two forms (orthorhombic and monoclinic form) as well as with the Pro138-Pro139 segment of AQP4 at 1.8 Å and 3.2 Å resolutions.

The peptide $C_{14}H_{26}N_2O_5$ was obtained in two polymorphic forms **(2** and **3),** both exist in the monoclinic space group *P*21/c and *P*21/n, respectively with one molecule in the asymmetric unit. The Aib residues in Boc-Aib-Aib-OMe adopt (φ, ψ)-values which are characteristics of helical conformations. The dihedral angles of the peptide backbone show that the Aib residues lie in left- or right-handed 3_{10}- /α-helical regions in the Ramachandran plot. The torsion angles indicate values for folded conformations.

Peptide **4**, $C_{16}H_{30}N_2O_5$, was designed and synthesized to the corresponding Val141-Val142 segment of the AQP4 loop C. It was crystallized in the orthorhombic space group $P2_12_12_1$ with three molecules in the asymmetric unit. Each molecule in the asymmetric unit adopts a β- strand/polyproline II backbone conformation. The main chain functional groups are hydrogen bonded into tapes carrying the characteristics of parallel β-sheets. Each tape has a left-handed twist and thus forms a helix, with six peptide molecules needed to complete a full 360° rotation. A comparison of hydrogen bond lengths and twisting mode is made with other related structures of protected dipeptides. Additionally, a comparison of the backbone conformation is made with that of the Val141-Val142 segment of the water channel aquaporin-4.

Peptide **5**, $C_{21}H_{37}N_3O_7$, crystallize in the monoclinic space group $C2$ with a single molecule in the asymmetric unit. A single crystal X-ray diffraction studies of **5** reveals that it adopts a bend (or turn-like structure) without any intramolecular hydrogen bonding. Most of the dihedral angles of the tripeptide **5** fall within the helical region of the Ramachandran plot.

CHAPTER ONE

1. INTRODUCTION

In all living cells, coordination of solute and water transport across cell membranes is of critical importance for osmotic balance. Water is quantitatively the major component of all the organisms that maintain high water flux through plasma membranes. It can pass directly through the lipid bilayer of the plasma membrane, but this form of water flux is slow and not subject to regulation.Yet many processes critically depend on the efficient exchange of water between the cell and its environment. It is therefore essential to have a mechanism for fluid homeostasis. The existence of protein channels for nonionic compounds and, in particular, water has important implications for water management in living organisms.

1.1. Structure, function and cellular expression of aquaporins

1.1.1. Aquaporins

Aquaporins (AQPs) are membrane channel proteins which enable passive yet remarkably efficient permeation of water molecules across cellular membranes in all tissues for which water balance is crucial, including the kidney, lung, brain, eye lens, skin and red blood cells [2]. Aquaporins have been identified in virtually every living organism, including higher mammals, other vertebrates, invertebrates, plants, eubacteria, archaebacteria, and other microbes, indicating that this newly recognized family of proteins is involved in diverse biological processes throughout the natural world. They also have been implicated in numerous physiological and pathological processes in humans and other mammalian species [3].

Peter Agre received the 2003 Nobel Prize in Chemistry for his discovery of the first aquaporin, first named CHIP28 for ‘channel-like integral membrane protein of 28 kDa’, which later named as aquaporin-1(AQP1) [4]. AQP1, whose structure has been

determined by electron crystallography, was first identified as an integral membrane protein in red blood cells and renal proximal tubules, where it functions as a water-selective membrane pore. The landmark discovery of AQP1 and subsequent identification of homologous water channel proteins have advanced the understanding of the mechanism of water transport across the cell membrane [5]. AQPs constitute a large family of integral membrane proteins which facilitate bidirectional water transport across the lipid bilayer of cell membranes [6] and are present in all domains of life [7, 8]. A subclass of the aquaporins also appears to be designed for the selective passage of small, uncharged amphipathic molecule such as glycerol across cellular membranes [9, 10]. They are expressed in many tissues (Table 1) and are mainly involved in the regulation of the water balance, since they function largely as water-conducting pores through cell membranes and thus allowing the cell to regulate its volume and internal osmotic pressure according to hydrostatic and/or osmotic pressure differences across the cell membrane.

1.2. Water channels: The Aquaporin family

1.2.1. Aquaporins classification

Member of the AQP family fall into two classes; aquaporins, pure water channels that only permit water passage, and the aquaglyceroporins, which are channels that also permit passage of other small neutral (uncharged) solutes, such as glycerol [11-13]. So far 13 mammalian aquaporins (AQP0-AQP12) with varying degree of homology have been identified [14-16]. AQPs with high water permeability are AQP1, AQP2, AQP4, AQP5, and AQP8, while aquaglyceroporins with glycerol and water permeability include the group AQP3, AQP7, and AQP10 [13, 16]. In addition, certain AQPs also conduct a variety of other molecules, including larger solutes. For example, AQP9 mediates passage of a wide variety of non-charged solutes including carbamides, polyols, purines, and pyrimidines in a phloretin- and mercury-sensitive manner, whereas amino acids, cyclic sugars, Na^+, K^+, Cl^-, and deprotonated monocarboxylates are excluded [17]. According to the permeability characteristics of its members, the aquaporin family can alternatively be

divided into three functional groups: the aquaporins, the aquaglyceroporins, and the neutral solute channels [18]. The most remarkable feature of the AQP channels are perhaps their high selectivity and efficiency with regard to water or glycerol passage and the strict exclusion of protons [2, 19-21].

1.2.2. Tissue distribution of mammalian aquaporins

In mammals, aquaporins are widely distributed in the cells of tissues that are actively involved in fluid secretion and absorption processes, and cells that require rapid or regulated water movement in response to an osmotic gradient [22]. Table 1 summarizes the complex tissue, cellular and subcellular expression patterns of the 13 mammalian aquaporins known to date. As can be inferred from Table 1, certain organs and tissues, like the kidney, liver, and brain exhibit a very complex pattern of expression of several aquaporins, which match the complexity of their functions and their regulation by neuronal and/or hormonal factors. In mammals, they are also expressed in cell types that are thought not to carry out fluid transport, such as skin, fat and urinary bladder cells [16].

Table 1. Function and expression pattern of aquaporins. Adapted from [16]

AQP	Permeability	Tissue expression
AQP0	Water?*	Eye lens fiber cells
AQP1	Water	Kidney tubules, endothelia, erythrocytes, choroid plexus, ciliary epithelium, intestinal lacteals, corneal endothelium
AQP2	Water	Kidney collecting duct
AQP3	Water, glycerol	Kidney collecting duct, epidermis, airway epithelium, conjunctiva, large airways, urinary bladder
AQP4	Water	Astroglia in brain and spinal cord, kidney collecting duct, glandular epithelia, airways, skeletal muscle, stomach, retina
AQP5	Water	
AQP6	Chloride?*	Kidney collecting duct intercalated cells
AQP7	Water, glycerol	Adipose tissue, testis, kidney proximal tubule
AQP8	Water	Liver, pancreas, intestine, salivary gland, testis, heart
AQP9	Water, small solutes	Liver, white blood cells, testis, brain
AQP10	Water, glycerol	Small intestine
AQP11	?*	Kidney, liver
AQP12	?*	Pancreatic acinar cells

N.B: * in the Table 1 is to indicate uncertainly explanations given by the author.

1.3. Molecular structure of the Aquaporins

1.3.1. Structural features of AQPs

X-ray structures of AQPs from all three kingdoms, bacteria, archae, and eukaryote, have been determined [23]. The configuration of AQP1 reflects the common structural features of the aquaporin family [18]. All members of the family contain structural motifs similar to AQP1, but each probably has special features needed for function or regulation [24]. They share the same basic AQP fold, which consists of two tandem domains, each containing a bundle of three transmembrane alpha-helices and a short pore helix in loop B and E (Figure 1). The two repeats are connected by long loop C, extracellular loop (Figure 3) [25]. They form tetramers with each monomer functioning as an independent water pore

and van der Waals interactions between the proline residues of two almost completely conserved Asn-Pro-Ala (NPA) motifs stabilize the stacking of the B and E short helices at the center of the water pore [10].

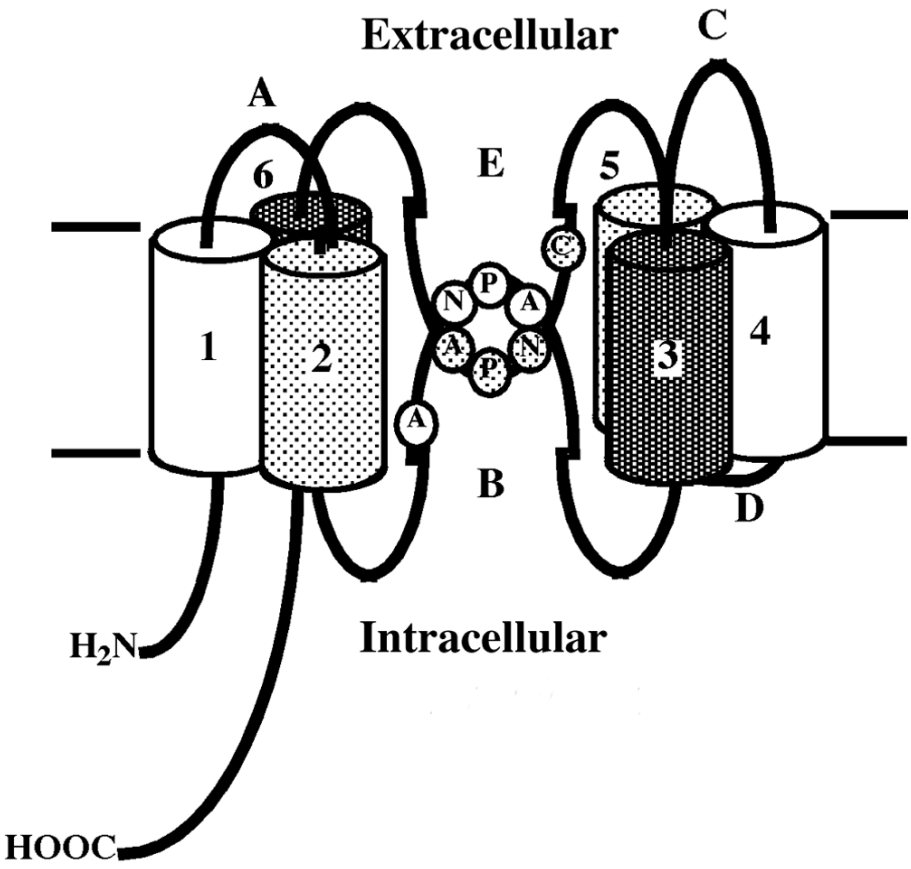

Figure 1. The Hour-glass model of AQP1; Loops B and E dip into the membrane from the intracellular (loop B) and extracellular (E) surfaces of the lipid bilayer, surrounded by the six transmembrane helices. Adapted from [26]

At this motif, the channel form a constriction and only one water molecule can pass through this constriction [19]. This may form a size-exclusion pore, giving the channel its high selectivity. The intracellular loop B and extracellular loop E fold into the membrane and interact with one another, forming what has come to be known as the 'hour-glass model' (Figure 1), characterized by wide external openings to the channel with a narrow central constriction where the NPA motifs interact, forming the functional water pore [3].

Protein conformation analysis of the amino acid sequences of the aquaporin family suggested that the six-transmembrane-spanning helices for each AQP molecule are arranged in two hemipores with cytosolic amino and carboxy termini, extracellular loops A, C and E and intracellular loops B and D (Figure 1). Primary amino acid sequence analysis shows a strong similarity between the two halves of the molecule, where the N-terminal half of the protein is sequence related to the C-terminal half [26].

1.4. Aquaporin-4

Aquaporin-4 (AQP4) is the predominant water channel in the mammalian brain and is concentrated in the astrocytic end-feet [27, 28]. It plays an important role in maintaining water homeostasis in the brain and in the development of brain edema, which is an abnormal increase in brain water content [1, 29]. AQP4 is also expressed in glial lamellae of the hypothalamus, where it may also play a role in osmo-sensing, thermo-sensing and glucose-sensing [11].

Over the last decade AQP4 has emerged as an attractive, novel target for development of drugs against brain edema, which is a common consequence of stroke and trauma. Regarding the role of AQP4 associated with brain edema, it was found that mice lacking AQP4 show less edema and suffer less damage to the brain in an ischemic stroke and acute water intoxication models than wild-type mice. AQP4 inhibition by

pharmacological blockers might provide a new therapeutic option for some forms of cerebral edema [30], and also provide for therapeutic agents that might reduce brain damage from stroke, tumor-associated edema, epilepsy, traumatic head injury, and other CNS disorders associated with brain water imbalance [23].

AQP4 is unique in having two spliced isoforms, one starting translation initiation with methionine, M1 (AQP4M1) and the second with M23 (AQP4M23) isoforms [23, 31, 32].

Few inhibitors of aquaporins are known and all are toxic, irreversible and/or unspecific, for example, silver nitrate and mercurials are aquaporin inhibitors [1]. This member of the aquaporin family, AQP-4, is not sensitive to mercurial inhibition and lacks a cysteine preceding the NPA motif in loop E which is known to confer mercurial sensitivity to AQP1 [3, 23]. Searching for a way to approach the problem of developing AQP4 selective inhibition, Jacobsen and co-workers turned to the significant amount of structural information that has accumulated in recent years from electron diffraction (ED) and X-ray diffraction studies of aquaporins and aquaglycoporins [1]. In 2006 Fujiyoshi and co-workers published the first near-atomic resolution structure of AQP4 from rat (rAQP4), an electron diffraction structure to 3.2 Å resolution [25]. This has later been improved to 2.8 Å [19]. This aquaporin is also homotetrameric channel protein, like other aquaporins.

Two of the AQPs, namely AQP0 and AQP4, are, in addition to their function as water channels, believed to play a role in cell-cell adhesion [11]. The term ‘adhennel’ has been proposed for membrane proteins that function both as a cell adhesion molecule and a membrane channel [11]. Hiroaki and co-workers expressed rAQP4M23 in L-cells, cells with no endogenous adhesion molecules, which later was able to develope cell-adhesion. The electron diffraction structure of rAQP4M23 suggests that the 3_{10}-helix in the C loop (residues 139 to 142; Figure 2), is the main region responsible for AQP4-mediated cell–cell adhesion in opposing tetramers. The involvement of loop C, which is part of the extracellular vestibule, in cell-cell adhesion appears to be conserved across all kingdoms [23]. The structure at 3.2 Å resolution revealed that AQP4 tetramers in the two membranes interact with each other through their extracellular surfaces. However, unlike the AQP0

tetramers, which exactly stacked, the AQP4 tetramers are shifted, a tetramer in one membrane is at the center of the four tetramers in the adjoining membrane. It has also been pointed out that unlike the AQP0 monomer, which forms three interactions involving five residues with a monomer in the adjoining membrane; an AQP4 monomer forms only one interaction involving two residues, which are Val142 and Pro139 (Figure 2).

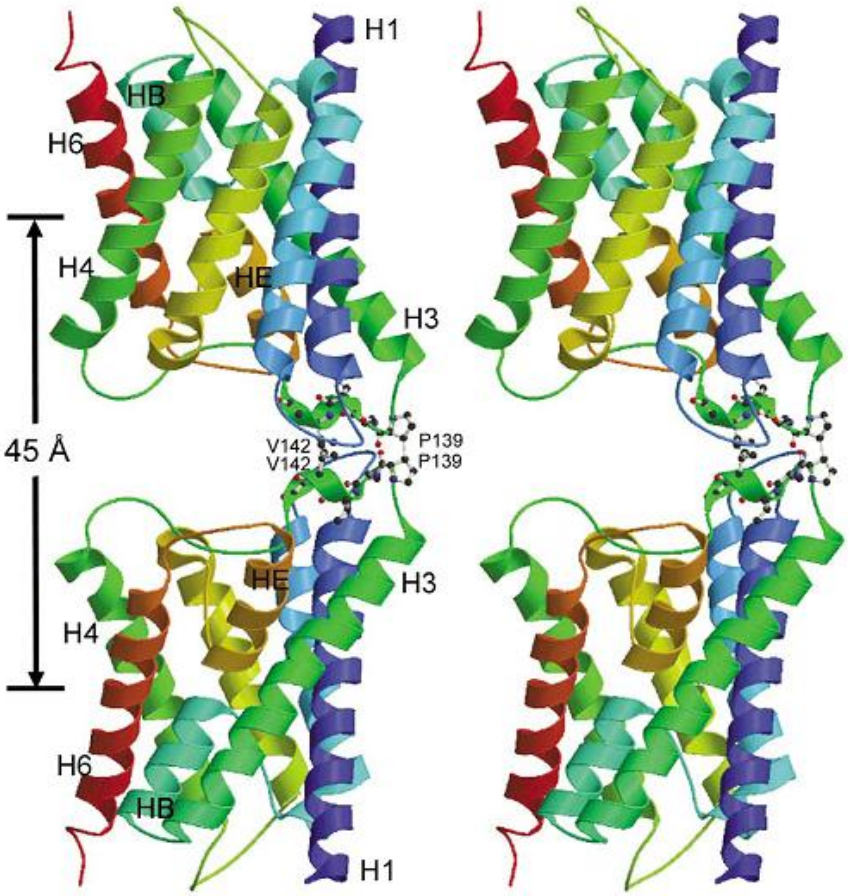

Figure 2. Stereo view of the interactions between rAQP4 monomers in adjoining membranes, AQP4 molecules are shown in ribbon representation, while residues Pro139 and Val142 in the 3_{10}- helix, are shown in ball-and-stick representation, adapted from [25]

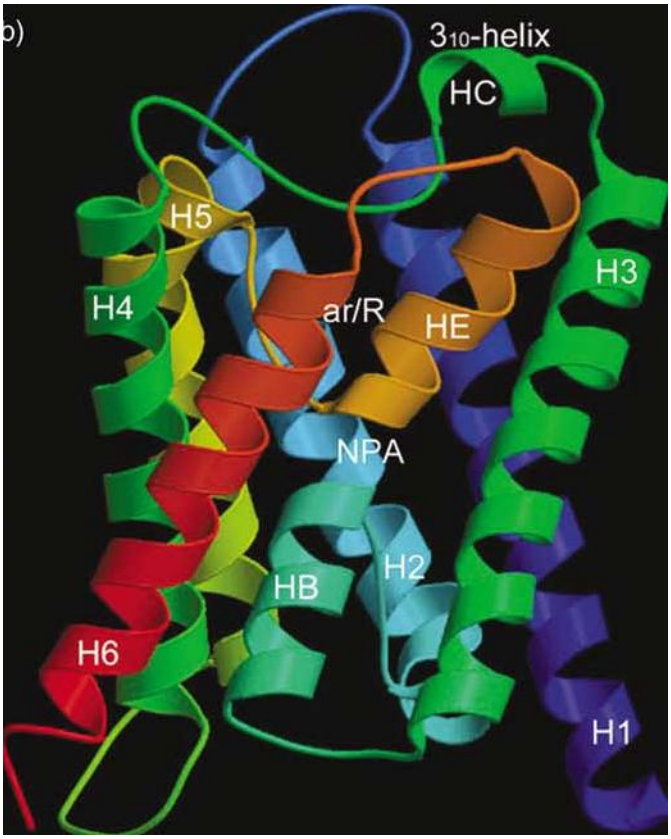

Figure 3. Ribbon diagram of rAQP4 structure: H1-H6, transmembrane helices; HB and HE, pore helices in loop B and E; HC, 3_{10}- helix in loop C. Adapted from [25].

1.4.1. Comparison of Rat AQP4 (rAQP4) and Human AQP4 (hAQP4)

Recently, the X-ray structure of human AQP4 (hAQP4) has been determined at 1.8Å resolution [23]. It shows water molecules throughout the channel, five glycerol, and one octyl glucoside molecule whereas the rAQP4 structure, at 3.2Å, no water or glycerol molecules observed [23]. Both structures crystallized in the same space group ($P42_12$); however their crystal lattice contacts lie on different surfaces of the protein. The hAQP4 3D crystal contains head to head contacts only; this is because tetramers within the horizontal plane are too far apart to make contacts with each other. The 2D crystal lattice of rAQP4 on the other hand has tetramers close together and contains both in- plane and between plane contacts of the latticed tetramers [23]. The 3_{10}-helix in the C loop is the main region that provides for rAQP4-mediated cell–cell adhesion in opposing tetramers

[25]. Even though the sequences of loop C in both rAQP4 and hAQP4 are the same, hAQP4 doesn't adopt the dihedral angles (φ, ψ) of the 3_{10}-helix in this region because this loop is not involved in crystal packing. However, Ho *et al*. suggested that the 3_{10}-helix in the loop C is a conformation that may be induced when two cells expressing AQP4 on the surface are in close proximity bringing two C loops into direct contact.

1.5. Aim of the study

Over the last decade AQP4 has emerged as an attractive, novel target for development of drugs against brain edema, which is a common consequence of stroke and trauma. In the perivascular AQP4 pool (i.e. the AQP4 pool that is thought to constitute the main influx pathway for water during the development of edema) the targeted binding site is not engaged in binding to contiguous AQP4 tetramers and thus should be freely available for ligand binding [1]. This thesis project is part of an ongoing project to design, synthesize and structurally characterize linear and cyclic peptide analogues of the 3_{10}-helical Pro138-Gly144 segment of human aquaporin-4 by olefin metathesis'. The ultimate objective of this project is to develop drug candidates against brain edema. Jacobsen and co-workers have designed and synthesized a series of peptides mimicking the Pro138-Gly144 segment of human AQP4. The structures of several of these peptides have been studied qualitatively in solution by circular dichroism (CD) and 2D NMR spectroscopy. However, none of these studies have provided atomic resolution detail of the conformation of the peptides.

One aim of the present study was therefore to obtain the crystal structures of some of these synthetic peptides, using X-ray diffraction, in order to facilitate a comparison with the structure of the Pro138-Gly144 segment in its native protein environment. Through the X-ray structural analysis we will be provided with the information of the bond lengths, bond angles, conformation, coordination and other crystallographic information of the molecular structure of the synthetic peptides. The results of these peptides structure through X-ray analysis will provide vital input to synthetic chemists regarding how the

peptides should be modified to more closely mimic this 3_{10}-helical segment. Hopefully, this and future X-ray structural studies will result in more potent ligands and eventually inhibitors of AQP4. For a start, we have crystallized and determined the crystal structure of the dipeptides, Boc-Pro-Pro-OH (**1**), Boc-Aib-Aib-OMe in two polymorphs (**2** and **3**), Boc-Val-Val-OMe (**4**), and the tripeptide Boc-allylSer-Aib-Val-OMe (**5**).

The structure descriptions in this thesis are written in the format of Acta Crystallographica journals. For instance, the peptides Boc-Val-Val-OMe and Boc-Aib-Aib-OMe are planned to be submitted in Acta Crystallographica section C in May 13, 2011, and Boc-allylSer-Aib-Val-OMe in Acta crystallographica section E.

CHAPTER TWO

2. Methods-Brief background theories on X-ray crystallography

2.1. Why use X-ray crystallography?

The knowledge of accurate molecular structures is a prerequisite for rational drug design and for structure based functional studies to aid the development of effective therapeutic agents and drugs [33, 34]. Several methods exist that allow the detailed three-dimensional characterization of protein structures and their ligand complexes, such as NMR, X-ray crystallography, neutron diffraction and electron microscopy. Crystallography provides the most direct way of forming three-dimensional images of molecules (including macromolecules, e.g., proteins and nucleic acids, and small molecules) ranging from global folds to atomic details of bonding. This structural knowledge then provides part of the basis for understanding and predicting the chemistry of the whole molecule, or one or more of its subcomponents (or functional groups) and give detailed information about their activity, their mechanism for recognizing and binding substrates and effectors, and the conformational changes which they may undergo [35]. X-ray diffraction studies of single crystals are a vital tool for structure determination. It can be applied to a wide range of sizes of structures ranging from very small molecules and simple salts to complex minerals, synthetically prepared inorganic and organometallic complexes, natural products and biological macromolecules (such as proteins and nucleic acids and even viruses). Of all the current methods for structural characterization of chemical compounds, X-ray crystallography is therefore the only one capable of providing detailed information on interatomic distances, bond angles, molecular architecture, absolute configuration, thermal vibration parameters, crystal packing, as well as possible order-disorder and/or non-stoichiometry from the same experiment [36]. The other methods are either limited in the range of problems and precision (NMR ~ 30-40 kDa), resolution (Electron microscopy), or are very specialized with limited applicability (Neutron crystallography).

2.2. Basic principles of X-ray Crystallography

Single-crystal X-ray diffraction, referred to as X-ray crystallography, is a study of crystal structure through X-ray diffraction techniques. This leads to an understanding of the molecular and crystal structure of a substance. Because a single molecule does not have enough diffraction power, the regular arrangement of molecules in a crystal is a necessary to reinforce scattering from one molecule by all others. Crystals are objects (molecules, atoms, and ions) arranged in a regularly repeating pattern in three dimensions from smaller units, so-called 'unit cells'. It generates the complete crystal by 3D translation along the unit cell axis. The unit cell is characterized by six parameters: three axial lengths (a, b and c) and three interaxial angles *(α, β, γ*) (Figure 4).

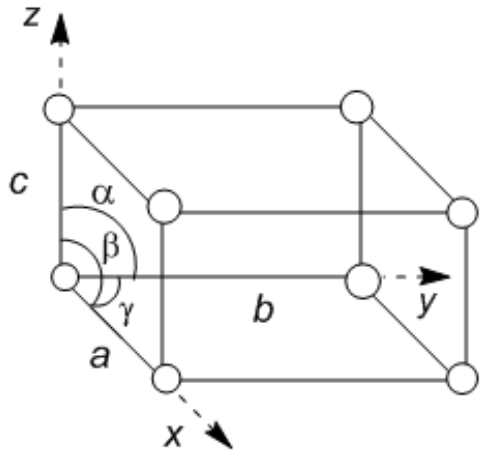

Figure 4. Schematic representation of unit cell where a, b and c are axial lengths, α, β, and γ are the interaxial angles between them, and the coordinates x, y, and z are measured along a, b, and c respectively. Redrawn using ChemBioDraw Ultra-12 from [35].

The basis of X-ray crystallography is the interaction of matter in the crystalline state with X-rays. Since the wave-lengths of X-rays (in the nanometer range) are of the same order

of magnitude as of the interatomic distances within the crystal, the interaction results in the X-ray diffraction. This method can be used to determine the structure of a crystalline molecule at atomic resolution: the composition of atoms, their relative orientation, and the chemical bonds between the atoms (both bond lengths and bond angles).

The determination of a crystal structure by X-ray crystallography normally proceeds in different stages. First, obtaining crystals of the peptides or proteins of interest is a prerequisite. Second, the intensities of the Bragg reflections are measured and from this data can be reduced to a common scale, corrections made for various geometrical and physical factors, and observed structure amplitudes calculated. The third stage is solving the phase problem of X-ray diffraction, the problem that only the intensities of the diffraction pattern are recorded, whereas the phases of the reflections cannot be measured directly (the phase information is lost). We must therefore find a way to assign initial, approximate phases (solve the structure). For small molecules, for example, the structures can be solved by so- called 'direct methods' using the SHELXS program. The fourth stage involves refining the approximate atomic positions in order to obtain the best possible agreement between the observed structure factors and the calculated structure factors.

2.3. X-ray diffraction and Bragg's law

Radiation incident upon a crystal is scattered in a variety of ways. When the wave length of the radiation (λ) is on the same scale as the atom spacing in a crystal, the scattering which is termed diffraction, gives rise to a set of well defined beams arranged with a characteristic geometry, thus forming a diffraction pattern. X-ray diffraction data collection is the result of relative intensity (I) for each reflection with a set of planes in crystal, known as Miller indices (h, k, l) along with the corresponding scattering angle (2θ) for that reflection. The positions and intensities of the diffracted beams are a function of the arrangements of the atoms in space and some other atomic properties. Thus, if the positions and the intensities of the diffracted beams (frequently referred to as

reflections, spots or lines) are recorded, it is possible to deduce the arrangement of the atoms in the crystal and their chemical nature.

A beam of radiation will only be diffracted when it impinges upon a set of planes in a crystal if the geometry of the situation fulfils quite specific conditions, defined by Bragg's law (constructive interference, Figure 5):

$$n\lambda = 2d_{hkl}\sin\theta \qquad (1)$$

Where, n = an integer, for peak order

λ= Wave length of the radiation (X-ray)

d_{hkl} = interplanar spacing of the hkl planes in the crystal lattice

θ = Bragg angle or diffraction angle

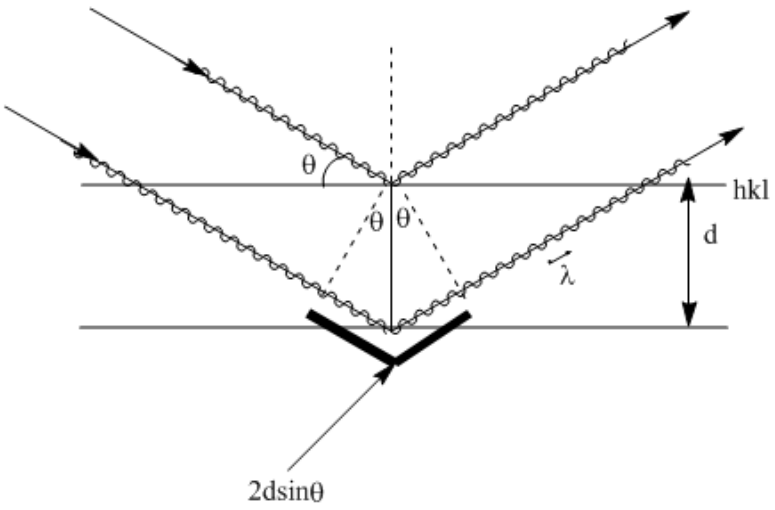

Figure 5. Schematic drawing of Bragg's law, redrawn using ChemBiodraw Ultra-12 from (C.H. Görbitz Lecture)

2.4. The X- Ray Diffractometer

A diffractometer is an instrument used for collection of intensities of diffracted radiation by counting the number of X-ray photons that arrive at a suitable placed detector. It allows for crystal orientation and the position of the counter to be controlled accurately while the crystal is kept in X-ray beam. The SMART APEXII system, a diffractometer used in this study, consists of horizontally oriented D8 goniometer base with 2-theta, omega and phi drives, dovetail tracks for the X-ray source and detector, and an additional mounting track for accessories such as the video camera and optional low-temperature attachment, and a high speed computer for data analysis.

2.4.1. X-rays and X-ray generator

2.4.1.1. X-rays

The diffraction of X-rays by crystals was first demonstrated by Walther Friedrich, Paul Knipping and Max von Laue; seventeen years after Wilhelm Konrad Röntngen discovered X-rays in 1895. From their experimental X-ray diffraction on a copper sulphate crystal, they concluded that X-rays are electromagnetic radiation with wave lengths of the order 10^{-8} cm (a unit of length equivalent to Ångeström unit, 1Å) [37]. X-rays having wave length of more than about 2Å are known as 'soft' X-rays. They are significantly absorbed by air and strongly by water, and wave lengths of 0.2 Å or less are very penetrating. The range of wave lengths between about 0.5 Å and 1.6 Å is the most suitable for X–ray crystallography. These waves are sufficiently penetrating to study samples up to a millimeter or so in size, but are scattered strongly by matter [35]. X-ray crystallography is used extensively nowadays in the elucidation of crystal and molecular structures, the wide application of X-rays is shown in Figure 6.

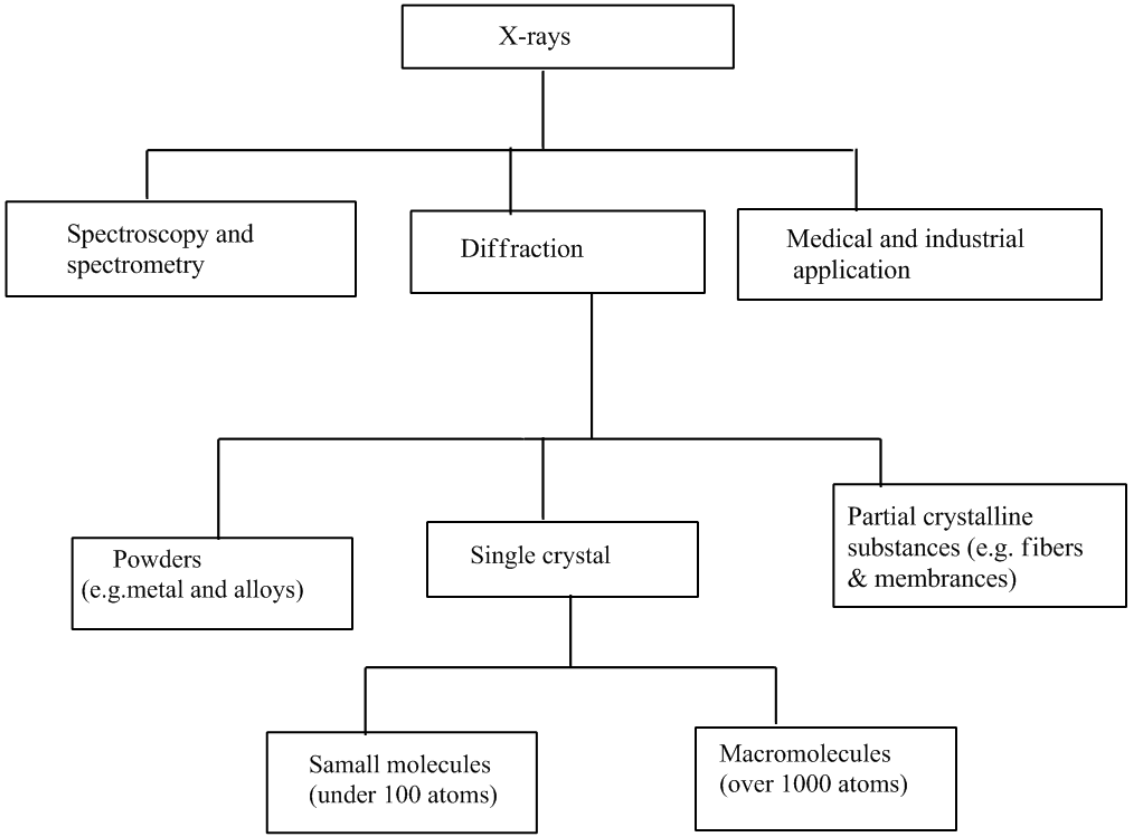

Figure 6. Schematic drawing for application of X-rays in modern science and technology, redrawn using ChemBiodraw Ultra-12 from [36].

2.4.1.2. Generation of X-Rays

In the laboratory, X-rays can be produced by focusing a beam of electrons towards a metallic target (anode) in vacuum which then the anode is bombarded with accelerating electrons and thereby caused to emit X-rays of specific wave length, so called monochromatic X-rays. The high voltage rapidly heating up the metal plate is cooled by

water. X-ray sources include; ordinary sealed X-ray tube, generator with rotating anode, and synchrotron radiation. Laboratory X-ray generators usually produce characteristic radiation from an anode made of copper (CuKα, 1.54 Å wavelength) or, if a shorter wave length is required, molybdenum can be used where a tunable graphite crystal monochromator selects only the Kα line emitted (MoKα, 0.71073 Å). The X-ray source used to investigate the crystal structure of small molecules, including this thesis work, is the sealed X-ray tube with MoKα radiation at 0.71073 Å wave length. X-rays are produced in a device called an X-ray tube (Figure 7) where electrons from the heated cathode are accelerated by high voltage towards the anode and x-rays are emitted from the anode target; leave the tube through Beryllium windows.

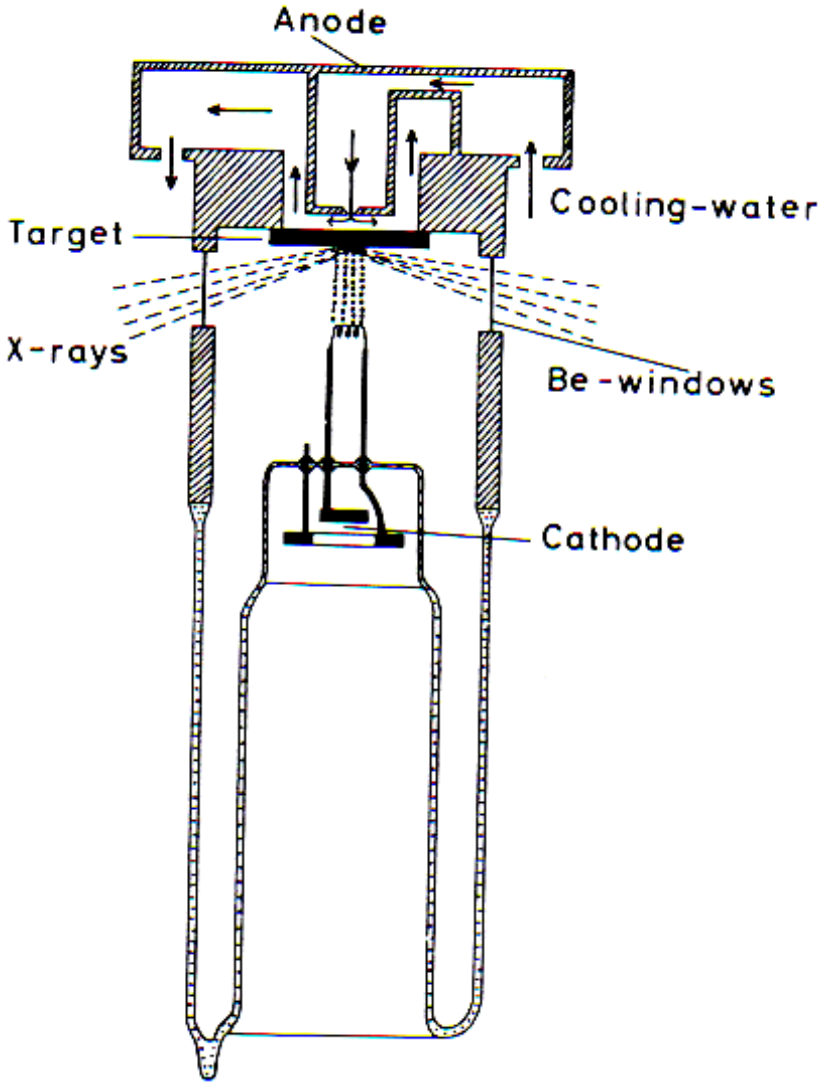

Figure 7. Schematic representation of X-ray tube [38]

If very powerful X-rays are needed, synchrotron radiation can be used. This is produced in synchrotron storage rings where electrons (or positrons) travel close to speed of light. These particles emit very strong radiation at all wave lengths ranging from gamma rays to visible light. Whenever an X-ray source is needed from the synchrotron radiation, only radiation of suitable wave length is selected from the storage ring. The main advantages of this source are; tunable wave length (useful for solving the phase problem) and high intensity radiation for weakly diffracting crystals.

2.4.2. X-ray detectors

The intensities of the diffracted beams are measured by intercepting the beams with something that is sensitive to X-rays. X-ray detectors respond to the energy of the diffracted beam, called intensity, which (at a given wave length) is proportional to the number of photons it delivers. Nowadays the diffracted spots are usually recorded on image plates rather than on X-ray films, the classic method, or by an electronic detector. Electronic area detectors feed the signals they detect directly in a digitized form into a computer, hence its name. Various forms of X-ray detectors can be available; some may count single photons, some providing only measurements of count rate or total flux, others measuring the energy, position, and/or incidence time of each X-ray. Most common detectors for single crystal X-ray crystallography are discussed below.

2.4.2.1. Charge-Coupled Device (CCD) detectors

Charged-coupled device (CCD) detectors have been widely accepted as detectors for collecting X-ray diffraction images for both macromolecules and small-molecule crystals, including this work. They offer rapid read-out diffraction images (faster data collection) and large reciprocal-space coverage as compared with other detectors [39]. These detectors are suited for both home-laboratory, and synchrotron X-ray sources with a relatively short exposure times are used, i.e. small-molecule X-ray diffraction and large-molecule crystallography at high-intensity synchrotron sources. In most systems, phosphorous screen converts the incident X-rays into to visible light that can be registered on the CCD –chip. Compared to imaging plate area detectors (IP), discussed below, CCD detectors have smaller detector area.

2.4.2.1. Imaging plates area (IP) detectors

IP are quite popular detectors with an excellent performance as an X-ray area detector. The diffraction pattern recorded on the plate is scanned and stored in a computer. The image plate is then erased and ready for the next exposure. It can be used with synchrotron radiation because it has high dynamic range (compared with X-ray film, for example, has the order of $1:10^5$) also has larger detector area, high count-rate capability and high spatial resolution. It can help to obtain more accurate data sets with a reduced X-ray dosage and a shortened exposure time on protein crystals. However, the images stored in the IP decreases, so called fading, with time after exposure to X-rays. Fading increases at higher temperature but does not depend on the exposure time or on the X-ray photon energy of the image [40]. They are made with a plate containing a photosensitive material that on exposure to X-rays creates color centers that can be read out in a scanning mode with a laser as a digital image.

2.4.3. The goniometer

In crystallography, 'goniometer' denotes all the gears required to position and orient a crystal in the X-ray beam during data collection. The simplest systems give rotation about three or four axes. In four-circle diffractometer, a crystal can be rotated around three axes (χ, ϕ and ω) independently, and the detector can be rotated around a fourth angle (2θ, concentric with ω), which give this the name 'four-circle diffractometer'. The 2θ and ω angles are measured relative to the rotation of the detector (corresponds to the Bragg angle for angular spread), and rotation of the base of the goniometer head, respectively. The ϕ and χ angles are measured due to rotation of the goniometer head around its own axis and rotation of the ϕ-axis relative to the reflection plane, respectively. For example, the Kappa apex II goniometer features the Kappa 4-axis goniometer where it uses a horizontally oriented Kappa goniometer with 2θ, ω, kappa (κ) and ϕ drives while the SMART APEX II goniometer (Figure 8), the three-circle instrument uses a horizontally oriented D8 goniometer base with 2θ, ω and ϕ drives. This three-axis system incorporates

a fixed chi stage with χ angle of 54.74° and a ϕ drive with 360° rotation, which is so compact that it swings into the incident beam collimator, allowing free rotation in ω.

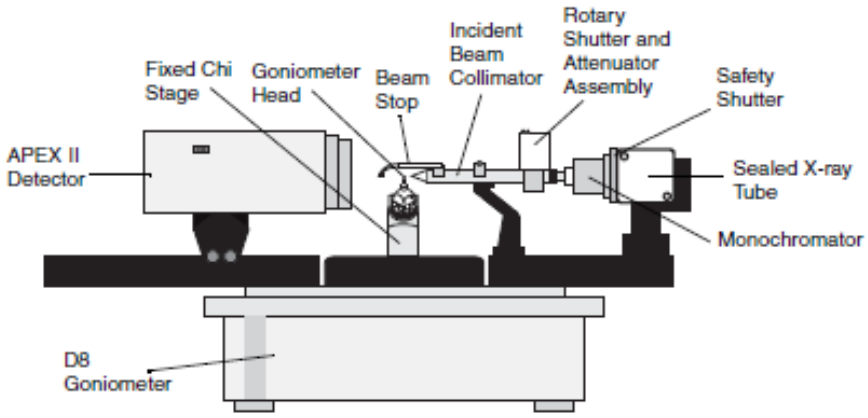

Figure 8. SMART APEXII goniometer components-adapted from (Bruker advanced X-ray solutions- APEXII user manual version 1.22)

2.4.3.1. Goniometer head

A goniometer head is simply a device allowing the crystallographer to put the crystal in the center of the beam, and perhaps to orient it. It has various possible adjustments (height, and X and Y adjustments or lateral adjustments) which are used to center the crystal in the crosswire of video microscope and in the X-ray beam so that a crystal can be bathed in a radiation. It also has a brass rod which holds glass fiber. This in turn is used to mount a crystal on it.

2.4.4. Computers

Computers have special remarkable features in the X-ray crystallography. Data may be generated by fast detectors (e.g. CCD) at several megabytes per second, so the real rate of data collection might be handled by the power of computers that accepts its output. The

SMART APEXII system, for instance, uses a high speed single computer to control the experiment, store raw frame data, integrate the data, and solve structure solution and refinement of the structure.

2.4.5. Cooling device with a liquid nitrogen

Concerning the conditions at the crystal during data collection, the most important choice is the temperature. Most of the crystals used for data collection in this thesis were investigated under cooled nitrogen. Showering a crystal with cold dry nitrogen during data collection reduces thermal vibrations of atoms so that better data quality is possible. Our crystals for example, were exposed to cold nitrogen at 100(2), 105(2) or 150(2) K during data collection. Cooling with liquid nitrogen can also be used in an alternative, lower and higher, range of temperatures on a single crystal, which is useful for studies of phase transitions [41]. However, at a very low temperature, e.g., 4 K, X-ray diffraction data collection is also possible using closed-cycle helium refrigerators, but helium is expensive and the device needs considerably more maintenance than an N_2 open-flow device [42].

CHAPTER THREE

3. METHODOLOGIES

This chapter focuses mainly on the methods and materials, with a general crystals growth procedures for the compounds studied, selection and orientation of crystal for data collection, the basic software or programs used (in the APEXII CCD diffractometer) for data collection, structure solution, and refinement are also discussed. In addition, the Cambridge Structural Data base (CSD), used for structure retrieving, visualizing and analysis is discussed. Finally, the crystallographic information file, CIF, which was used for editing the crystallographic data, is also discussed.

3.1. Experimental methods and crystal growth

3.1.1. Materials and reagents

The peptides to be crystallized (Table 2) were synthesized by[1] and received for crystallization.

Table 2. Peptides with different crystallizing solvents

Name of peptide sequences	Best crystal contain	System/method	X-ray data
Boc-allylSer-Aib-Val-OMe	block-shaped single crystal (s)	ethyl acetate/ water	**5**
Boc-allylSer-Val-Val-OMe	amorphous-like	ethyl acetate/water	-
Boc-allylSer-Val-Val-allylSer-Gly-OMe	no crystal formed	MeOH/water, ethyl acetate/water, TFE/AcN	-
Boc-Val-Val-OMe	needle-shaped single crystal (s)	ethyl acetate/water	**4**
Boc-BnSer-Aib-Val-OMe	very small single crystals	ethyl acetate/water	-
Boc-Pro-Pro-BnSer- Aib-Val-OMe	no crystal formed	TFE/Et_2O, ethyl acetate/water, MeOH/water	-
Boc-Pro-Pro-allylSer-Aib-Val-OMe	no crystal formed	MeOH/water, ethyl acetate/water, TFE/AcN	-
Boc-Pro-Pro-allylSer-Val-Val-OMe	precipitate like formed	ethyl acetate/water	-
Boc-Pro-Pro-OH	need-shaped single crystal (s)	ethyl acetate/water, MeOH/water	**1**
Boc-allylSer-Aib-Val-allylSer-Gly-OMe	no crystal formed	ethyl acetate/water, MeOH/AcN	-
Boc-Pro-BnSer-Aib-Val-OMe	no crystal formed	TFE/Et_2O, ethyl acetate/water	-
Boc-Aib-Aib-OMe	needle-shaped single crystal (s)	ethyl acetate/ water	**2** and **3**
CH_3N^+- allylSer-Val-Val-Gly-OMe	amorphous-like	MeOH/water	-

3.1.2. Crystal Growth Procedures

The crystallization methods to each of the peptides listed in Table 2 were about the same procedure: about 5mg each of the above peptides were added to labeled 30 x 6 mm test tubes. To dissolve the compounds, 50 µl of ethyl acetate was added to each test tube, which was then immediately covered by parafilm. A small hole was pricked in the parafilm, and then each test tube was placed inside a larger test tube, filled with about 1.5 ml of water. Finally, the larger test tubes were capped and left for a couple of weeks at room temperature. Crystals started growing as water diffused into the solution at room temperature. The same procedures were also performed using different solvents (Table 2) such as methanol (MeOH)/water, trifluroethanol (TFE) /Acetonitril (AcN), and TFE/Diethyl ether (Et_2O). The crystal dimensions, colours and shapes of each specimen for data collection and refinement are discussed in the result and discussion part.

3.1.3. Selection and orientation of a crystal

Good crystals are the preconditions for structure determination of a given compounds either small molecules or macromolecules. To select a suitable crystal for X-ray structure determination, crystal samples from each test tube were placed on the glass microscope slides. Looking through the microscope, larger crystals were cut down to size (to be compatible with the beam diameter) using a razor blade and knife. A great care was taken on some crystals, which were sticky and fragile.

Looking through the microscope, the crystals of interest were attached to a glass fiber tip of the goniometer head with a grease (for data collection at cooled temperature) where the longest dimension of the crystal of interest for each compound was facing approximately upwards along the length of the fiber. Glue should not be used at low temperature because it contracts during cooling which cause to crack the crystal and is usually difficult to remove the crystal from the glue (i.e., crystal can be destroyed). The crystal attached on the goniometer head was then mounted on the instrument (diffractometer) for data collection.

Once the goniometer head along with the crystal attached was mounted on the goniometer, the crystal was centered in the X-ray beam using the setting screws on the goniometer head.

3.2. Software used

This section generally focuses on the basic software used; starting from data collection to the final structure refinement.

3.2.1. Data Collection

Apex2 program controls the instrument in collecting data used by the other program in the systems program suit (SHELXTL). Before the regular data collection began, a small

test run called matrix was performed, which was containing information on how the crystal was attached to the goniometer head and determining unit cell parameters. The actual data collections were then performed in three separate runs (1, 2 and 3) in which the ω angle set to 30 º. The detector set to 2θ = 30 º (with default crystal-to-detector distance of 5cm). The ϕ angles were set to 0 º, 90 º and 180 º, and the sets of exposures each taken over 0.5º ω rotation scan. Exposure times were ranging from 60 to 90 seconds and the sweep range was set to 185 º.

3.2.2. Data integration and data reduction

The data set collected has to be integrated. The program SAINT sets up and carries out the integration and reduction processes, and is also useful in unit cell refinement. Integration of the intensity in a spot is a matter of separation of the background counts from the reflections.

3.2.3. Space Group Determination

The XPREP program provides extensive menu-driven facilities to aid the user in determining the correct cell and space group and to prepare the file for structure determination. It is designed to perform all operations that involve analysis and manipulation of intensity data, e.g. space group determination, reciprocal lattice displays, empirical and face-indexed absorption corrections, intensity statistics (including resolution shells, data, theory, % completeness, redundancy, mean I, mean I/σ(I), R_{int}, and R_{sigma}), scaling and merging of different data sets, and preparation of the input files for structure solution with the SHELXTL program. XPREP reads the raw data file extension with .raw (list of the reflection intensities sorted by Miller index) and the parameter file extension with .p4p (containing, among others, information on the cell parameters a, b, c, α, β, and γ), which then make the instruction file extensions with .ins and reflection data file .hkl for use by the programs XS and XL for structure solution and refinements.

The program suggests different options, which can guide us to work with the different menus or options, e.g. the proposed option [S] is the one chosen to find a space group with no prior knowledge about the given compound. The different steps can be confirmed by pressing 'enter' key to the selected or proposed option through the program and move to the sub-menus. There are several criteria to consider while determining the correct space group (s). Among them;

i) The mean | E*E-1| value statistics

The distributions of E-values, which are normalized structure factors (the square-roots of the intensities), can indicate as a hint if the space group is chiral (no-centrosymmetric) or centrosymmetric. For centrosymmetric space groups, the theoretically expected mean | E*E-1| value is 0.968, and 0.736 for non-centrosymmetric.

ii) The systematic absences (systematic extinctions)

During data collection, many reflections (or spots) with intensities (I_{hkl}), related to miller indices (hkl), are recorded while at certain places on the frame of data some reflections are missing or absent. This absence occur when $I_{hkl} = 0$. The presences of translational symmetry elements or centered lattices cause some series of reflection to be absent. For example, a screw axis gives sets of reflections along the axis with no (or very low) intensities (e.g. 2-fold screw axis along b with indices 0*k*0, where k is odd) and a glide plane gives systematic absences in the plane (e.g. $P2_1/c$ reflections with indices *h*0*l* where *l* is odd). In the space group determination, the systematic extinction is observed under the line N (int > 2sigma) (as for our case).

iii) The frequency of the space group

Apart from the above two criteria, the number of known structures which crystallize in a certain space group becomes an important indicator for the probability that this space group is also correct for the new structure, i.e. it helps to prevent errors in space group determination by considering all possible space groups in the Cambridge structural data bases (CSD). Space group-frequency table may be used in routine structure work, which helps to check a list of space-group frequencies as soon as a space group has been assigned or limited to a few possibilities [43].

In addition to the above criteria, another criterion to put into account is the weighted figure of merit where the possible space groups with low figures of merit are listed. Usually a figure of merit less than one is very likely to indicate the correct space group.

3.2.4. Crystal Structure Solution

The structure solution program SHELXS is primarily designed for single crystal data and uses direct methods (like for our small structures) or Patterson method (if containing

heavy atoms) for phasing. The XS needs two input files, a .hkl file for reflection data, and a .ins file containing essential crystallographic information plus the phasing instruction(s). It then writes the best solution (a list of atomic coordinates and other information) to the results file .res, and a detailed listing of the program's activities is written to the .lst files. The .ins files usually begin with the instructions:

TITL (title of the structure)

CELL (this line contains X-ray wave length (λ) and the cell parameters a, b, c, α, β, and γ)

ZERR (the Z-value or number of molecules in the unit cell)

LATT (type of crystal lattice, e.g.1= P (primitive), 2= I (body center etc). if it is negative number, indicates the structure is non-centrosymmetric)

SYMM (symmetry operation)

SFAC (atomic scattering factors or elements)

UNIT (number of atoms of each type in the unit cell, in SFAC order)

TREF (for specifying the phasing method (for direct methods-just like our cases) or PATT (instruction for Patterson phasing)

HKLF 4 (the standard HKL file format, listing squared structure factors)

END (usually closes the instruction).

At the beginning of solving a crystal structure, the peaks generated by XS, assigned by the letter Q and number n, are either non-hydrogen atoms or noise peaks. The highest peak, Q1 is the one peak with the largest electron density/$Å^3$, where as the last Qn peak has the smallest electron density density/$Å^3$. Peaks with large peak heights are possibly due to real non-hydrogen atoms in the structure. The real peaks end and noise peaks start can often be determined by looking in the peak list. If we are able to see a sharp peak height decrease, we can assume that the peaks below are noise peaks, which can be ignored in the subsequent refinement. We can recognize the molecule of interest on the screen if the XS is able to solve the structure. All the structures solutions in this thesis were solved by XS.

3.2.5. Structure Refinement

XL is the structure refinement part of SHELXTL which refined all structures, often found by XS, step by step. During refinement, heavy atoms not found initially (if any) are introduced. Atomic displacement parameter may be isotropic (with equal displacement in all direction) or anisotropic (with different values in different directions in the crystal). By writing ANIS in an .ins file, atoms are refined anisotropically. Anisotropic refinement is related to the thermal vibrations of an atom which need not be the same in all directions, and the motion is therefore described by anisotropic displacement parameters (ADP). In this case the motion is described by an ellipsoid that can be rotated in any direction. The ellipsoid is described in 6 parameters: U11, U22, and U33, specify the magnitude of the movement in the three axes, and U12, U13, U23, specify the rotation of the ellipsoid off the principal axes. HFIX introduces hydrogen atoms in theoretical positions. It is difficult to locate the hydrogen atoms accurately using X-ray data because of their low scattering power and poor electron density. The HFIX command is carried out to fix the hydrogen atoms in a well predicted position, and we want to keep the number of refinement parameters to a minimum. For example, HFIX 33 command fix the hydrogen atoms for methyl group, 23 for methylene, 13 for methane, 43 for hydrogen bonded to sp^2 hybridized atom (e.g. NH in an amide, an atom in an aromatic ring). The least-squares refinement proceeds in cycles, and brief descriptions of the results are displayed on the screen. We changed manually the instructions and continued refining, which was usually after repeatedly having copied the .res file to the .ins file with subsequent refinement by XL. The .lst file (listing file), a list of the contents of the .ins files, contains information about what is really happening during the least-square refinement. While refining the structure, the brief descriptions displayed often have to look at (to complete the refinement in the best possible manner) is (are);

- The weighting scheme (WGHT) - this helps the refinement by putting the most weight on the data that have the smallest error. The WGHT instruction in the .ins file controls wR2 (a least-squire residual) and Goof (goodness of fit) = S. Refining of structure was continued until the value of WGHT reached as small as

possible. wR and S are based on F^2, which is ~I, such that S should be close to 1.0 (showing the weighting function is satisfactory) and wR2 is about 2xR(F). Turning atoms anisotropic usually makes the wR2 factor to decrease and this usually indicates a 'better' structure.

- R_{int}-value, which is the internal consistency of the data and the same magnitude as R(F) (the measure of the agreement between the observed data (Fobs) and the calculated structure factors, Fcal), should be as low as possible (0.03-0.04) for better structure quality or 0.05-0.07 is also reasonable for good structures.

XP, which is part of SHELXTL, helps to visualize post-script illustrations with thermal ellipsoids. The XSHEL program unites the functions of XS, XL and XP (Figure 9).

3.2.6. Absorption Correction

Intensities can be affected by variable crystal volume in the beam (if a crystal is greater than beam diameter), incident beam inhomogeneity, absorption by the glass rod, absorption in air, and crystal decay. SADABS provides useful diagnostics and can correct for such errors and corrects all intensities accordingly.

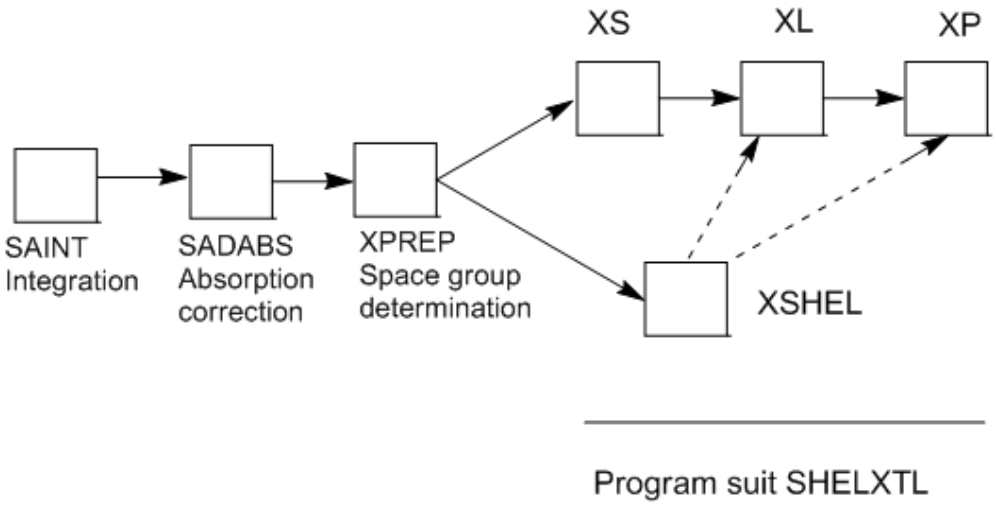

Figure 9. Schematic drawing of steps for structure solution and refinement after the data are collected, redrawn using ChemBioDraw Ultra-12 (adapted from C.H.Görbitz Lecture)

3.3. Cambridge structural databases (CSD)

The results of X-ray structure analyses of small molecules are stored on the CSD. It records bibliographic (Author name, journal name, etc), chemical and crystallographic information for organic and metal organic compounds whose 3D structure have been known. CSD is a product of the Cambridge Crystallographic Data Center (CCDC, http://www.ccdc.cam.ac.uk/). From this database, known structures or portions of structures give detailed information on experimental conditions, a reference to original papers and structural information. For example, CSD is important in searching for similar or related crystal structures, visualization of the crystal structures including crystal packing, detailed hydrogen bonding information, bond angle, bond distance, detailed torsion angles, statistical analysis and display of geometric and other data etc.

3.3.1. Mercury

Mercury offers a comprehensive range of tools for structure visualization and the exploration of crystal packing, which can be accessible from the CCDC (http://www.ccdc.cam.ac.uk/products/csd_systm/mercury/). The crystal structure illustrations in this thesis were prepared using this program.

Some of the basic benefits using Mercury provide:

- Several structure display style options, including displacement ellipsoids (ORTEP), wireframe, and ball-and-stick, capped-stick, or space filling model.
- The ability to measure and display bond distances, angles and torsion angles involving atoms, centroids and planes.
- Location and display of intermolecular and/or intramolecular hydrogen bonds, short nonbonded contacts, and user-specified types of contacts
- The ability to build and visualize a network of intermolecular contacts
- Structure overlay display (to measure the root mean square deviations, r.m.s.d of related structures), e.g. the r.m.s.d of Boc-Val-Val-OMe of the three molecules in the asymmetric unit was measured.
- Manually editing structures, or to automatically assign bond-types, standardizes bond-types to CSD conventions and to add missing hydrogen atoms.
- Visualization of the crystal packing, to show how the molecules interact within the unit cell etc.

3.3.2. ConQuest

This program is important for searching and retrieving information from the CSD, which can provide a full range of text or numerical database search options. By selecting ‘peptide’ from the menu, a selected amino acid sequence (Aib-Aib, or Pro-Pro, for example) were searched to get crystal structure information from similar or related structures.

3.3.3. Vista

This program provides statistical analysis and display of geometric and other data. It reads the files automatically generated by ConQuest e.g., the average hydrogen bonds for each/or similar group of structure searched were calculated using this program.

3.4. Crystallographic Information File (CIF)

CIF is a standardized file format for presentation of crystallographic data. A CIF file is created by the refinement program (SHELXL). It contains a text part which describes the author(s), structure, experiment such as the refinement, crystallization, figure legends, etc, and a data part (provides all the necessary data for description of data collection and refinement, as well as the experimental results including atomic coordinates, tables with bond lengths, bond angles, torsion angles etc). The program publCIF, a freeware from http://journals.iucr.org/e/services/authorservices.html/ can be used to give an on-line help for checking CIF structure data (checkCIF) and also corrects errors after some changes made.

CHAPTER FOUR

4. RESULTS AND DISCUSSION

This part mainly focuses brief explanations on: the experimental results, data collection and structure solution, structure refinement, and structure conformation discussion of the five compounds (**1, 2, 3, 4 and 5**).

4.1. Crystal structure of *N*-(*tert*-Butoxycarbonyl)-L-prolyl-L-proline (Boc-Pro-Pro-OH) (1): an N-terminally protected dipeptide

4.1.1. Introduction

Proline (Pro) is unique among the 20 naturally occurring (genetically coded) amino acids in that its side chain is cyclically closed (forming pyrrolidine ring) so that the peptide nitrogen cannot act as a hydrogen bond donor, only as a hydrogen bond acceptor. Due to this ring formation, the L-Pro residue N-C^{α} torsion angle (φ) is restricted to -60° (±20°) and the D-Pro with 60° (±20°), giving proline an exceptional conformational rigidity compared to other amino acids [44, 45]. As a consequence, the local conformations of L-Pro are largely limited to ψ ≈ -30° (±20°) [α_R] or ψ ≈+120° (±30°) (polyproline, PPII) conformations. Two clusters of observed conformations characterized by distinct ψ values are observed in protein dataset. The most commonly occurring conformations for L-Pro are φ = -60° (±20°), ψ = -30° (±20°) and φ = -60° (±20°), ψ = +120° (±20°), which are compatible with the *i*+1 position of type I/III and type II beta-turns, respectively [46].

Proline acts as a structural disruptor in the middle of regular secondary structure elements such as α-helices and β-sheets, where both the hydrogen bonding and torsion angle requirements are not accommodated [47]; however, when it occurs in a helix, it is more often located at the first two residue than in the middle [48]. Proline is also commonly found in turns and loop segments of proteins and peptides [47, 49]. In protein structures, proline is considered as α-helix terminator, and kinks and turns inducer despite its propensity to occur at the N-terminus region of the helices [50]. Diproline segments have

emerged as important templates in the designed synthetic peptides with defined structures. It has been shown that diproline segment promotes as a folding nuclei in helices when positioned at the N-terminus of synthetic sequences [45].

4.1.2. Data collection and structure solution

X-ray data on a colorless needle-shaped single crystal of peptide **1** was collected at 100(2) K on ApexII CCD diffractometer using APEX2 software [51]. Intensity measurements were performed using MoKα radiation (λ= 0.71073 Å). Determination of integral intensities, unit cell refinement and data reduction were performed with SAINT-Plus [52].

Subsequent data absorption correction was done by SADABS[53] using multi-scan technique. The space group $P2_12_12_1$ with Z = 4 and Z' = 1 for the formula unit $C_{15}H_{24}N_2O_5$, was determined by XPREP. The structure was solved by direct methods using SHELXTL[54]. The crystallographic data for peptide **1** are reported in Table 3.

Table 3. Crystal data and structure refinement for Boc-Pro-Pro-OH (**1**)

Chemical name	Boc-Pro-Pro-OH
Chemical formula	$C_{15}H_{24}N_2O_5$
Formula weight (M_r)	312.36
Temperature	100 (2) K
Dx	1.295 Mgm^{-3}
Wave length (λ)	0.71073 Å
Crystal system	orthorhombic
Space group	$P2_12_12_1$
Unit cell dimensions	
a	6.5380 (18) Å
b	14.651 (4) Å
c	16.840(5) Å
Volume (V)	1613.0 (8) $Å^3$
Z	4
Absorption coefficient	0.10 mm^{-1}
Crystal size	0.75 × 0.21 × 0.1 mm
Absorption correction	multi-scan
(Max. and min. absorption corrections)	0.9903 and 0.8518
F(000)	672
Theta(θ) range for data collection	1.8-26.6°
Index ranges	h = -6→6, k = -14→14, l = -16→12
$N_{measured}$	5729
N_{unique}	1488
$N_{observed}$ ($I > 2\sigma(I)$)	1412
Refinement method	Full-matrix least-squares on F^2
Data/restraints/parameter	1944/0/205
GooF (S) on F^2	1.13
R_{int}	0.034
$R(F^2>2\sigma(F^2))$	0.036
$wR(F^2)$	0.091
Peak differences in electron density map	$\Delta\rho_{max}$ = 0.13 e $Å^{-3}$, $\Delta\rho_{min}$ = −0.14 e $Å^{-3}$

4.1.3. Structure refinement

Full-matrix least-square refinement on F^2 against all reflections was carried out by SHELXTL[54]. All non-hydrogen heavy atoms were refined anisotropically. All H atoms were positioned with idealized geometry and fixed C-H distances for CH_2 and CH_3 at 0.99 and 0.98 Å, respectively. Free rotation was permitted for methyl groups. U_{iso} (H) values were set to $1.2U_{eq}$ of the carrier atom or $1.5U_{eq}$ for methyl groups. Complete crystal data for peptide **1** are given in Appendix B.

4.1.4. DISCUSSION

4.1.4.1. Structural conformation of Boc-Pro-Pro-OH

Peptide **1** (with a chemical diagram depicted in Figure 10) is part of the N-terminal Pro138-Pro139 segment of the 3_{10}-helix loop C (Pro138-Pro139-Ser140-Val141-Val142-Gly143-Gly144) segment of AQP4. The compound was crystallized and its crystal structure determined.

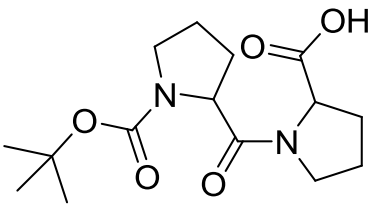

Figure 10. Schematic illustration of Boc-Pro-Pro-OH, drawn using ChemBioDraw Ultra-12.0

A search for similar structures in the Cambridge structural database (CSD), using the peptide fragment Pro-Pro, was performed. Two compounds with refcodes: BOCPRO and BOCPRO01, an orthorhombic form of tBoc-Pro-Pro-OH in space group $P2_12_12_1$ [55] and monoclinic form in space group $P2_1$ [50] respectively, were found. Both structures represent the same compound, but in different crystallizing solvents. The orthorhombic form was crystallized from ethyl acetate and petroleum ether while the monoclinic form was crystallized with four molecules in the asymmetric unit from an aqueous methanol

solution. The different space groups attained could be due to solvent polarity difference in the method of crystallization, as pointed out by [50]. Both of the searched structures show similar back bone torsion angles (φ, ψ, and ω), Table 4.

Table 4. Selected torsional angles: orthorhombic (refcode: BOCPRO) and monoclinic (refcode: BOCPRO01).

	Pro1			**Pro2**		
	φ	ψ	ω	φ	ψ	ω
Orthorhombic (refcode: BOCPRO)	-66.6	-95.5	-168.7	-95.1	-168.7	-175
Monoclinic (refcode: BOCPRO01)	-65	145	1	-85	-175	-175

Table 5. Selected torsion angles for the main backbone of **1**

C8—N6—C7—C11 (φ_1)	−66.5 (3)
N6—C7—C11—N3 (ψ_1))	139.4 (2)
O1—C8—N6—C7(ω_1)	−8.1 (3)
C11—N3—C13—C10 (φ_2)	−96.1 (3)
N3—C13—C10—O2 (ψ_2)	−166.8 (2)
C7—C11—N3—C13 (ω_2)	−174.12 (19)

The torsion angles of both proline residues, Pro1 and Pro2, in the two structures, place them in the incipient polyproline type I (PPI) and polyproline type II (PPII) turn region, respectively [50]. Poly-L-proline can form two regular conformations known as poly (Pro) II (PPII) and poly(Pro) I (PPI) in the solid state and in solution [56]. An ideal left-handed PPII helix has backbone dihedral angles (φ, ψ) = (−75°, +145°), which is adopted by homopolymers of proline in aqueous solution. The right-handed PPI has similar backbone dihedral angles but has all peptide bonds in the *cis* conformer ($\omega = 0°$) [57] while PPII is a left-handed helix with all trans peptide bonds [56]. PPII is a dominant backbone conformation in unfolded peptides and proteins [58]. Poly-L-proline-type structures are formed in polypeptides containing three or more contiguous or successive three proline

residues [50, 59], but the incipient formation of Poly-L-proline type I and II structure requires only two consecutive proline residues [50].

Compared to other amino acids, proline readily isomerizes between its *cis* ($\omega = 0°$) and *trans* ($\omega = 180°$) conformers [60]. The probability distribution for *cis*-*trans* prolyl bonds is affected by neighboring amino acids, pH and ionic strength, solvent and chain length [61]. The right-handed polyproline I helical conformation is observed for homopolymers of proline in organic solvents and is disfavored in aqueous solution [57], where as PPII conformation predominates in aqueous media or in the presence of aliphatic acids [61, 62], which commonly found on the surface of proteins [60].

As far as the structure of **1** is concerned, the backbone conformation as well as the main dihedral angles (Table 5), shows similar structure to those of two previously determined structures. Here, in the molecular structure of **1** (Figure 11), the Pro-Pro peptide bond is in the *trans*-conformation along the peptide bond (C11-N3). The *t*Boc-Pro bond shows *cis*-geometry roughly with $\omega = -8.1^{o}$ while the *trans*-conformation with $\omega = -174.12^{o}$ (Table 5), which are both comparable to the normal 0° and ±180° for peptide bonds with a *cis* and *trans* configurations, respectively. The peptide bond preceding Pro has a relatively high intrinsic probability (~5-6%) of having a *cis* arrangement as compared with other amino acids (~0.03%) [63].

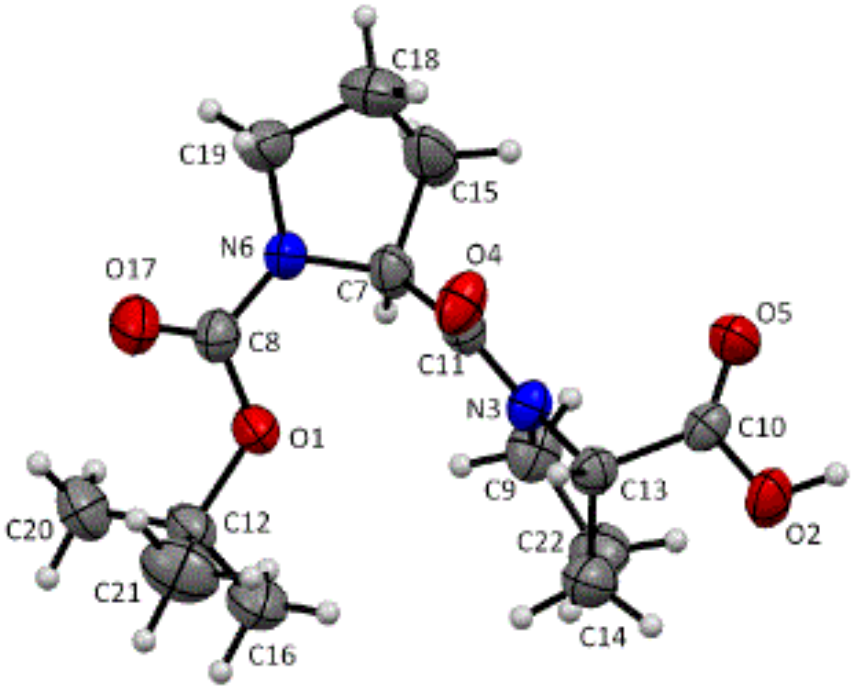

Figure 11. Molecular structure of **1** (*ORTEP* diagram) with atomic numbering indicated. Displacement ellipsoids are shown at the 50% probability level for non H-atoms. H atoms are shown as spheres of arbitrary size.

4.1.4.2. Hydrogen Bonding and crystal packing

Molecules in **1** are linked in pairs by a single O2—H1···O4 ($x-1/2$, $-y+3/2$, $-z+1$) hydrogen bond with 1.75 (3) Å bond length (Table 6), which runs from O-H end of the first to the carbonyl oxygen of the second residues. The intermolecular hydrogen bonds (expansion of the molecule along the crystallographic *b*-axis) form a helical like shape with the Boc-groups pointing out from the helix (Figure 12). Similar type of helical

characteristics were observed with the related molecules of the same compound (monoclinic and orthorhombic forms) when forming intermolecular hydrogen bonding along their respective crystallographic *a*- and *b*- axes (Figure 12b and c, respectively). In addition, the backbone conformations of the three related structures are also very similar.

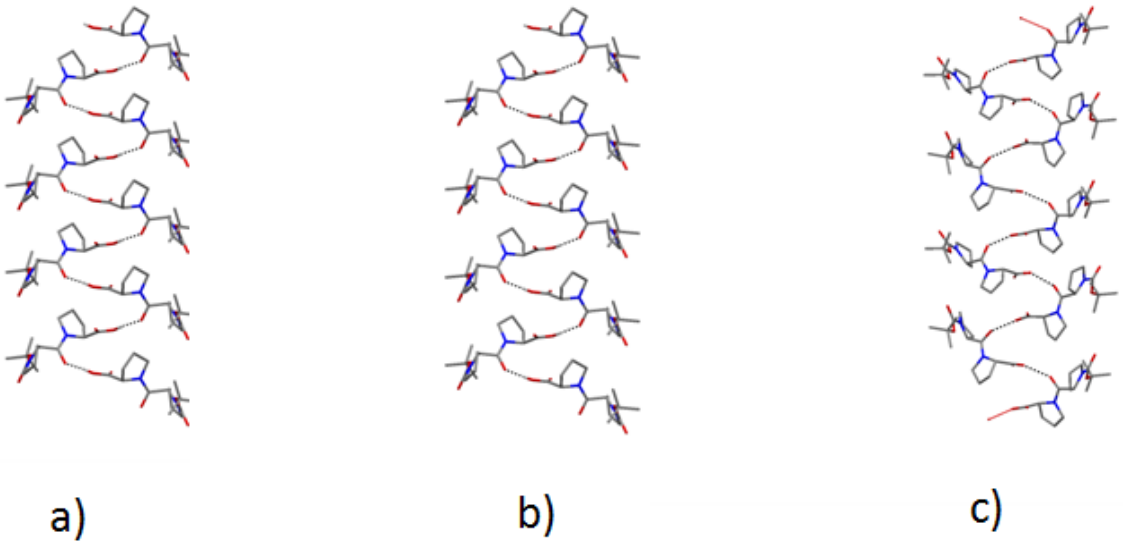

Figure 12. Capped-stick model for helix forming molecules when expanding by intermolecular hydrogen-bonding: a) for **1**; b) orthorhombic, $P2_12_12_1$ form (refcode: BOCPRO); c) monoclinic, $P2_1$ form (recode: BOCPRO01), illustrations have been made using the Mercury program.

Table 6. Hydrogen-bond geometry (Å, °) of **1**

D—H···*A*	*D*—H	H···*A*	*D*···*A*	*D*—H···*A*
O2—H1···O4^{i}	0.88 (3)	1.75 (3)	2.615 (3)	167 (3)

Symmetry codes: (i) *x*−1/2, −y+3/2, -z+1.

The molecular packing of **1** along the *c*-axis (Figure 13) shows that molecules are arranged in helix like manner when the molecules are connected through the intermolecular O—H···O type of hydrogen bond.

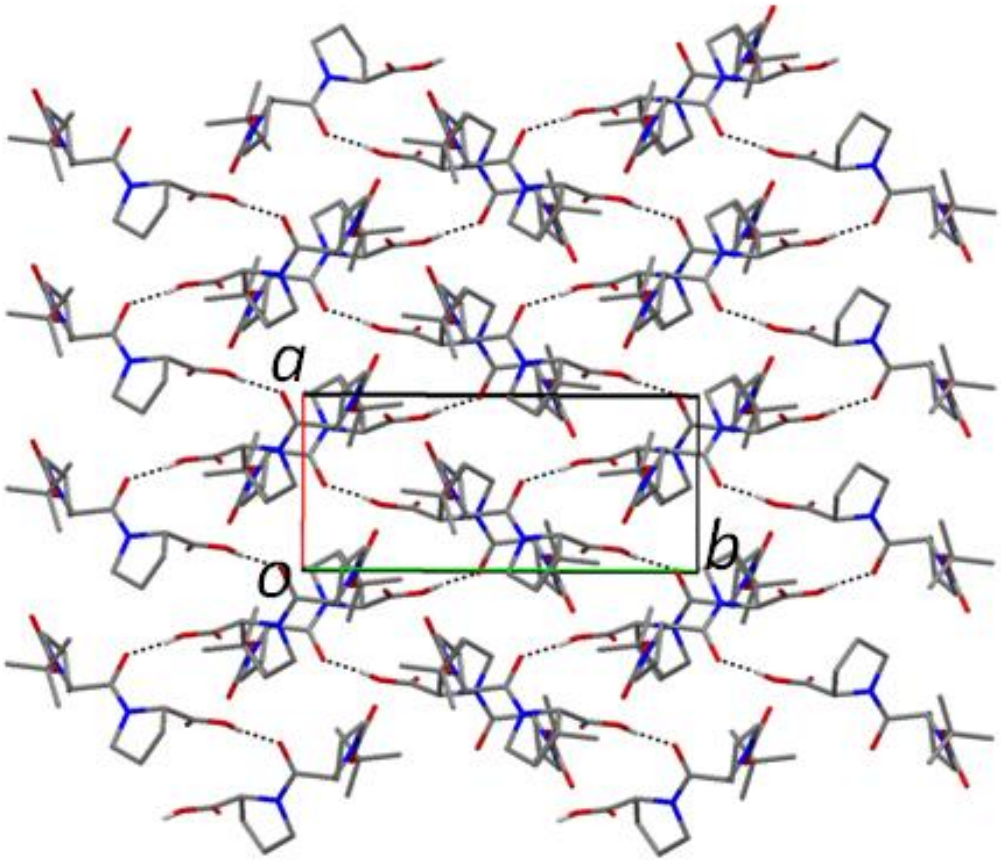

Figure 13. The molecular packing of **1** viewed along the crystallographic *c* axis. Dashed lines indicate hydrogen bonds. Hydrogen atoms not involved in hydrogen bonding have been omitted for clarity.

4.1.4.3. Torsion angles as criteria for structure conformation

The torsion angles for the structure **1**, Boc-Pro-Pro-OMe, can be assigned according to the main chain (or polypeptide backbone) or side chain torsion angles (torsion angle of the proline rings).

i) ***The main chain (or polypeptide backbone) torsion angles***

According to IUPAC-IUB Commission on Biochemical Nomenclature [64], the main torsion angle describing rotation about N-C^{α} is denoted by φ, rotation about C^{α}-C is denoted by ψ, and rotation describing about C-N is denoted by ω. The symbols φ_i, ψ_i, and ω_i are used to denote torsion angles of bonds within the *i*th residue in the case of φ_i and ψ_i, and between the *i*th and (*i*+1)th residues in the case of ω_i; specifically, they denote the torsion angles the sequences of atoms C_{i-1},N_i,C^{α}_i,N_{i+1}, N_i,C^{α}_i,C_i,N_{i+1}, and C^{α}_i,C_i,$N_{i+1}C^{\alpha}_{i+1}$, respectively. The dihedral angle ω_i for the Boc-Pro bond can be assigned with regard to the O atom of the Boc group (Table 5).

The main backbone dihedral angles (φ, ψ, ω) (Table 5) of **1** show that the two proline residues Pro1 and Pro2 adopt incipient Poly-L-proline type I (PPI) and type II (PPII) backbone conformations, respectively.

ii) ***Side chain torsion angles of proline rings (pyrrolidine rings)-five member ring puckering conformations***

Atoms are lettered, or lettered and numbered, from C^{α}, and bonds are numbered from C^{α}, working outwards away from the main chain. Atoms other than hydrogen are designated by Greek letters α, β, γ, δ, etc. Figure 14, denotes the assigned atoms of the proline rings where the carbon atoms in the rings are assigned by the Greek letters giving α to C11, β to C15, γ to C18, and δ to C19. The number given to the atoms is based on the *ORTEP* diagram (Figure 11).

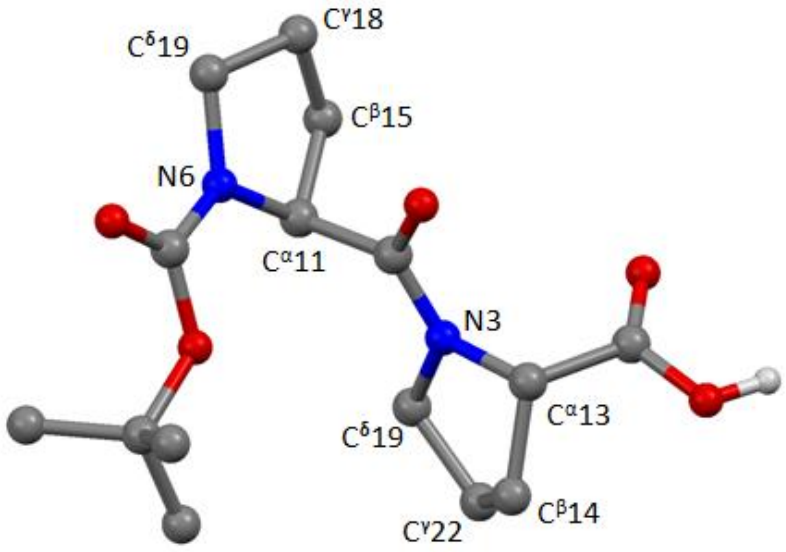

Figure 14. Ball and stick model showing labeled and assigned atoms of proline rings.

For pyrrolidine rings of proline residues, there are two groups of preferred conformations that are about equally energetically favourable. They are distinguished by the direction the C^{γ} atom protrudes from the average plane of the ring and are referred to as either: up and down, A and B or C^{γ}-exo and C^{γ}-endo [65]. The down and up ring puckering are defined as the C^{γ}, and C=O group of the Pro residue lie on the same and opposite sides, respectively, of the plane defined by C^{δ}, N and C^{α} atoms [63, 66]. In the pyrrolidine rings classified as A and B conformations, A has the negative dihedral angle χ_1, and the C=O and C^{γ} are on opposite side of the planar $NC^{\alpha}C^{\beta}C^{\gamma}$ (C^{γ}-*exo*) while B has positive χ_1, and the two atoms are on the same side of the plane (C^{γ}-*endo*) [67]. Thus, the pyrrolidine ring of the proline pucker can assume C^{γ}-*exo* and C^{γ}-*endo*, or up and down, respectively. It has been shown that the puckering of the Proline ring can be influenced by the surrounding environment, either the solvent or neighboring residues [50].

Table 7. The torsion angles of all the five bonds of the pyrrolidine rings for Pro1 and Pro2 of **1**

Pro_1	Values (°)	Pro_2	Values (°)
N6 $C^{\alpha}7$ $C^{\beta}15C^{\gamma}18$ (χ_1)	27.9 (3)	N3 $C^{\alpha}13C^{\beta}14C^{\gamma}22$ (χ'_1)	39.3 (2)
$C^{\alpha}7$ $C^{\beta}15$ $C^{\gamma}18$ $C^{\delta}19$ (χ_2)	−33.2 (3)	$C^{\alpha}13$ $C^{\beta}14$ $C^{\gamma}22C^{\delta}9$ (χ'_2)	−37.7 (3)
$C^{\beta}15$ $C^{\gamma}18$ $C^{\delta}19$ N6 (χ_3)	24.9 (3)	$C^{\beta}14$ $C^{\gamma}22$ $C^{\delta}9$ N3 (χ'_3)	21. (3)
$C^{\gamma}18$ $C^{\delta}19$ N6 $C^{\alpha}7$ (χ_4)	−7.0 (3)	$C^{\gamma}22$ $C^{\delta}9$ N3 $C^{\alpha}13$ (χ'_4)	4.1 (3)
$C^{\gamma}19$ N6 $C^{\alpha}7$ $C^{\beta}15$ (θ_1)	-13.0 (3)	$C^{\gamma}9$ N3 $C^{\alpha}13$ $C^{\beta}14$ (θ'_1)	−27.74(2)

From Table 7, χ_1 and χ'_1 both contain positive dihedral angles, 27.7º and 39.5º, respectively. According to [67], Boc-Pro-Pro-OH of **1** belongs to conformation B, i.e. down puckered conformation (C^{γ}-*endo*).

4.1.4.4. Comparison of the dihedral angles of the Pro138-Pro139 segment in the structure of rAQP4 and hAQP4 with the main backbone of the Pro-Pro residues in the crystal structure of (1)

The first reported structure of rAQP4 was solved by electron diffraction to 3.2 Å resolution [25], and the crystal structure of human hAQP4 was recently solved by X-ray diffraction to 1.8 Å resolution [23]. The dihedral angles for Pro138 and Pro139 in AQP4 loop C (in both structures) have been measured and the following values were observed. From the first reported structure of rAQP4, it was found that φ (Pro138) = -57.54°, ψ (Pro138) = -23.65°, φ (Pro139) = -90.97° and ψ (Pro139) = 6.32°. The dihedral angles place Pro138 in the 3_{10}-helical region of the Ramachandran plot. On the other hand, the values for hAQP4 are φ (Pro138) = - 55.07 and ψ (Pro138) = 134.95, and φ (Pro139) = -51.58 and ψ (Pro139) = -33.46. In this case, the Pro138 residue adopts a polyproline II (PII) conformation and the Pro139 residue a

3_{10}-helical conformation. The difference in backbone structure between (I) and the Pro138-Pro139 segment of loop C is that **1** is too short to form a 3_{10} helix or polyproline II helix, since they are formed by at least three residues per turn [50, 59]. But the incipient polyproline type I (PPI) and polyproline type II (PPII) turns, with which **1** formed, are characterized by only two consecutive proline residues [50].

4.2. Crystal structures of two polymorphic forms (2 and 3) of Boc-Aib-Aib-OMe *N*-(*tert*-Butoxycarbonyl-α-aminoisobutyryl-α-aminoisobutyric acid methyl ester): a fully protected dipeptide

4.2.1. Introduction

The achiral residue α-aminoisobutyric acid (Aib) is one of the non-standard amino acids found in a class of polypeptides known as peptaibiotics [68, 69]. It is believed that these peptides exert their antibiotic effect by forming voltage-gated transmembrane ion channels through the cell membrane [70-72]. These residues are also useful in synthetic analogues of protein sequences to increase helix stability [69, 73, 74], either with α-helical or 3_{10}-helical hydrogen bonding patterns [45, 75]. The 3_{10}-helix is a common secondary structural motif in peptides and proteins which is characterized by three amino acids per turn and ten atoms in the pseudo-ring formed by an intramolecular i→i+3 hydrogen bond [76, 77].

Introduction of Aib residues into polypeptide chains limits the range of accessible conformations due to the presence of extra methyl group at the C^{α}-carbon and forces the peptide chain into a left-or right-handed helical conformation [72], or nucleates β-turns and helical structures [68]. Shorter Aib peptides preferentially adopts type III β-bends and 3_{10}-helices while longer Aib containing peptides are able to form α-helical structures [70]. It has been shown by X-ray diffraction studies on numerous Aib-based short model peptides that they form 3_{10}-helical structures [69, 77, 78]. In fact, a review on crystal structures of synthetic tri-, tetra-, and peptapeptides containing at least one Aib residue showed that all except one contained an incipient 3_{10}-helix [69]. The Aib residue is almost invariably restricted to the dihedral angles ((φ,ψ)-values) of -60° (±20°) and -30°(±20°), right handed 3_{10}- or α-helix (α_R) [46] or just limited to the helical region of the Ramachandran map (φ = ±60±20 ; ψ = ±30±20) [73].

Another investigation on Aib has been shown that these peptides do not tend to form β-sheet structures and they are proved to be best beta-sheet breaker amino acid [79, 80]. From

the concept of the conformational entropy change that accompanies binding, Aib has less conformational entropy loss thus it improves binding affinity by reducing the loss of conformational entropy upon binding. Increased helicity in solution also results in improved proteolytic stability. Low proteolytic stability is a major problem with peptide based drugs in vivo [81].

4.2.2. Data collection and structure solution

X-ray data on colorless needle-shaped single crystals of **2** and **3** were collected at 296(2) and 105(2) K, respectively on ApexII CCD diffractometer using APEX2 software [51]. Intensity measurements were performed using MoKα radiation (λ= 0.71073 Å). Determination of integral intensities, unit cell refinements and data reductions were performed with SAINT-Plus [52]. Table 8 and 9 provide crystal data and structure refinement information of **2** and **3**, respectively.

Subsequent data absorption correction was done by SADABS [53] using multi-scan technique. The space group $P2_1/c$ (**2**) and $P2_1/n$ (**3**), each with Z=4 and Z' =1 for the formula unit $C_{14}H_{26}N_2O_5$, were determined by XPREP. The structures were solved by direct methods using SHELXTL [54].

4.2.3. Structure refinement

Full-matrix least-square refinements on F^2 against all reflections were carried out by SHELXTL [54]. All non-hydrogen heavy atoms were refined anisotropically. All H atoms were positioned with idealized geometry and fixed C-H distances for CH_3 at 0.98 for **2** and 0.96 for **3**. Free rotations were permitted for methyl groups. U_{iso} (H) values were set to $1.2U_{eq}$ of the carrier atom (N-H) and $1.5U_{eq}$ for methyl groups. Complete crystal data for **2** are given in Appendix C and for **3** are in Appendix D.

Table 8. Crystal data and structure refinement for Boc-Aib-Aib-OMe (**2**)

Chemical name	Boc-Aib-Aib-OMe
Chemical formula	$C_{14}H_{26}N_2O_5$
Formula weight (M_r)	302.37
Temperature	296 (2) K
Dx	1.144 Mgm^{-3}
Wave length (λ)	0.71073 Å
Crystal system	Monoclinic
Space group	$P2_1/c$
Unit cell dimensions	
a /Å	6.5380 (18)
b/ Å	33.743 (9)
c /Å	8.583 (2)
β/ °	92.266(3)
Volume (V)	1756.0 (8) $Å^3$
Z	4
Absorption coefficient	0.09 mm^{-1}
Crystal size	0.8 × 0.1 × 0.1 mm
F(000)	656
Absorption correction	Multi-scan
(Max. and min. absorption corrections)	0.9900 and 0.9000
Theta (θ) range for data collection	2.41-25.06°
Index ranges	h = -6→7, k = -40→40, l = -8→10
$N_{measured}$	10165
N_{unique}	3105
$N_{observed}$ ($I > 2\sigma(I)$)	1584
Refinement method	Full-matrix least-squares on F^2
Data/restraints/parameter	3105/0/197
GooF (S) on F^2	0.99
R_{int}	0.052
$R(F^2>2\sigma(F^2)$	0.042
$wR(F^2)$	0.1257
Peak differences in electron density map	$\Delta\rho_{max}$ = 0.15 e $Å^{-3}$, $\Delta\rho_{min}$ = −0.18 e $Å^{-3}$

Table 9. Crystal data and structure refinement for Boc-Aib-Aib-OMe (**3**)

Chemical name	Boc-Aib-Aib-OMe
Chemical formula	$C_{14}H_{26}N_2O_5$
Formula weight (M_r)	302.37
Temperature	105 (2) K
Dx	1.178 Mgm^{-3}
Wave length (λ)	0.71073 Å
Crystal system	Monoclinic
Space group	$P2_1/n$
Unit cell dimensions	
a /Å	6.116 (3)
b/ Å	15.662 (7)
c /Å	17.967 (8)
β/º	97.878(3) °
Volume (V)	1704.7 (13) $Å^3$
Z	4
Absorption coefficient	0.09 mm^{-1}
Crystal size	0.79 × 0.22 × 0.13 mm
F(000)	656
Absorption correction	Multi-scan
(Max. and min. absorption corrections)	0.9880 and 0.9170
Theta (θ) range for data collection	1.7-28.3°
Index ranges	h = -7→7, k = -20→20, l = -19→23
$N_{measured}$	11873
N_{unique}	4100
$N_{observed}$ ($I > 2\sigma(I)$	2595
Refinement method	Full-matrix least-squares on F^2
Data/restraints/parameter	4100/0/190
GooF (S) on F^2	1.02
R_{int}	0.048
$R(F^2>2\sigma(F^2)$	0.051
$wR(F^2)$	0.129
Peak differences in electron density map	$\Delta\rho_{max}$ = 0.28 e $Å^{-3}$, $\Delta\rho_{min}$ = −0.24 e $Å^{-3}$

4.2.4. Discussion

4.2.4.1. Structure conformations of (2) and (3)

The crystal structures of **2** and **3** (schematic drawing in Figure 15) crystallize in the monoclinic space groups with $Z' = 1$. The molecular structure of **2** is shown in Figure 16 and **3** in Figure 17.

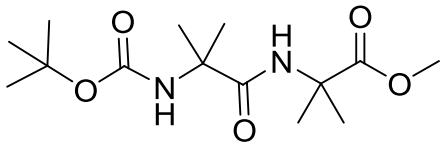

Figure 15. Schematic illustration of Boc-Aib-Aib-OMe, drawn using ChemBioDraw Ultra-12.0

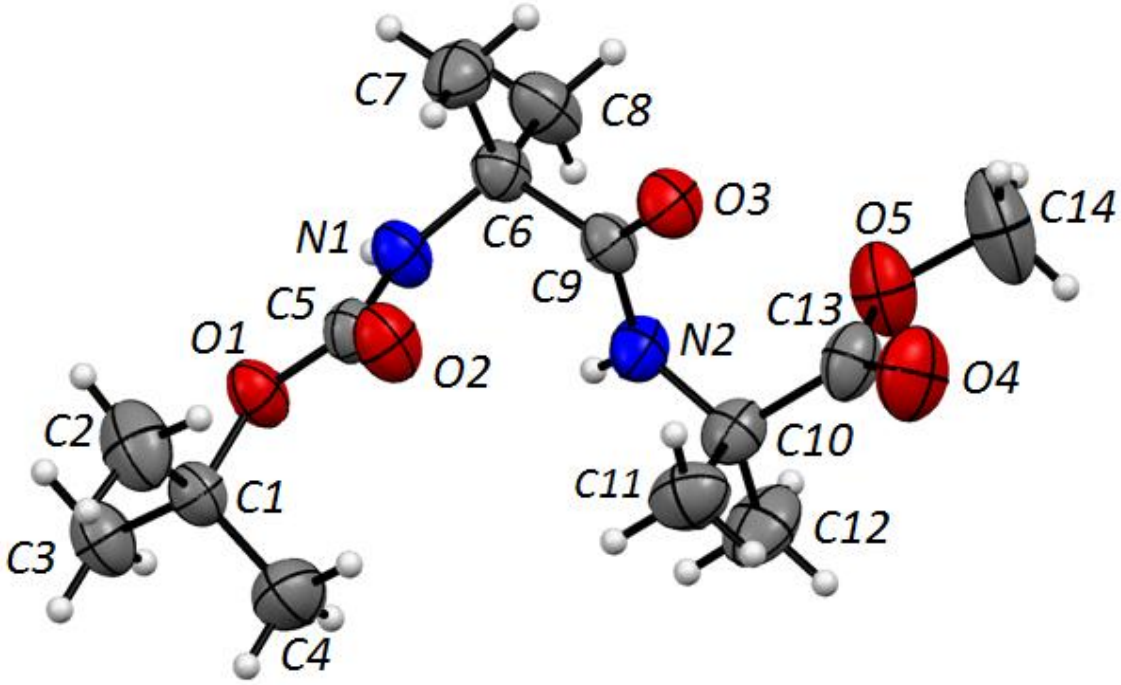

Figure 16. Crystal structure of **2** (*ORTEP* diagram) with atomic numbering indicated**.** Displacement ellipsoids are shown at the 50% probability level for non H-atoms. H atoms are shown as spheres of arbitrary size.

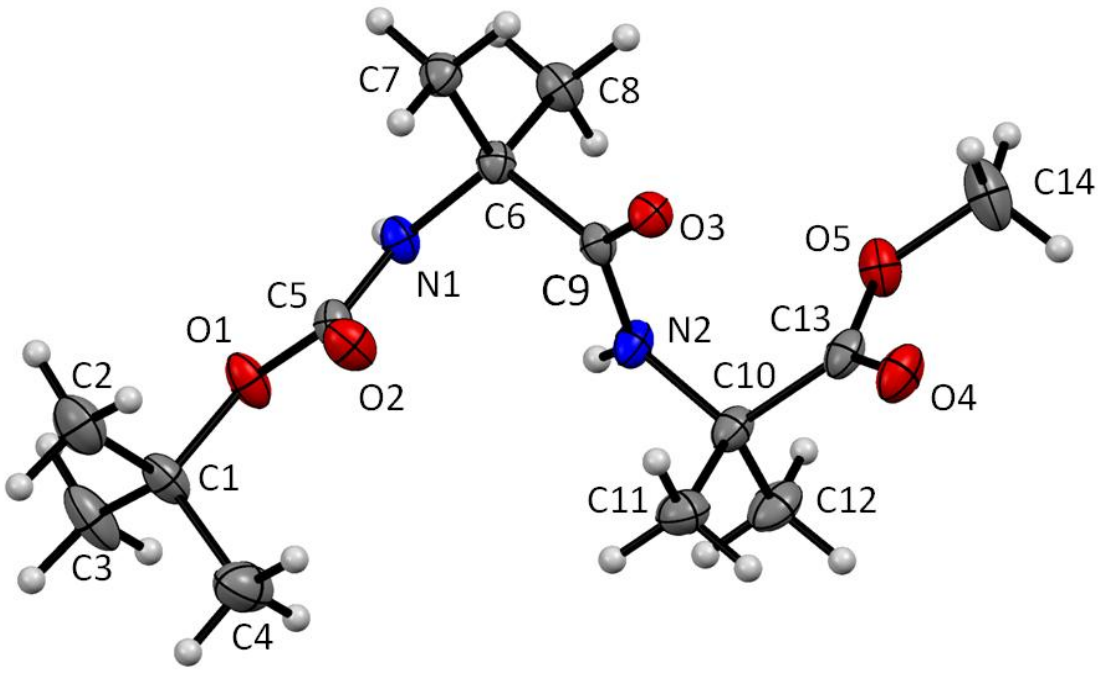

Figure 17. Crystal structure of **3** (*ORTEP* diagram) with atomic numbering indicated. Displacement ellipsoids are shown at the 50% probability level for non H-atoms. H atoms are shown as spheres of arbitrary size.

The Aib residues in **2** and **3** adopt (φ,ψ)-values characteristics of helical conformations. The peptide backbone (φ,ψ)-values for the Aib1 and Aib2 residues in both polymorphs show that they adopt left-and right-handed 3_{10}-/α-helical conformations (Tables 10 and 11). These torsion angles are quite similar to the Aib residue positioned in the crystal structure of the dipeptides, Boc-Aib-Leu-OMe and Boc-Aib-Phe-OMe, one of the molecules in the asymmetric unit adopts a left-handed helical conformation and the Aib in the other molecule in the asymmetric unit adopts a right-handed helical conformations [82, 83]. Like **2** and **3** whose Aib residues adopt left- and right-handed 3_{10}-/α-helical

conformations, another fully protected dipeptide, Boc-Aib-Aib-OBzl with CSD refcode BAJROT10 [84] shows similar structural backbone arrangement (Figure 18b).

Table 10. Selected backbone torsional angles for Boc-Aib-Aib-OMe **2** (°)

O1—C5—N1—C6 (ω_1)	176.89 (19)
C5—N1—C6—C9 (φ_1)	56.4 (3)
N1—C6—C9—N2 (ψ_1)	42.5 (3)
C6—C9—N2—C10 (ω_2)	−175.7 (2)
C9—N2—C10—C13(φ_2)	−50.4 (3)
N2—C10—C13—O5 (ψ_2)	−49.1 (3)

Table 11. Selected backbone torsional angles for Boc-Aib-Aib-OMe **3** (°)

O1—C5—N1—C6 (ω_1)	178.14 (13)
C5—N1—C6—C9 (φ_1)	58.93 (19)
N1—C6—C9—N2 (ψ_1)	40.83 (19)
C6—C9—N2—C10 (ω_2)	178.15 (14)
C9—N2—C10—C13(φ_2)	−45.7 (2)
N2—C10—C13—O5 (ψ_2))	−50.44 (18)

The reversal in handedness of the C-terminal residue relative to the previous residues is frequently observed in peptides when this residue is not involved in intramolecular hydrogen bonding and reduces intramolecular contacts that would otherwise occur [84]. Since the Aib residue does not have an asymmetric C^{α}-atom, both the $\alpha_L$and α_R-conformations are equally possible in achiral residues [69, 73]. Thus, both the Aib residues can adopt either a left- or right-handed helix. The Aib-Aib bonds adopt *trans*-conformation along the peptide bond (C9-N2) with ω = −175.7 (2) º (Table 10) or 178.15 (14) º (Table 11).

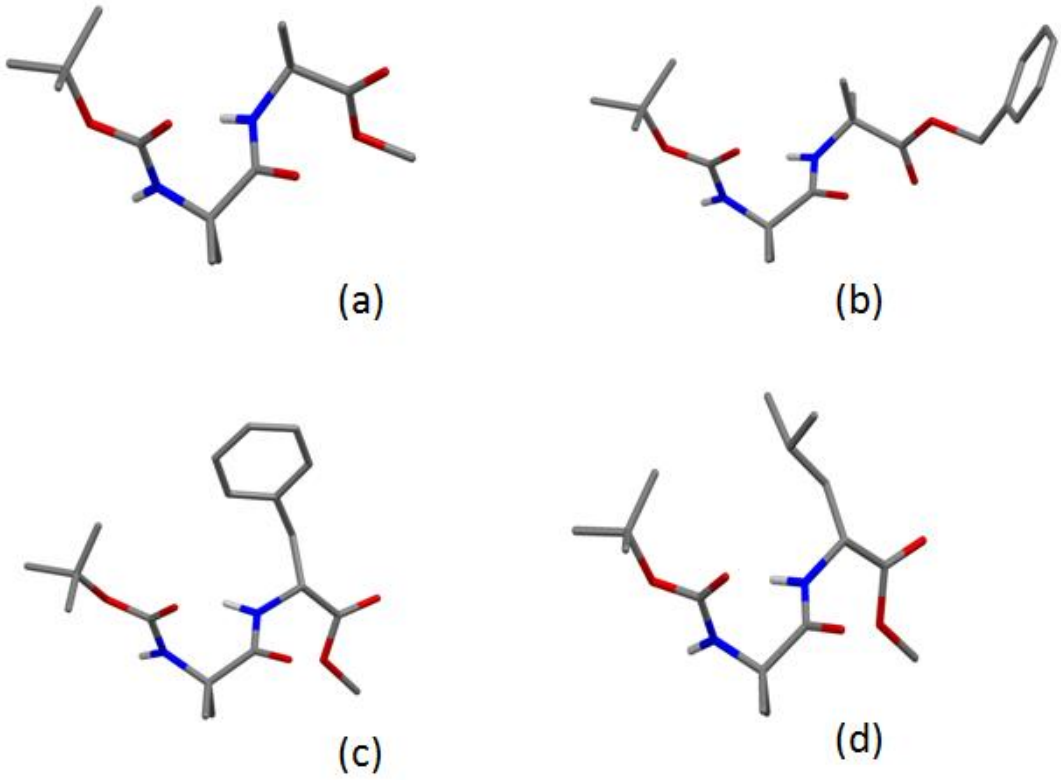

Figure 18. Capped-stick model backbone conformations for: a) Boc-Aib-Aib-OMe; b) Boc-Aib-Aib-OBz (refcode: BAJROT10); C) Boc-Aib-Phe-OMe (refcode: PASGUL); d) Boc-Aib-Leu-OMe (refcode: XOWVAG).

The main backbone conformations of the fully protected dipeptides in Figure 18 show similar arrangements, but the C-terminal side of Boc-Aib-Aib-OBz (Figure 18b) has different arrangement around the –COO group where the C=O is positioned upward and –OMe group downward in the other structures while the reverse arrangements are observed in Boc-Aib-Aib-OBz, i.e. down and up respectively.

Figure 19 shows the intermolecular hydrogen bonding of **2** and **3** structures. The peptide molecules are arranged in a β-sheet like manner when the molecules are linked to each other by N1—H1···O3 and N2—H2···O4 type of hydrogen bonds (Tables 12 and 13) .

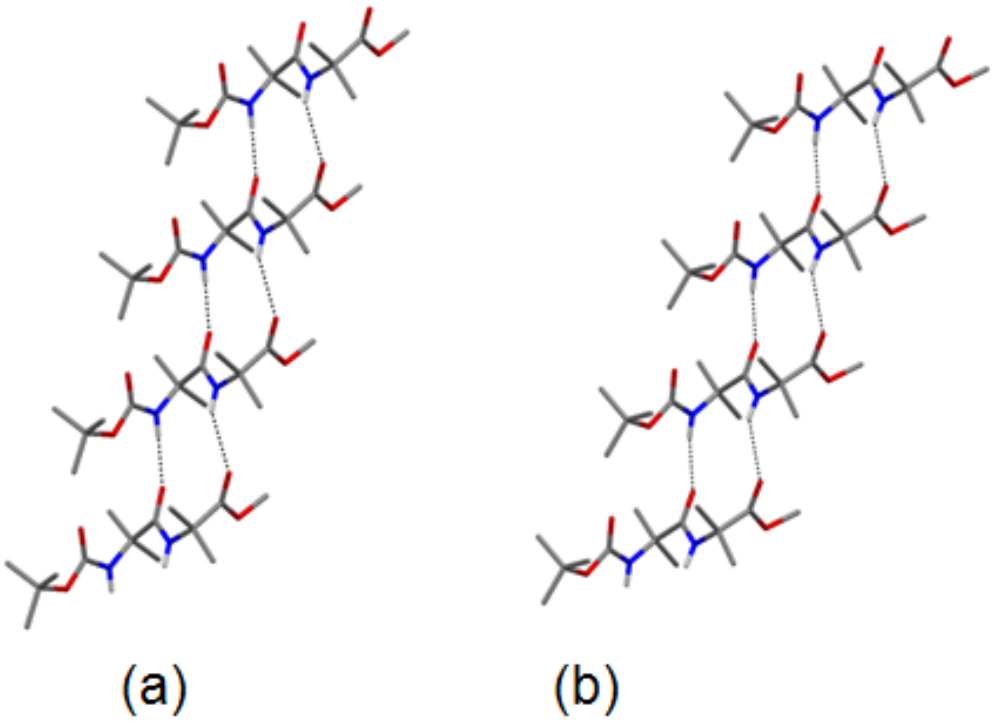

Figure 19. Capped-stick model for intermolecular hydrogen bonds of Boc-Aib-Aib-OMe when the molecules are viewed along the crystallographic c axis: a) molecules in **3** and b) molecules in **2**.

Table 12. Hydrogen-bond geometry (Å, °) of **2**

D—H···*A*	*D*—H	H···*A*	*D*···*A*	*D*—H···*A*
N1—H1···O3^{i}	0.87 (2)	2.15 (2)	3.007 (3)	170 (2)
N2—H2···O4^{i}	0.86 (2)	2.43 (2)	3.197 (3)	148 (2)

Symmetry codes: (i) x+1, y, z

Table 13. Hydrogen-bond geometry (Å, °) of **3**

D—H···*A*	*D*—H	H···*A*	*D*···*A*	*D*—H···*A*
N1—H1···O3^{i}	0.86	2.10	2.962 (2)	175
N2—H2···O4^{i}	0.86	2.45	3.227 (2)	151

Symmetry codes: (i) *x*−1, *y*, *z*.

The intermolecular hydrogen bonding of Boc-Aib-Aib-OMe is also shown in Figure 20a just for comparisons with the other related structures. Even though the backbone conformations of the reference compounds show similar geometries to Boc-Aib-Aib-OMe, their intermolecular hydrogen bonding patterns are different.

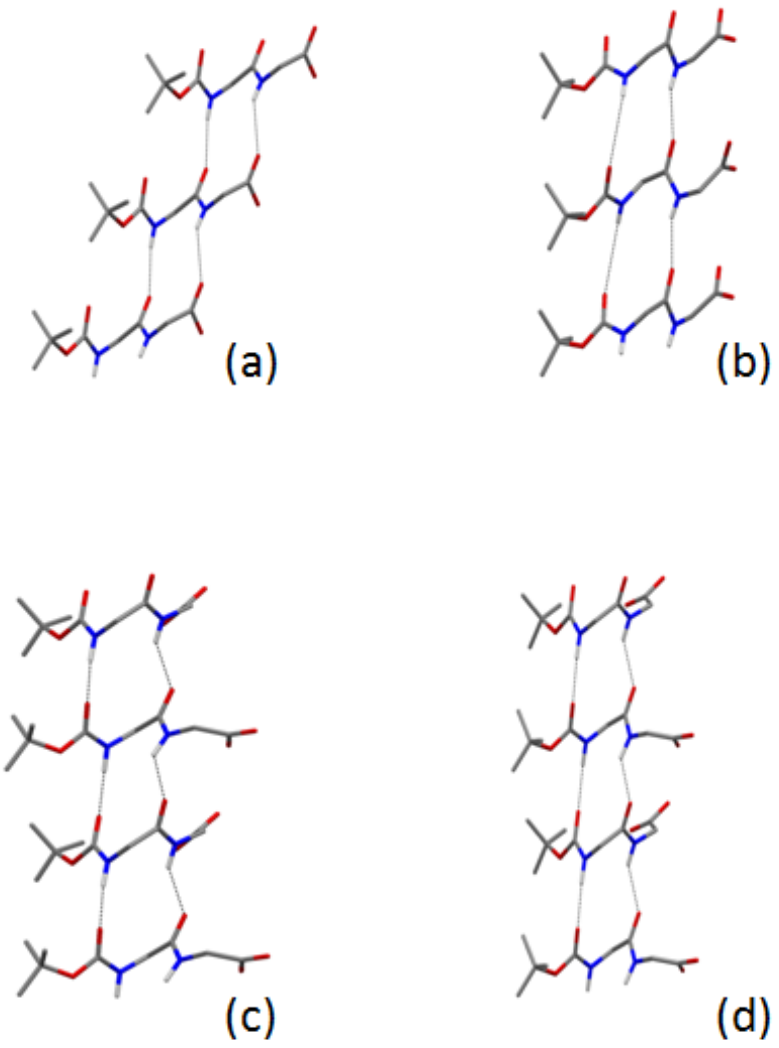

Figure 20. Intermolecular hydrogen bonding of molecules are shown where hydrogen bonds with N-H donors and O=C acceptors are indicated as dashed lines and some side chains, and all hydrogen atoms except those forming H-bonding are not shown for clarity. a) Boc-Aib-Aib-OMe; b) Boc-Aib-Aib-OBz (refcode: BAJROT10); C) Boc-Aib-Phe-OMe (refcode: PASGUL); d) Boc-Aib-Leu-OMe (refcode: XOWVAG).

The intermolecular hydrogen-bonding arrangements of Boc-Aib-Aib-OMe **(2** and **3)** (Figure 19 and 20a) shows that molecules are displaced from each other, i.e. tilted from the hydrogen-bond axis and run diagonally (or just in a slant way). This type of

arrangement is not observed in the other three structures; they are exactly stacking one above the other. Unlike the other compounds whose H-bond acceptors are C=O of the Boc group and C=O of the first Aib group, the acceptors for the **2** and **3** are C=O of the Aib residues.

Even though the molecular structure conformations of **2** and **3** are the same, their crystal packing modes (Figure 21) and unit cell dimensions (Table 8 and 9) are different. All the molecules in **3** are in close contact to each other through their hydrophobic side chains, as can be seen from Figure 21a. However, the interaction of molecules in **2** (Figure 21b) are different; the close contacts are only in between two neighbor molecules. The hydrophobic interactions between the molecules can be important for stabilizing the structure.

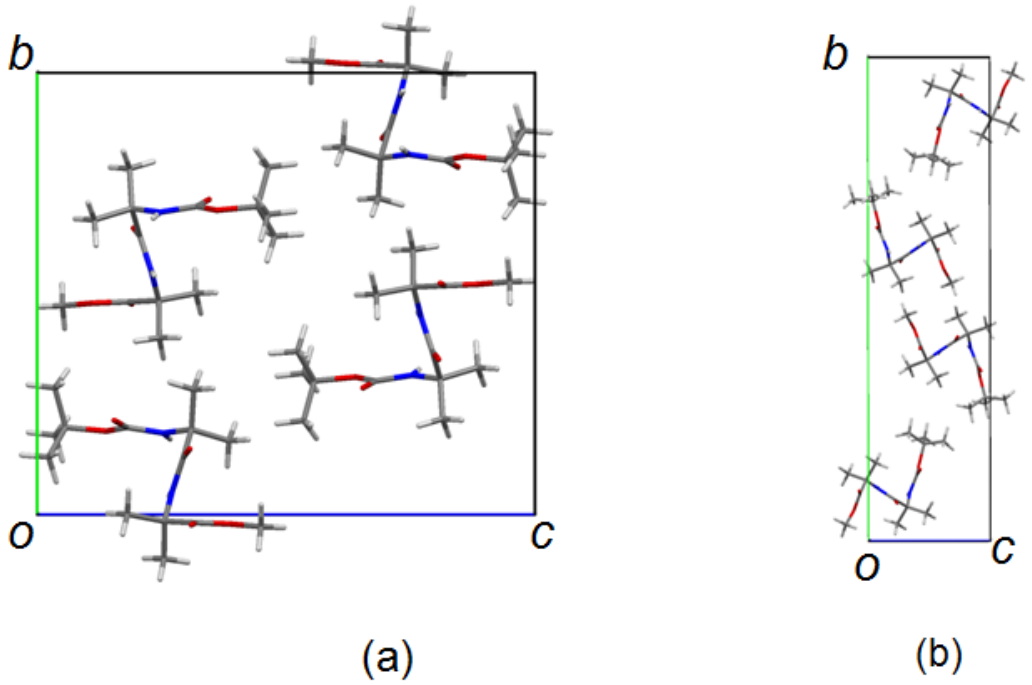

Figure 21. Molecular packing of Boc-Aib-Aib-OMe viewed along the *a* axis. (a) for **3** (b) for **2**

4.3. Crystal structure of Boc-Val-Val-OMe *N*-(*tert*-Butoxycarbonyl-L-valyl-L-valine methyl ester): a twisted, parallel β-sheet in the crystal structure of a fully protected dipeptide

4.3.1. Introduction

Valine, an essential amino acid with hydrophobic side chain, is usually found in the interior of proteins. Aliphatic amino acids such as valine, alanine, leucine and isoluecine have high propensity for forming extended conformations [85]. Peptides containing valine residue have the least tendency to form a β-turn, but have a high propensity to form β-sheet structures [86]. As part of the ongoing synthetic and structural studies of AQP4 loop C mimics [1] peptide **4**, corresponding to the Val141-Val142 segment of the 3_{10}-helical loop C (Pro138-Pro139-Ser140-Val141-Val142-Gly143-Gly144) segment of AQP4, was crystallized and its X-ray structure determined.

4.3.2. Data collection and structure solution

X-ray data on a colorless needle-shaped single crystal was collected at 150(2) K on ApexII CCD diffractometer using APEX2 software [51]. Intensity measurements were performed using MoKα radiation (λ= 0.71073 Å). Determination of integral intensities, unit cell refinement and data reduction were performed with SAINT-Plus [52] . The crystallographic data for peptide **4** are reported in Table 14.

Subsequent data absorption correction was done by SADABS [53] using multi-scan technique. The space group $P2_12_12_1$ with Z = 12 and Z' = 3 for the formula unit $C_{16}H_{30}N_2O_5$ was determined by XPREP. The structure was solved by direct methods using SHELXTL [54].

Table 14. Crystal data and structure refinement for Boc-Val-Val-OMe (**4**)

Chemical name	Boc-Val-Val-OMe
Chemical formula	$C_{16}H_{30}N_2O_5$
Formula weight (M_r)	330.42
Temperature	150 (2) K
Dx	1.116 Mgm^{-3}
Wave length (λ)	0.71073 Å
Crystal system	orthorhombic
Space group	$P2_12_12_1$
Unit cell dimensions	
a/Å	11.6937 (12) Å
b/Å	18.6458 (19) Å
c/ Å	27.047 (2)
Volume (V)	5897.3 (10) $Å^3$
Z	12
Absorption coefficient	0.08 mm^{-1}
Crystal size	0.72 x 0.15 x 0.11 mm
F(000)	2160
Absorption correction	multi-scan
(Max. and min. absorption corrections)	0.9800 and 0.9000
Theta (θ) range for data collection	1.9-25.0°
Index ranges	h = -13→13, k = -22→22, and l = -32→32
$N_{measured}$	38750
N_{unique}	5757
$N_{observed}$ $(I > 2\sigma(I))$	4918
Refinement method	Full-matrix least-squares on F^2
Data/restraints/parameter	5757/6/618
GooF (S) on F^2	1.03
R_{int}	0.044
$R(F^2>2\sigma(F^2))$	0.037
$wR(F^2)$	0.091
Peak differences in electron density map	$\Delta\rho_{max}$ = 0.19 e $Å^{-3}$, $\Delta\rho_{min}$ = −0.18 e $Å^{-3}$

4.3.3. Structure refinement

Full-matrix least-square refinement on F^2 against all reflections was carried out by SHELXTL [54]. The L-Val side chain of residue 2 (Figure 23) in molecule C is disordered over two positions, and atoms of the major orientation with occupancy 0.843(7) were refined in a normal manner. The covalent geometry of the 0.157(7) minor orientation was loosely tied to the geometry of the major component by a SHELX SAME restraint. C^{α} (C11D) and C^{β} (C12D) received the same set of thermal displacements parameters as their major counterparts (C11C and C12C), while a common isotropic temperature factor was refined for $C^{\gamma 1}$ (C13D) and $C^{\gamma 2}$ (C14D). Positional parameters were refined for H-atoms bonded to N, with a mild restraint on N-H distances imposed by a SHELX DFIX 0.88 0.02 command. Other H atoms were positioned with idealized geometry and fixed C–H distances at 0.98 and 1.00 Å for CH_3 and CH, respectively. Free rotation was permitted for methyl groups. U_{iso} (H) values were set to $1.2U_{eq}$ of the carrier atom (N-H) or $1.5U_{eq}$ for methyl groups. Complete crystal data for peptide **4** are given in Appendix E.

4.3.4. Discussion

4.3.4.1. Structure conformation of Boc-Val-Val-OMe

Peptide **4**, with a chemical diagram depicted in Figure 22, crystallize in the orthorhombic $P2_12_12_1$ space group with three molecules in the asymmetric unit. Its molecular structure is shown in Figure 23.

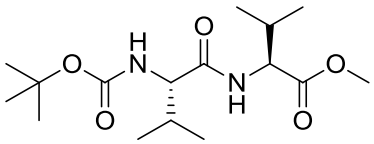

Figure 22. Schematic illustration of Boc-Val-Val-OMe, drawn using ChemBioDraw Ultra-12.0

The molecular conformations (Figure 23) are roughly similar, and in particular the RMS value for the best overlay between molecules A and C is only 0.3 Å. Molecule B has a different orientation for the side chain of the C-terminal valine residue, Val2, as defined by the N2-C11-C12-C13 and N2-C11-C12-C14 torsion angles as in Table 15, which together with larger main chain C5-N1-C6-C10 torsion angle contribute to the slightly higher RMS values of 0.79 Å and 0.69 Å for the best overlays with molecule A and molecule C, respectively. The average values for the torsion angles C5-N1-C6-C10 and N1-C6-C10-N2 (φ, ψ) of Val1 are -94º and 130º respectively, which are quite close to the ideal values for a parallel β-beta sheet [87]. β-pleated sheets can be found in silk however, they are common structural elements found in globular proteins [88]. The Val2 residue adopts polyproline II conformation, with the average dihedral angles being -59 º and 130 º respectively. Polyproline II is one of the dominating conformations in unfolded peptides and proteins [58]. The two Val1-Val2 residues are nearly *trans*-conformation for each of the three molecules in the asymmetric unit along the peptide bond (C10-N2) with torsion angles C6—C10—N2—C11 close to ± 180 º (Table 15).

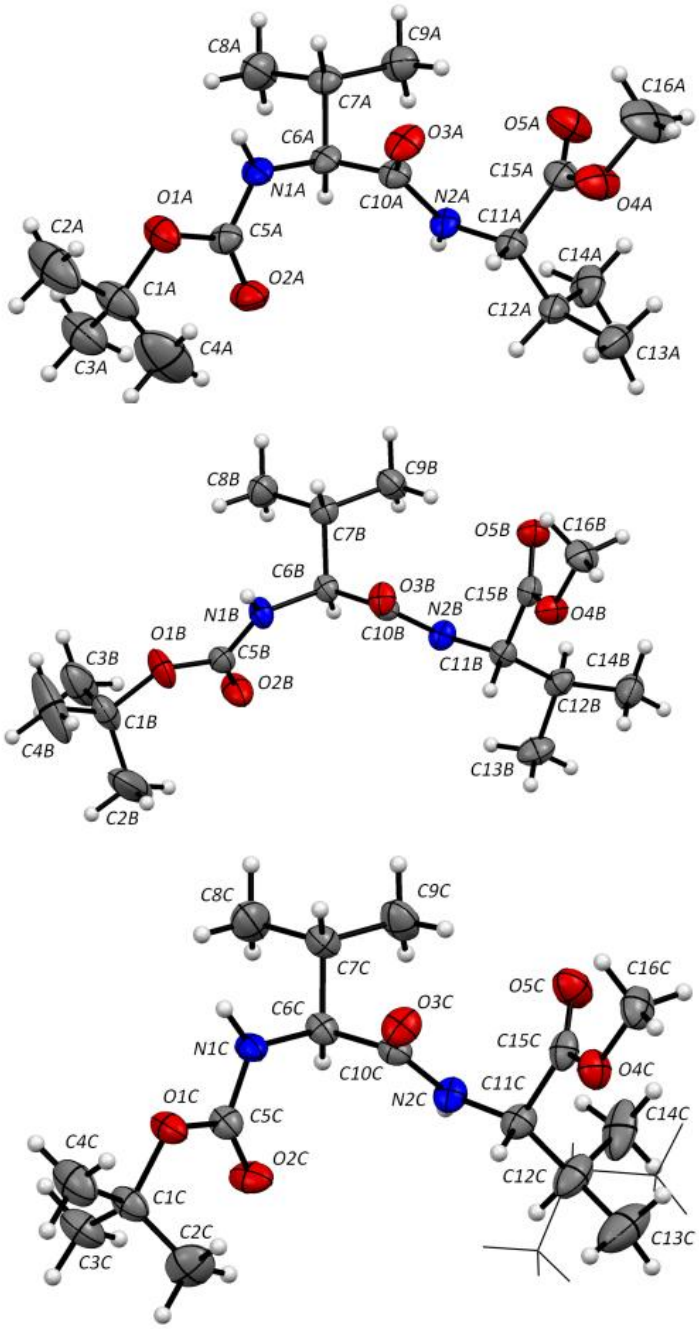

Figure 23. Molecular structure of **4** with atomic numbering scheme for each molecule in the asymmetric unit (A, B, C). Displacement ellipsoids are shown at the 50% probability level. H atoms are shown as spheres of arbitrary size. The minor orientation of the second Val of molecule C (occupancy 0.157 (7)) is shown in wireframe representation.

Table 15. Selected torsional angles for each of the three molecules (A, B, C) in the asymmetric unit **4**

Torsion angle	A	B	C
C1—O1—C5—N1	−178.4.(3)	174.5 (2)	177.0 (2)
O1—C5—N1—C6	−177.4 (2)	−174.1 (2)	168.0 (2)
C5—N1—C6—C10	−87.6 (3)	−117.6 (2)	−76.2 (3)
N1—C6—C10—N2	126.2 (2)	134.3 (2)	129.5 (2)
C6—C10—N2—C11	−176.4 (2)	177.5 (2)	−176.4 (2)
C10—N2—C11—C15	−62.6 (3)	−57.0 (3)	−58.3 (3)
N2—C11—C15—O4	149.1 (2)	141.6 (2)	145.5 (2)
C11—C15—O4—C16	178.2 (3)	176.6 (2)	−178.0 (2)
N1—C6—C7—C8	−64.3 (3)	−179.5 (2)	−60.2 (3)
N1—C6—C7—C9	172.9 (2)	−56.3 (3)	176.3 (2)
N2—C11—C12—C13	−168.9 (2)	−67.2 (3)	73.9 (5)
N2—C11—C12—C14	65.2 (3)	170.2 (2)	−157.8 (4)

In contrast to the dipeptide **4**, the dihedral angles of Val141 and Val142 in loop C of rAQP4 are (-63º, -26º) and (-26º, -39º) respectively, placing the Val141-Val142 segment in the 3_{10}- or mixed 3_{10}/α-helical region of the Ramachandran plot. However, the difference in backbone structure between **4** and the Val141-Val142 segment of rAQP4 loop C could be explained by the fact that **4** is too short to form the stabilizing intramolecular $i \rightarrow i+3$ H-bonds which are characteristic of 3_{10}-helices.

4.3.4.2. Crystal packing and Hydrogen-bonding

The molecular packing of **4** is shown in Figure 24. The molecules are hydrogen bonded in a parallel β-sheet like manner along the c axis into ribbons with a left-handed twist.

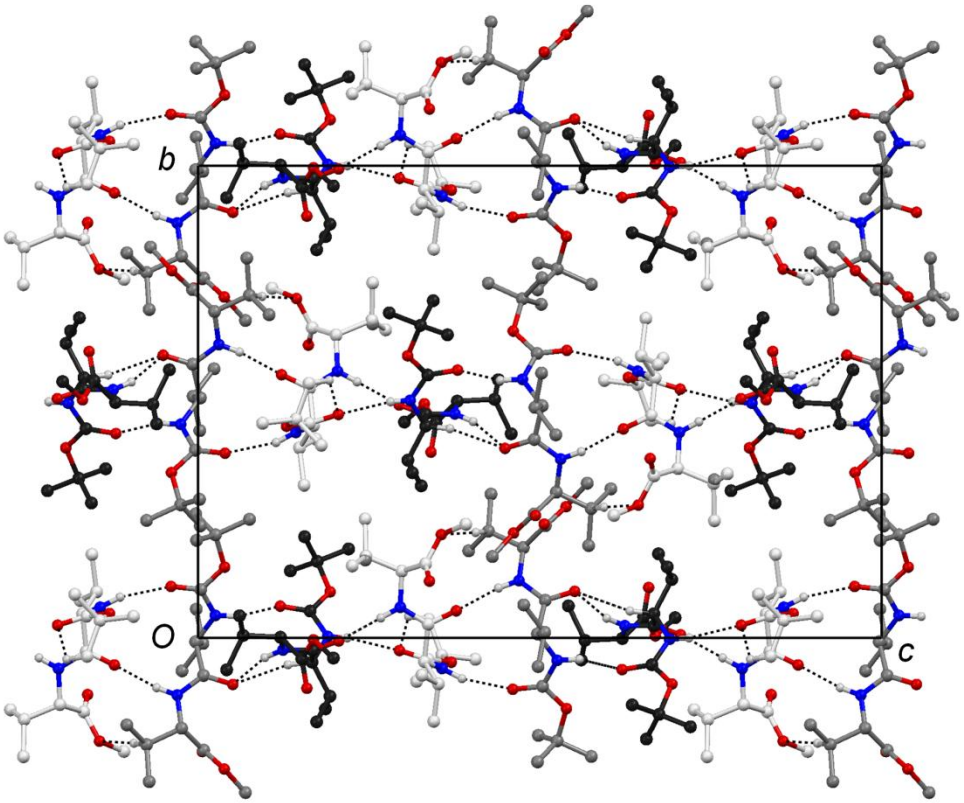

Figure 24. The molecular packing of (**4**) viewed along the *a* axis. Dashed lines indicate hydrogen bonds. H atoms not involved in hydrogen bonding have been omitted. The C-atoms of the molecule A, B, and C have been coloured in black, grey, and white, respectively.

A structural analogy in protein is provided by the β-sheet of a Rossmann fold [89], which is frequently found in nucleotide binding proteins, e.g., in the NADP(H) –binding proton pump transhydrogenase [90]. The Rossmann fold is a supersecondary structural motif

which consists of a β-sheet containing three or more parallel β-strands that are connected by α-helices, β-strands or unfolded loops. The topological structure of the Rossmann fold is β-α-β-α-β. The structure of NAD(P)-dependent dehydrogenases feature two Rossmann folds with left-handed twisting of the β-sheets in their cofactor binding domain [91].

Table 16. Hydrogen-bond geometry (Å, °) **4**

D—H···*A*	*D*—H	H···*A*	*D*···*A*	*D*—H···*A*
N1A—H1A···O2C^{i}	0.851 (17)	2.080 (18)	2.920 (3)	169 (3)
N2A—H2A···O3B	0.865 (17)	2.031(18)	2.874 (3)	165 (3)
C6A—H61A···O3B	1.00	2.45	3.295 (3)	142
N1B—H1B···O2A	0.854 17)	2.14 (2)	2.948 (3)	157 (3)
N2B—H2B···O3C	0.855 (17)	1.965 (18)	2.810 (3)	170 (3)
C6B—H61B···O3C	1.00	2.52	3.367 (3)	142
N1C—H1C···O2B	0.865 (17)	2.124 (19)	2.966 (3)	164 (3)
N2C—H2C···O3A^{ii}	0.859 (17)	1.924 (18)	2.782 (3)	177 (3)
C6C—H61C···O3A^{ii}	1.00	2.75	3.559 (3)	138

Symmetry codes: (i) −*x*+3/2, −*y*, *z*+1/2; (ii) −*x*+3/2, −*y*, *z*−1/2.

N—H···O and C—H···O types of intermolecular interactions (Table 16) stabilized the molecules of **4** in a parallel β-sheet like manner with a left-handed twist as in Figure 24 and 26c.

To get an overview of small molecule structures containing parallel β-sheets, the CSD was searched for peptide structures (not just dipeptides) containing the search fragment depicted in Figure 25, where the dashed C—N bonds have bond types "any", the central N—C bonds have been defined as acyclic, the number of H atoms on the central C^{α} atom can be 1 or 2 (V= variable) and the atom type of QA is either C or O. The two hydrogen bonds HB1 and HB2 were defined as intermolecular contacts with N—H···O hydrogen bonds may additionally be connected by C— H···O hydrogen bonds, but these were not specified in the search.

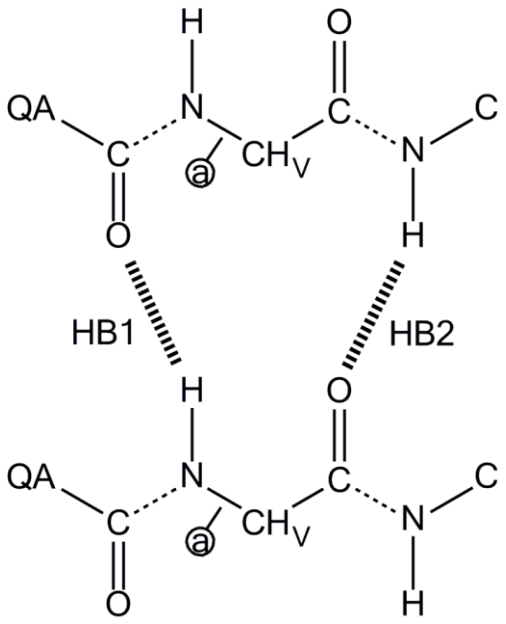

Figure 25. Schematic illustration of parallel-beta sheet for the search fragment

The query returned a total of 86 CSD entries, and subsequent manual scrutiny revealed infinite tapes in 67 structures of the N- and C- protected peptides, including 55 regular dipeptides, two structures where two dipeptides are linked by a disulphide bridge, nine tripeptides and one pentapeptide, as well as one psuedopeptide structure. Most tapes (49 observations out of 67 structures, Appendix A) are planar and straight, as seen in Figure 26a, but some structures have tapes that are twisted into helices, as seen for **4** in Figure 24.

This second group of 18 peptides may be subdivided into smaller groups depending on the number of molecules required to complete a full turn of the helix. The only example with eight peptides for a full turn is shown in Figure 26b. There is also just a single example of a structure with Z'= 7. The structure of **4** (Figure 26c) adds to a larger group of nine other structures with a repeating unit of six peptide molecules. Seven of these belongs to the hexagonal space group $P6_5$ with Z' = 1, one, with a rare central 2-methylvaly residue, belongs to $P6_1$, while the last structure, like **4**, is orthorhombic,

$P2_12_12_1$, with Z' = 3. The last group, with a repeating unit of four peptide molecules (Figure 26d) comprises seven structures, of which five are tetragonal with Z' = 1 and two are monoclinic with Z' = 2.

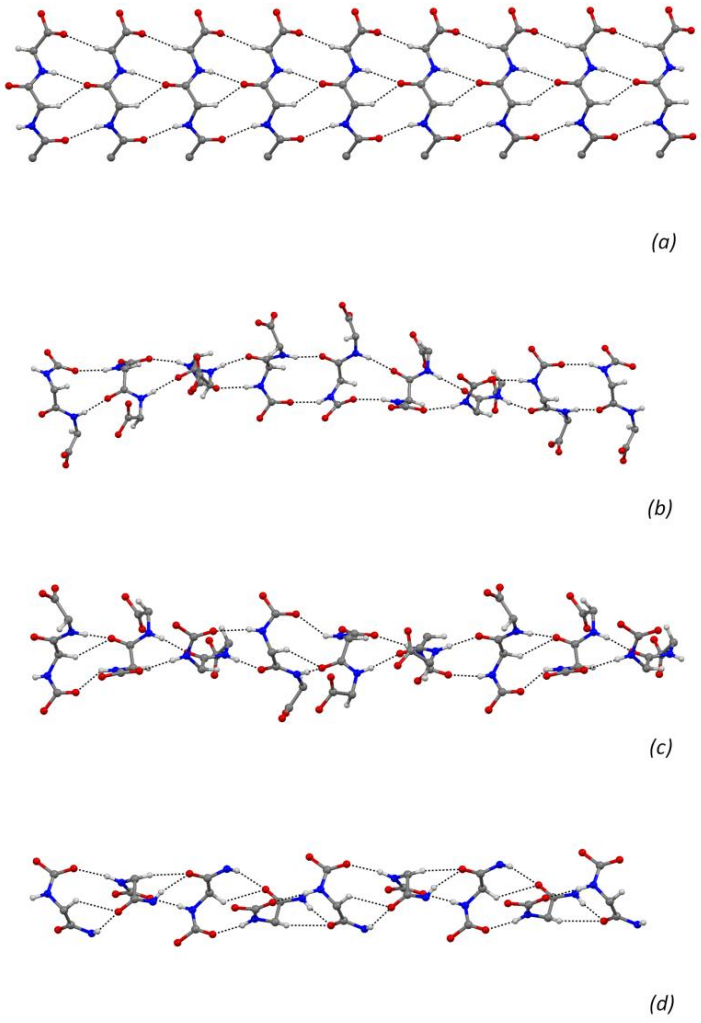

Figure 26. (a) A straight parallel β-sheet (CSD refcode CEPQOE [92]) with a single strand is observed in the structure. Side chains are not shown. H-bonds with N—H and C—H donors are shown as dashed lines. (b) a twisted parallel β-sheet with eight peptide molecules for one complete turn (CSD refcode PIYSAS [93]). (C) The twisted parallel β-sheet of (**4**) with six peptide molecules for one complete turn. (d) A twisted parallel β-sheet with four peptide molecules for one complete turn (CSD refcode FABLUP10 [94]).

It is interesting to find that when only regular amino acids in their L-configuration are involved (16 out of 18 structures), the twist is always left-handed. This is in accordance with the preferred sense of twist observed for β-sheets in proteins [95]. Another important observation is that the hydrogen bonds appear to get shorter when the twist increases. Thus, the average of the two hydrogen bonds lengths HB1 and HB2 scheme in Figure 25 is 2.131 Å, for the flat tapes (or 2.094 Å when three clear outlier structures are removed from the statistics), but 2.079 and 2.057 Å for twisted tapes with a repeating unit of six and four molecules, respectively. The hydrogen bond data for **4** are given in Table 16. After normalization of N—H bonds to 0.88 Å, the average length of six N—H···O hydrogen bonds in the structure of **4** is 2.023 Å, which is short for this type of pattern.

4.4. Crystal structure of Boc-allylSer-Aib-Val-OMe *N*-(*tert*-Butoxycarbonyl-*O*-allyl-L-seryl-α-aminoisobutyryl-L-valine methyl ester): a fully protected tripeptide with allylated serine residue

4.4.1. Introduction

One aim of [1] was to develop AQP4 mimics of loop C compounds. The presence of a serine residue in the 3_{10}-helix loop C (Pro138-Pro139-Ser140-Val141-Val142-Gly143-Gly144), Ser 140, which could be easily allylated, and a Gly residue in the *i* +3 position which did not seem to be involved in any key interactions, was an important aspect of their current project. Using the concept of ring-closing olefin metathesis (RCM) reaction and standard solution phase technique, the synthetic peptides (pentapeptides and heptapeptides), which are of potential significance for the development of AQP4 inhibitors, were synthesized. RCM is a useful method for altering the conformational and metabolic stability of α-helical peptides [76].

Th tripeptide **5**, Boc-allylSer-Aib-Val-OMe, is part of the acyclic pentapeptide Boc-allylSer-Aib-Val-allylSer-Gly-OMe, was crystallized and its X-ray structure determined.

4.4.2. Data collection and structure solution

X-ray data on a block-shaped single crystal was collected at 105(2) K on ApexII CCD diffractometer using APEX2 software [51]. Intensity measurements were performed using MoKα radiation (λ= 0.71073 Å). Determination of integral intensities, unit cell refinement and data reduction were performed with SAINT-Plus [52]. The crystallographic data for peptide **5** are reported in Table 17. Subsequent data absorption correction was done by SADABS [53] using multi-scan technique. The space group *C*2, with $Z = 4$ and $Z' = 1$ for the formula unit $C_{21}H_{37}N_3O_7$, was determined by XPREP. The structure was solved by direct methods using SHELXTL [54].

Table 17. Crystal data and structure refinement for Boc-allylSer-Aib-Val OMe (**5)**

Chemical name	Boc-allylSer-Aib-Val OMe
Chemical formula	$C_{21}H_{37}N_3O_7$
Formula weight (M_r)	443.54
Temperature	105 (2) K
Dx	1.200 Mgm^{-3}
Wave length (λ)	0.71073 Å
Crystal system	Monoclinic
Space group	*C*2
Unit cell dimensions	
a/Å	19.753 (4)
b/Å	5.9369 (12)
c/ Å	21.343 (5)
β	101.271(3)º
Volume (V)	2454.7(9) $Å^3$
Z	4
Absorption coefficient	0.09 mm^{-1}
Crystal size	0.60 x 0.43 x 0.24 mm
F(000)	2160
Absorption correction	Multi-scan
(Max. and min. absorption corrections)	0.9790-0.8390
Theta (θ) range for data collection	2.0-25.2°
Index ranges	h = -23→23, k = --7→6, and l = -25→25
$N_{measured}$	7153
N_{unique}	3852
$N_{observed}$ ($I > 2\sigma(I)$)	3184
Refinement method	Full-matrix least-squares on F^2
Data/restraints/parameter	3852/1/280
GooF(S) on F^2	1.04
R_{int}	0.030
$R(F^2>2\sigma(F^2))$	0.046
$wR(F^2)$	0.112
Peak differences in electron density map	$\Delta\rho_{max}$ = 0.28 e $Å^{-3}$, $\Delta\rho_{min}$ = −0.19 e $Å^{-3}$

4.4.3. Structure refinement

Full-matrix least-square refinement on F^2 against all reflections was carried out by SHELXTL [54]. All non-hydrogen heavy atoms were refined anisotropically. All H atoms were positioned with idealized geometry and fixed C/N-H distances for N-H, CH_3 and CH_2 at 0.88, 0.99 and 0.98 Å, respectively. Free rotation was permitted for methyl group. U_{iso} (H) values were set to $1.2U_{eq}$ of the carrier atom (N-H) and $1.5U_{eq}$ for methyl groups. Complete crystal data for **5** are given in Appendix F.

4.4.4. Discussion

4.4.4.1. Structure conformation of (Boc-allylSer-Aib-Val OMe)

Peptide **5 (**schematic drawn as in Figure 27) crystallized in the monoclinic *C*2 and its molecular structure is shown in Figure 28.

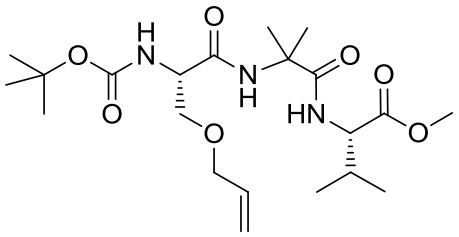

Figure 27. Schematic drawing of Boc-allylSer-Aib-Val-OMe, drawn using ChemBioDraw Ultra-12.0

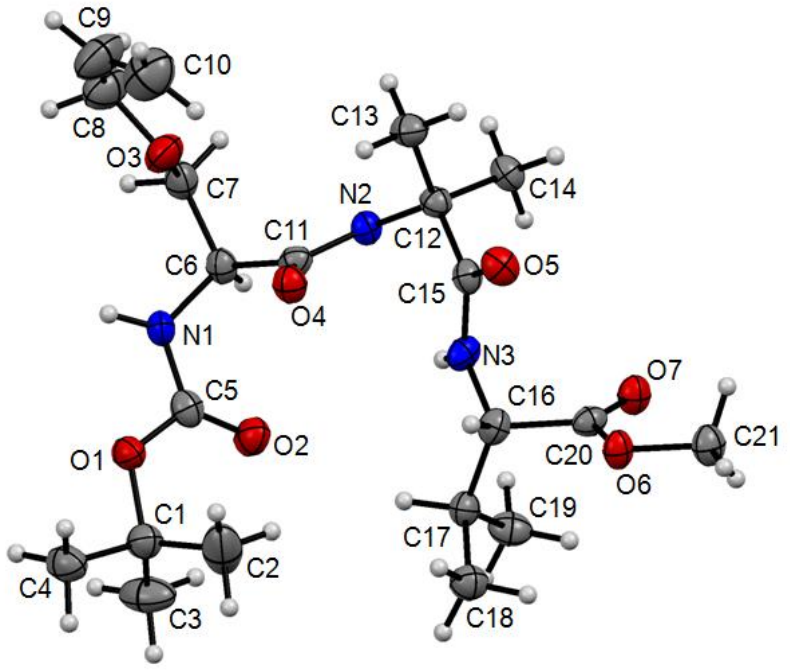

Figure 28. Molecular structure of Boc-allylSer-Aib-Val-OMe (*ORTEP* diagram) with atomic numbering indicated. Displacement ellipsoids are shown at the 50% probability level for non H-atoms. H atoms are shown as spheres of arbitrary size.

The tripeptide **5** contains a centrally placed conformationally constrained non-coded amino acid (Aib) residue. The main dihedral angles for **5** are shown in Table 18. Most of the dihedral angles of **5** (except ψ_1 and $\psi 3$) fall within the helical region of the Ramachandran plot. The molecular structure of **5** (Figure 28) adopts a bend or turn-like structure even though it fails to form any intramolecular hydrogen bonds as in the prototype β-turn conformation. The Ser residue in **5** adopts (φ_1, ψ_1) values of −59.1 (3) º and 159.3 (2) º respectively, which are a characteristic of polyproline II conformation. The second residue Aib adopts 3_{10}-/α- helix with (φ_2, ψ_2) being 58.7 (3) º and 33.2 (3) º, respectively. The third residue Val has (φ_3, ψ_3) of −70.3 (3) º and 143.5 (2) º, respectively which place it in the polyproline II conformation.

Table 18. The main backbone torsion angles (°) for **5**

O1—C5—N1—C6 (ω1)	166.4 (2)
C5—N1—C6—C11 (φ1)	−59.1 (3)
N1—C6—C11—N2 (ψ1)	159.3 (2)
C6—C11—N2—C12 (ω 2)	166.3 (2)
C11—N2—C12—C15 φ2)	58.7 (3)
N2—C12—C15—N3 (ψ2)	33.2 (3)
C12—C15—N3—C16 (ω3)	179.0 (2)
C15—N3—C16—C20 (φ3)	−70.3 (3)
N3—C16—C20—O6 (ψ3)	143.5 (2)

4.4.4.2. Hydrogen bonding and crystal packing

In peptide **5** there are two intermolecular N—H···O types of hydrogen bonds (Table 19), i.e. N1—H1···O7 (x-1/2, y-1/2, z) and N2—H2···O5 (x, y-1, z) with hydrogen-bond length 2.23 Å and 2.05 Å respectively, which are responsible for connecting individual peptide molecules to form and stabilize in parallel β-sheet like arrangement (Figure 29).

Table 19. Hydrogen-bond geometry (Å, °) of **5**

D—H···*A*	*D*—H	H···*A*	*D*···*A*	*D*—H···*A*
N1—H1···O7^{i}	0.88	2.23	3.058 (3)	157
N2—H2···O5^{ii}	0.88	2.05	2.901 (3)	164

Symmetry codes: (i) *x*−1/2, *y*−1/2, *z*; (ii) *x*, *y*−1, *z*.

The intermolecular hydrogen bonds (expansion of molecules) generate a β-sheet like arrangement when the molecules are expanded along the crystallographic *b* axis as in Figure 29.

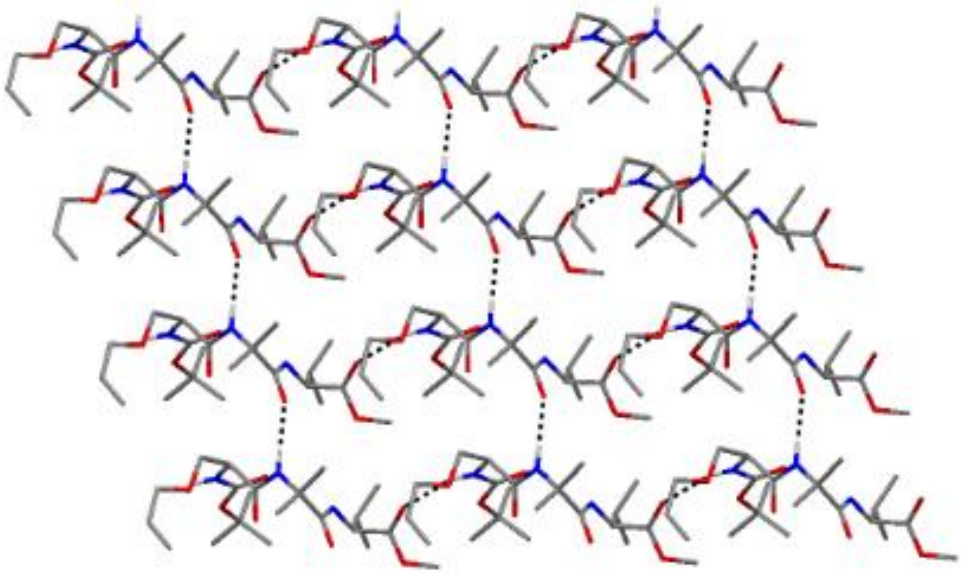

Figure 29. Intermolecular hydrogen bonds (dashed lines) forming when the molecules of **5** are expanded along the b axis, they form continuous β-sheet like structure. Hydrogen atoms except those forming H-bonds are not shown for clarity.

.

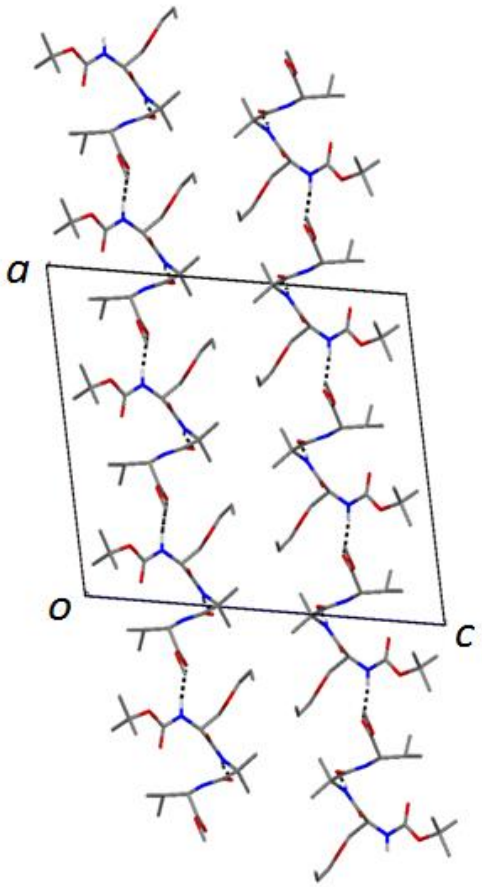

Figure 30. The molecular packing of **5** viewed along the *b* axis. Dashed lines indicate hydrogen bonds. H atoms not involved in hydrogen bonding have been omitted.

The molecular packing of **5** is shown in Figure 30. When the packing of molecules are viewed along the *b* axis, molecules are stacking one above the other forming layers.

CHAPTER FIVE

5. CONCLUSIONS

Using ethyl acetate and water as crystallizing solvents, compounds **1** and **4** were crystallized in the orthorhombic $P2_12_12_1$ space groups while **2, 3**, and **5** were in the monoclinic $P2_1/c$, $P2_1/n$, and $C2$ space groups, respectively. All peptides except **4** (which contain Z'= 3) were crystallized with a single molecule in the asymmetric unit (Z' = 1).

The main chain functional groups **2**,**3**, and **5** were observed to form β-sheet like arrangements when the molecules are linked to each other by two N—H···O type of hydrogen bonds. When the molecules in **4** are hydrogen bonded by two N—H···O and single C—H···O type of hydrogen bonds, twisted parallel β-sheet with six peptides molecules for one complete turn are formed. However, the molecules in **1** were able to form helix like shape when they are connected by single O—H···O type of hydrogen bonds.

The main backbone dihedral angles (φ, ψ) of proline residues in **1** adopt incipient poly-L-proline type I (PPI) and type II (PPII) backbone conformations. The pyrrolidine rings for Pro1 and Pro2 in Boc-Pro-Pro-OH of **1** belong to conformation B, i.e. down puckered conformation (C^{γ}-*endo*).

The average vales for the torsion angles (φ, ψ) Val1 in **4** are close to the ideal values for the parallel β-sheet while the Val2 residues adopt values for polyproline II conformations.

Boc-Aib-Aib-OMe contains two polymorphs (**2** and **3)** and its structural study shows that the Aib residues adopt (φ, ψ)-values characteristics of helical conformations. The dihedral angles adopt values for 3_{10}-/α-helical conformations in the Ramachandran plot. The centrally placed Aib residue in **5** also adopts values for the helical conformation. The

backbone conformation of peptide **3** is the same as peptide **2**. However, the molecular packing of **2** and **3** are different, showing to exist in two polymorphic forms.

The molecular structure of peptide **5** adopts a bend (or turn)-like structure even though it fails to form any intramolecular hydrogen bonded as in the prototype β-turn conformation.

Recommendation

The observed dihedral angles for most of the peptides are promising and fall in the helical regions of the Ramachandran plot even though they are too short to form the stabilizing intramolecular $i \rightarrow i+3$ H-bonds which are characteristics of 3_{10}-helix. However, if the longer peptides (Table 2) are able to form crystals (using suitable crystallizing solvents) or modified by inserting more Aib residues to most of the shorter peptides, as Aib-based short model peptides are able to form 3_{10}-helical structures [69], they could more mimic the 3_{10}- helix loop C of AQP4, and use as potent drugs for AQP4 inhibitors.

6. REFERENCES

[1] Jacobsen, O.; Klaveness, J.; Petter, O. O.; Reza, A.-M. M.; Rongved, P., *Org. Biomol. Chem.*, (2009) **7**, 1599.

[2] de Groot, B. L.; Grubmüeller, H., *Curr. Opin. Struct. Biol.*, (2005) **15**, 176.

[3] Agre, P.; King, L. S.; Yasui, M.; Guggino, W. B.; Ottersen, O. P.; Fujiyoshi, Y.; Engel, A.; Nielsen, S., *J. Physiol. (Cambridge, U. K.)*, (2002) **542**, 3.

[4] Knepper, M. A.; Nielsen, S., *J. Am. Soc. Nephrol.*, (2004) **15**, 1093.

[5] King, L. S.; Agre, P., *Annu. Rev. Physiol.*, (1996) **58**, 619.

[6] De Jongh, R.; Nuydens, R.; Smets, A.; Vissers, K.; Meert, T., *Curr. Top. Pharmacol.*, (2008) **12**, 37.

[7] Tajkhorshid, E.; Nollert, P.; Jensen, M. O.; Miercke, L. J. W.; O'Connell, J.; Stroud, R. M.; Schulten, K., *Science (Washington, DC, U. S.)*, (2002) **296**, 525.

[8] Murata, K.; Mitsuoka, K.; Hirai, T.; Walz, T.; Agre, P.; Heymann, J. B.; Engel, A.; Fujiyoshi, Y., *Nature (London)*, (2000) **407**, 599.

[9] Savage, D. F.; O'Connell, J. D.; Miercke, L. J. W.; Finer-Moore, J.; Stroud, R. M., *Proc. Natl. Acad. Sci. U. S. A.*, (2010) **107**, 17164.

[10] Wu, B.; Beitz, E., *Cell. Mol. Life Sci.*, (2007) **64**, 2413.

[11] Engel, A.; Fujiyoshi, Y.; Gonen, T.; Walz, T., *Curr Opin Struct Biol*, (2008) **18**, 229.

[12] Borgnia, M.; Nielsen, S.; Engel, A.; Agre, P., *Annu. Rev. Biochem.*, (1999) **68**, 425.

[13] Agre, P.; Kozono, D., *FEBS Lett.*, (2003) **555**, 72.

[14] Frigeri, A.; Nicchia, G. P.; Svelto, M., *Curr. Pharm. Des.*, (2007) **13**, 2421.

[15] Karabasil, M. R.; Hasegawa, T.; Azlina, A.; Purwanti, N.; Yao, C.; Akamatsu, T.; Tomioka, S.; Hosoi, K., *Biol. Cell*, (2011) **103**, 69.

[16] Verkman, A. S., *J. Cell Sci.*, (2005) **118**, 3225.

[17] Tsukaguchi, H.; Shayakul, C.; Berger, U. V.; Mackenzie, B.; Devidas, S.; Guggino, W. B.; Van, H. A. N.; Hediger, M. A., *J. Biol. Chem.*, (1998) **273**, 24737.

[18] Badaut, J.; Lasbennes, F.; Magistretti, P. J.; Regli, L., *J. Cereb. Blood Flow Metab.*, (2002) **22**, 367.

[19] Tani, K.; Mitsuma, T.; Hiroaki, Y.; Kamegawa, A.; Nishikawa, K.; Tanimura, Y.; Fujiyoshi, Y., *J. Mol. Biol.*, (2009) **389**, 694.

[20] Fu, D.; Libson, A.; Miercke, L. J. W.; Weitzman, C.; Nollert, P.; Krucinski, J.; Stroud, R. M., *Science (Washington, D. C.)*, (2000) **290**, 481.

[21] Andrews, S.; Reichow, S. L.; Gonen, T., *IUBMB Life*, (2008) **60**, 430.

[22] Verkman, A. S.; Yang, B.; Song, Y.; Manley, G. T.; Ma, T., *Exp. Physiol.*, (2000) **85**, 233S.

[23] Ho, J. D.; Yeh, R.; Sandstrom, A.; Chorny, I.; Harries, W. E. C.; Robbins, R. A.; Miercke, L. J. W.; Stroud, R. M., *Proc. Natl. Acad. Sci. U. S. A.*, (2009) **106**, 7437.

[24] Agre, P.; Bonhivers, M.; Borgnia, M. J., *J. Biol. Chem.*, (1998) **273**, 14659.

[25] Hiroaki, Y.; Tani, K.; Kamegawa, A.; Gyobu, N.; Nishikawa, K.; Suzuki, H.; Walz, T.; Sasaki, S.; Mitsuoka, K.; Kimura, K.; Mizoguchi, A.; Fujiyoshi, Y., *J. Mol. Biol.*, (2006) **355**, 628.

[26] Heymann, J. B.; Agre, P.; Engel, A., *J Struct Biol*, (1998) **121**, 191.

[27] Yukutake, Y.; Yasui, M., *Neuroscience (Amsterdam, Neth.)*, (2010) **168**, 885.
[28] Amiry-Moghaddam, M.; Ottersen, O. P., *Nat. Rev. Neurosci.*, (2003) **4**, 991.
[29] Zador, Z.; Bloch, O.; Yao, X.; Manley, G. T., *Prog. Brain Res.*, (2007) **161**, 185.
[30] Manley, G. T.; Fujimura, M.; Ma, T.; Noshita, N.; Filiz, F.; Bollen, A. W.; Chan, P.; Verkman, A. S., *Nat. Med. (N. Y.)*, (2000) **6**, 159.
[31] Lu, M.; Lee, M. D.; Smith, B. L.; Jung, J. S.; Agre, P.; Verdijk, M. A. J.; Merkx, G.; Rijss, J. P. L.; Deen, P. M. T., *Proc. Natl. Acad. Sci. U. S. A.*, (1996) **93**, 10908.
[32] Jung, J. S.; Bhat, R. V.; Preston, G. M.; Guggino, W. B.; Baraban, J. M.; Agre, P., *Proc Natl Acad Sci U S A*, (1994) **91**, 13052.
[33] Michaux, C.; Wouters, J., *Chim. Nouv.*, (2006) **24**, 109.
[34] Deschamps, J. R., *AAPS J*, (2005) **7**, E813.
[35] Blow, D., *Outline of Crystallography for Biologists*, Oxford University Press: (2002); p 236 pp.
[36] Lee, M. R., *Meteoritics*, (1994) **29**, 898.
[37] Glusker, J. P.; Lewis, M.; Rossi, M., *Crystal Structure Analysis for Chemists and Biologists*, VCH: (1994); p 854 pp.
[38] Luger, P., *Modern X-Ray Analysis on Single Crystals*, de Gruyter: (1980); p 312 pp.
[39] Muchmore, S. W., *Acta Crystallogr., Sect. D: Biol. Crystallogr.*, (1999) **D55**, 1669.
[40] Amemiya, Y., *J. Synchrotron Radiat.*, (1995) **2**, 13.
[41] Görbitz, C. H., *J. Phys. Chem. B*, (2011) **115**, 2447.
[42] Goeta, A. E.; Thompson, L. K.; Sheppard, C. L.; Tandon, S. S.; Lehmann, C. W.; Cosier, J.; Webster, C.; Howard, J. A. K., *Acta Crystallogr., Sect. C: Cryst. Struct. Commun.*, (1999) **C55**, 1243.
[43] Mighell, A. D.; Himes, V. L.; Rodgers, J. R., *Acta Crystallogr., Sect. A: Found. Crystallogr.*, (1983) **A39**, 737.
[44] Kantharaju; Raghothama, S.; Aravinda, S.; Shamala, N.; Balaram, P., *Biopolymers*, (2010) **94**, 360.
[45] Rai, R.; Aravinda, S.; Kanagarajadurai, K.; Raghothama, S.; Shamala, N.; Balaram, P., *J. Am. Chem. Soc.*, (2006) **128**, 7916.
[46] Venkatraman, J.; Shankaramma, S. C.; Balaram, P., *Chemical Reviews*, (2001) **101**, 3131.
[47] Chatterjee, B.; Saha, I.; Raghothama, S.; Aravinda, S.; Rai, R.; Shamala, N.; Balaram, P., *Chem.-Eur. J.*, (2008) **14**, 6192.
[48] Cheng, S.-F.; Chang, D.-K., *Chem. Phys. Lett.*, (1999) **301**, 453.
[49] Chou, P. Y.; Fasman, G. D., *Journal of Molecular Biology*, (1977) **115**, 135.
[50] Thomas, L. M.; Ramasubbu, N.; Bhandary, K. K., *Int. J. Pept. Protein Res.*, (1994) **44**, 207.
[51] Apex2, Bruker AXS, Inc., In Madison, WI, (2007).
[52] SAINT-Plus, Bruker AXS, Inc., In Madison, WI, (2007).
[53] SADABS, Bruker AXS, Inc., In Madison, WI, (2007).
[54] Sheldrick, G. M., *Acta Crystallogr., Sect. A: Found. Crystallogr.*, (2008) **A64**, 112.
[55] Kamwaya, M. E.; Oster, O.; Bradaczek, H., *Acta Crystallogr., Sect. B*, (1981) **B37**, 1564.

[56] DeTar, D. F.; Luthra, N. P., *J. Am. Chem. Soc.*, (1977) **99**, 1232.
[57] Rucker, A. L.; Creamer, T. P., *Protein Sci.*, (2002) **11**, 980.
[58] Shi, Z.; Chen, K.; Liu, Z.; Kallenbach, N. R., *Chem. Rev. (Washington, DC, U. S.)*, (2006) **106**, 1877.
[59] Moyna, G.; Williams, H. J.; Nachman, R. J.; Scott, A. I., *J. Pept. Res.*, (1999) **53**, 294.
[60] Adzhubei, A. A.; Sternberg, M. J., *J Mol Biol*, (1993) **229**, 472.
[61] Moradi, M.; Babin, V.; Roland, C.; Darden, T. A.; Sagui, C., *Proc. Natl. Acad. Sci. U. S. A.*, (2009) **106**, 20746.
[62] Pujals, S.; Giralt, E., *Adv. Drug Delivery Rev.*, (2008) **60**, 473.
[63] Flores-Ortega, A.; Casanovas, J.; Zanuy, D.; Nussinov, R.; Aleman, C., *J. Phys. Chem. B*, (2007) **111**, 5475.
[64] *Biochemistry*, (1970) **9**, 3471.
[65] Milner-White, E. J.; Bell, L. H.; Maccallum, P. H., *J. Mol. Biol.*, (1992) **228**, 725.
[66] Kang, Y. K.; Choi, H. Y., *Biophys. Chem.*, (2004) **111**, 135.
[67] Asuda, T.; Kakudo, M., *Bull. Chem. Soc. Jap.*, (1974) **47**, 1129.
[68] Aravinda, S.; Shamala, N.; Roy, R. S.; Balaram, P., *Proc. - Indian Acad. Sci., Chem. Sci.*, (2003) **115**, 373.
[69] Karle, I. L.; Balaram, P., *Biochemistry*, (1990) **29**, 6747.
[70] Bosch, R.; Voges, K. P.; Jung, G.; Winter, W., *Acta Crystallogr., Sect. C: Cryst. Struct. Commun.*, (1983) **C39**, 481.
[71] Nagaraj, R.; Balaram, P., *Acc. Chem. Res.*, (1981) **14**, 356.
[72] Santagada, V.; Fiorino, F.; Perissutti, E.; Severino, B.; De, F. V.; Vivenzio, B.; Caliendo, G., *Tetrahedron Lett.*, (2001) **42**, 5171.
[73] Aravinda, S.; Shamala, N.; Balaram, P., *Chem. Biodiversity*, (2008) **5**, 1238.
[74] Burgess, A. W.; Leach, S. J., *Biopolymers*, (1973) **12**, 2599.
[75] Marshall, G. R.; Hodgkin, E. E.; Langs, D. A.; Smith, G. D.; Zabrocki, J.; Leplawy, M. T., *Proceedings of the National Academy of Sciences of the United States of America*, (1990) **87**, 487.
[76] Boal, A. K.; Guryanov, I.; Moretto, A.; Crisma, M.; Lanni, E. L.; Toniolo, C.; Grubbs, R. H.; O'Leary, D. J., *Journal of the American Chemical Society*, (2007) **129**, 6986.
[77] Toniolo, C.; Crisma, M.; Formaggio, F.; Peggion, C.; Broxterman, Q.; Kaptein, B., *Journal of Inclusion Phenomena and Macrocyclic Chemistry*, (2005) **51**, 121.
[78] Toniolo, C.; Benedetti, E., *Trends in Biochemical Sciences*, (1991) **16**, 350.
[79] Moretto, V.; Crisma, M.; Bonora, G. M.; Toniolo, C.; Balaram, H.; Balaram, P., *Macromolecules*, (1989) **22**, 2939.
[80] Toniolo, C.; Crisma, M.; Formaggio, F.; Peggion, C., *Biopolymers*, (2001) **60**, 396.
[81] Banerjee, R.; Basu, G.; Chene, P.; Roy, S., *Journal of Peptide Research*, (2002) **60**, 88.
[82] Nissa, M. N.; Banumathi, S.; Velmurugan, D.; Ramasubbu, N., *Cryst. Res. Technol.*, (2001) **36**, 499.
[83] Balakrishnan, R.; Parthasarathy, R.; Ramasubbu, N., *J. Pept. Res.*, (1997) **49**, 371.
[84] Van, R. P.; Smith, G. D.; Balasubramanian, T. M.; Marshall, G. R., *Acta Crystallogr., Sect. C: Cryst. Struct. Commun.*, (1983) **C39**, 894.

[85] Thirumuruhan, R. A.; Sony, S. M.; Shanmugam, G.; Ponnuswamy, M. N.; Jayakumar, R., *Mol. Cryst. Liq. Cryst.*, (2004) **414**, 39.
[86] Sukumar, N.; Ponnuswamy, M. N.; Jayakumar, R., *Bull. Chem. Soc. Jpn.*, (1993) **66**, 2101.
[87] Loughlin, W. A.; Tyndall, J. D. A.; Glenn, M. P.; Hill, T. A.; Fairlie, D. P., *Chem Rev*, (2010) **110**, PR32.
[88] Richardson, J. S., *Adv. Protein Chem.*, (1981) **34**, 167.
[89] Rao, S. T.; Rossmann, M. G., *J. Mol. Biol.*, (1973) **76**, 241.
[90] Jeeves, M.; Smith, K. J.; Quirk, P. G.; Cotton, N. P. J.; Jackson, J. B., *Biochim. Biophys. Acta, Bioenerg.*, (2000) **1459**, 248.
[91] Kutzenko, A. S.; Lamzin, V. S.; Popov, V. O., *FEBS Lett.*, (1998) **423**, 105.
[92] Gerhardt, W. W.; Weck, M., *J. Org. Chem.*, (2006) **71**, 6333.
[93] Oku, H.; Yamada, K.; Katakai, R., *Biopolymers*, (2008) **89**, 270.
[94] Varughese, K. A.; Angus, R. H.; Carey, P. R.; Lee, H.; Storer, A. C., *Can. J. Chem.*, (1986) **64**, 1668.
[95] Chothia, C., *J. Mol. Biol.*, (1973) **75**, 295.

7. APPENDICES

Appendix A. Structures with parallel beta sheets in the Cambridge Structural Database

Refcode, tape	Space group	*Z*'	peptide length	Note
Straight				
ADOFAB	$P2_1$	1	2	
BAJPIM	$P2_12_12_1$	1	2	Statistical outlier
BCMEGL	$P2_1$	1	2	
BIPHOX10	$P2_12_12_1$	1	3	
BIVLIB	$P2_1$	1	2	
BUSCGL	$P2_1$	1	2	
CEPQIY	$P2_12_12_1$	1	2	
CEPQOE	$P2_12_12_1$	1	2	
CEPQUK	$P2_1$	1	2	
COGKAL	$P2_1$	1	5	
COPBIS10	$C2$	1	2	
DALREO	$C2$	1	3	
DALRIS	$C2$	1	3	
DENNUF	$P2_1$	1	2	
FAFSUA	$P2_1$	1	2	
FAVLOD	$P2_12_12_1$	1	3	
FUJDET	$P2_1$	1	2	
GEMDEH	$P2_12_12_1$	1	2	
GPAGLM	$P2_12_12_1$	1	2	
HICNEM	$C2$	1	2	
HURDAZ	$P4_32_12$	1	2	
JECYUL	$P2_1$	1	3	

JOVWEW	$P2_1$	1	2	
KAXMIG	$C2$	0.5	2	Disulfide bridge
KEHXEB	$P2_1$	1	3	
KEHXIF	$P2_1$	1	3	
KEHXOL	$P1$	1	3	
KEHXUR	$P2$	2	3	
LECDIH	P21/n	1	3	
LECDON	P-42_1c	0.5	2	pseudopeptide[a]
LPTILL	P21	1	2	Statistical outlier
OCAWEV	$P2_12_12_1$	1	2	
PATFAR	$P2_12_12_1$	1	2	
PATWEN	$P2_12_12_1$	1	2	
QOWREZ	$P2_12_12_1$	1	2	
RUYLUS	$C2/c$	2	2	achiral (Gly residues)
SAMGAP	$P2_1$	1	2	
SEMQUX	$P2_1$	1	2	
SEMRAE	$P2_1$	1	2	
SEMREI	$P2_12_12_1$	1	2	
TAPYAL	P-1	1	2	racemate
UCIHEU	$C2$	0.5	2	
VAXROC	$P1$	1	2	
VISKUE	$P2_1$	1	2	
WISGAG	$P2_1$	1	2	
XIMQIU	$P2_12_12_1$	1	2	
YAQBOH	$P2_1$	1	2	
ZIGCIB	$P2_12_12_1$	1	2	
ZZZIFQ01	$P2_1$	2	2	Statistical outlier
Repeating unit 8				
PIYSAS	$P4_32_12$	2	2	

Repeating unit 7				
GUFWKEX	$P2_1$	7	2	
Repeating unit 6				
BIMGAF10	$P6_5$	1	2	
GUFWEJ	$P2_12_12_1$	3	2	
IDOFOX	$P6_5$	1	2	
JAYWUC	$P6_5$	1	2	
JEQKAS	$P6_5$	1	2	
REVJAE	$P6_5$	1	2	
WEVCUW	$P6_5$	1	2	amide H atoms misplaced[b]
XAHWOT	$P6_5$	1	2	
ZADJAP	$P6_1$	1	2	unusual 2-methylvaline central residue
Repeating unit 4				
BLEGLE	$P2_1/n$	2	2	racemate
ERIMAT	$P2_1$	2	2	disulfide bridge
FABLUP10	$I4_1$	1	2	
IGOLOF	$P4_3$	1	2	
LERHUM	$P4_3$	4	2	only one tape with parallel chains
MAKLEQ	$P4_3$	1	2	
XEZDUC	$I4_1/n$	1	2	achiral

[a] racemic N,N'-bis(t-butoxycarbonyl-valyl)ethane-1,2-diamine

[b] Amide sp^2 H atoms are in tetrahedral positions, structure not included in statistics

Appendix B. Complete data for Boc-Pro-Pro-OH (1).

Fractional atomic coordinates and isotropic or equivalent isotropic displacement parameters (Å^2) of (1)

	x	*y*	*z*	U_{iso}*/U_{eq}
O1	0.4126 (3)	0.37664 (11)	0.35221 (8)	0.0473 (4)
O2	0.1214 (3)	0.80374 (11)	0.43276 (10)	0.0517 (5)
H1	0.079 (4)	0.846 (2)	0.4660 (17)	0.062*
N3	0.1831 (3)	0.55967 (11)	0.44036 (10)	0.0359 (4)
O4	0.5073 (3)	0.55391 (10)	0.48471 (11)	0.0499 (5)
O5	0.1133 (3)	0.71020 (11)	0.53675 (10)	0.0531 (5)
N6	0.4958 (3)	0.36586 (12)	0.47843 (11)	0.0433 (5)
C7	0.3128 (4)	0.41750 (14)	0.49839 (14)	0.0426 (6)
H7	0.1886	0.3899	0.4734	0.051*
C8	0.5584 (4)	0.34913 (15)	0.40339 (14)	0.0438 (6)
C9	−0.0168 (4)	0.52052 (17)	0.41833 (18)	0.0519 (7)
H9A	−0.1028	0.5102	0.4659	0.062*
H9B	0.0003	0.4620	0.3897	0.062*
C10	0.1408 (3)	0.72385 (13)	0.46784 (14)	0.0368 (5)
C11	0.3398 (4)	0.51651 (13)	0.47308 (13)	0.0356 (5)
C12	0.4235 (4)	0.35455 (18)	0.26723 (13)	0.0469 (6)
C13	0.2060 (4)	0.65186 (14)	0.40807 (13)	0.0389 (5)
H13	0.3512	0.6624	0.3918	0.047*
C14	0.0702 (5)	0.64824 (18)	0.33552 (15)	0.0557 (7)
H14A	0.1399	0.6176	0.2906	0.067*
H14B	0.0276	0.7102	0.3188	0.067*
C15	0.3045 (6)	0.40983 (19)	0.58922 (16)	0.0680 (9)
H15A	0.2450	0.4656	0.6130	0.082*
H15B	0.2220	0.3564	0.6057	0.082*
C16	0.5901 (5)	0.4099 (2)	0.22806 (19)	0.0759 (10)
H16A	0.7235	0.3907	0.2487	0.114*
H16B	0.5691	0.4748	0.2395	0.114*
H16C	0.5860	0.4000	0.1705	0.114*
O17	0.7206 (3)	0.31518 (12)	0.38598 (10)	0.0589 (5)
C18	0.5225 (7)	0.3986 (2)	0.61330 (17)	0.0809 (11)
H18A	0.5321	0.3648	0.6641	0.097*
H18B	0.5889	0.4588	0.6199	0.097*
C19	0.6244 (5)	0.34504 (18)	0.54666 (14)	0.0610 (8)
H19A	0.7667	0.3658	0.5380	0.073*
H19B	0.6248	0.2788	0.5582	0.073*
C20	0.4509 (6)	0.25299 (18)	0.25511 (16)	0.0666 (9)
H20A	0.3503	0.2198	0.2872	0.100*
H20B	0.5892	0.2352	0.2714	0.100*
H20C	0.4311	0.2381	0.1989	0.100*
C21	0.2153 (5)	0.3833 (2)	0.23825 (16)	0.0620 (8)
H21A	0.1098	0.3490	0.2669	0.093*
H21B	0.2040	0.3708	0.1812	0.093*
H21C	0.1966	0.4487	0.2477	0.093*

C22	−0.1107 (5)	0.59292 (19)	0.36442 (17)	0.0601 (7)
H22A	−0.1837	0.5643	0.3193	0.072*
H22B	−0.2078	0.6318	0.3943	0.072*

Atomic displacement parameters (Å^2) of (1)

	U^{11}	U^{22}	U^{33}	U^{12}	U^{13}	U^{23}
O1	0.0521 (10)	0.0522 (10)	0.0375 (9)	0.0128 (8)	−0.0044 (8)	−0.0112 (7)
O2	0.0679 (13)	0.0306 (8)	0.0566 (10)	0.0093 (8)	0.0106 (9)	0.0059 (7)
N3	0.0364 (11)	0.0284 (9)	0.0431 (10)	−0.0018 (8)	0.0036 (9)	−0.0001 (8)
O4	0.0437 (10)	0.0326 (8)	0.0735 (12)	−0.0013 (8)	−0.0082 (9)	−0.0015 (8)
O5	0.0761 (13)	0.0439 (9)	0.0394 (9)	0.0101 (9)	0.0059 (9)	0.0002 (7)
N6	0.0592 (13)	0.0329 (9)	0.0377 (10)	0.0096 (9)	−0.0024 (10)	−0.0029 (8)
C7	0.0563 (16)	0.0301 (10)	0.0413 (12)	0.0022 (10)	0.0090 (12)	−0.0014 (9)
C8	0.0521 (16)	0.0333 (11)	0.0461 (13)	0.0057 (11)	−0.0028 (13)	−0.0058 (10)
C9	0.0436 (15)	0.0422 (12)	0.0699 (18)	−0.0044 (12)	−0.0041 (13)	−0.0025 (12)
C10	0.0360 (12)	0.0330 (11)	0.0413 (13)	0.0016 (9)	−0.0008 (11)	0.0025 (9)
C11	0.0419 (14)	0.0291 (10)	0.0357 (11)	−0.0001 (10)	0.0040 (10)	−0.0025 (9)
C12	0.0549 (16)	0.0517 (13)	0.0341 (12)	0.0004 (13)	0.0006 (12)	−0.0092 (10)
C13	0.0436 (14)	0.0334 (11)	0.0398 (11)	0.0025 (10)	0.0061 (11)	0.0045 (9)
C14	0.076 (2)	0.0494 (14)	0.0416 (13)	0.0059 (15)	−0.0068 (14)	−0.0028 (11)
C15	0.111 (3)	0.0481 (15)	0.0448 (14)	0.0118 (17)	0.0226 (18)	0.0056 (12)
C16	0.075 (2)	0.095 (2)	0.0583 (17)	−0.020 (2)	0.0074 (17)	0.0036 (16)
O17	0.0558 (12)	0.0640 (11)	0.0570 (11)	0.0206 (10)	−0.0037 (9)	−0.0117 (9)
C18	0.120 (3)	0.084 (2)	0.0386 (15)	0.014 (2)	−0.0099 (18)	0.0013 (14)
C19	0.088 (2)	0.0507 (14)	0.0439 (14)	0.0167 (16)	−0.0116 (15)	0.0036 (11)
C20	0.089 (3)	0.0563 (16)	0.0550 (16)	0.0078 (17)	−0.0022 (17)	−0.0187 (13)
C21	0.0683 (19)	0.0702 (18)	0.0477 (15)	0.0051 (16)	−0.0120 (14)	−0.0117 (13)
C22	0.0544 (18)	0.0607 (16)	0.0651 (17)	0.0037 (14)	−0.0172 (14)	−0.0058 (13)

Geometric parameters (Å °) of (1)

O1—C8	1.347 (3)	C13—H13	1.0000
O1—C12	1.469 (3)	C14—C22	1.514 (4)
O2—C10	1.317 (3)	C14—H14A	0.9900
O2—H1	0.88 (3)	C14—H14B	0.9900
N3—C11	1.324 (3)	C15—C18	1.491 (5)
N3—C13	1.464 (3)	C15—H15A	0.9900
N3—C9	1.475 (3)	C15—H15B	0.9900
O4—C11	1.240 (3)	C16—H16A	0.9800
O5—C10	1.191 (3)	C16—H16B	0.9800
N6—C8	1.350 (3)	C16—H16C	0.9800
N6—C7	1.455 (3)	C18—C19	1.522 (4)
N6—C19	1.456 (3)	C18—H18A	0.9900

C7—C11	1.522 (3)	C18—H18B	0.9900
C7—C15	1.535 (4)	C19—H19A	0.9900
C7—H7	1.0000	C19—H19B	0.9900
C8—O17	1.208 (3)	C20—H20A	0.9800
C9—C22	1.525 (4)	C20—H20B	0.9800
C9—H9A	0.9900	C20—H20C	0.9800
C9—H9B	0.9900	C21—H21A	0.9800
C10—C13	1.519 (3)	C21—H21B	0.9800
C12—C21	1.506 (4)	C21—H21C	0.9800
C12—C16	1.510 (4)	C22—H22A	0.9900
C12—C20	1.513 (4)	C22—H22B	0.9900
C13—C14	1.511 (3)		

C8—O1—C12	121.6 (2)	C22—C14—H14B	111.2
C10—O2—H1	111.5 (18)	H14A—C14—H14B	109.2
C11—N3—C13	121.07 (19)	C18—C15—C7	104.2 (3)
C11—N3—C9	127.21 (17)	C18—C15—H15A	110.9
C13—N3—C9	110.86 (18)	C7—C15—H15A	110.9
C8—N6—C7	124.0 (2)	C18—C15—H15B	110.9
C8—N6—C19	121.7 (2)	C7—C15—H15B	110.9
C7—N6—C19	113.66 (19)	H15A—C15—H15B	108.9
N6—C7—C11	109.6 (2)	C12—C16—H16A	109.5
N6—C7—C15	102.8 (2)	C12—C16—H16B	109.5
C11—C7—C15	110.67 (19)	H16A—C16—H16B	109.5
N6—C7—H7	111.2	C12—C16—H16C	109.5
C11—C7—H7	111.2	H16A—C16—H16C	109.5
C15—C7—H7	111.2	H16B—C16—H16C	109.5
O17—C8—O1	126.1 (2)	C15—C18—C19	106.0 (3)
O17—C8—N6	124.6 (2)	C15—C18—H18A	110.5
O1—C8—N6	109.3 (2)	C19—C18—H18A	110.5
N3—C9—C22	103.6 (2)	C15—C18—H18B	110.5
N3—C9—H9A	111.0	C19—C18—H18B	110.5
C22—C9—H9A	111.0	H18A—C18—H18B	108.7
N3—C9—H9B	111.0	N6—C19—C18	102.8 (2)
C22—C9—H9B	111.0	N6—C19—H19A	111.2
H9A—C9—H9B	109.0	C18—C19—H19A	111.2
O5—C10—O2	124.9 (2)	N6—C19—H19B	111.2
O5—C10—C13	124.84 (19)	C18—C19—H19B	111.2
O2—C10—C13	110.29 (19)	H19A—C19—H19B	109.1
O4—C11—N3	122.54 (19)	C12—C20—H20A	109.5
O4—C11—C7	118.7 (2)	C12—C20—H20B	109.5
N3—C11—C7	118.8 (2)	H20A—C20—H20B	109.5
O1—C12—C21	102.2 (2)	C12—C20—H20C	109.5
O1—C12—C16	110.0 (2)	H20A—C20—H20C	109.5
C21—C12—C16	111.2 (2)	H20B—C20—H20C	109.5
O1—C12—C20	110.7 (2)	C12—C21—H21A	109.5
C21—C12—C20	109.8 (2)	C12—C21—H21B	109.5
C16—C12—C20	112.5 (3)	H21A—C21—H21B	109.5
N3—C13—C14	102.00 (18)	C12—C21—H21C	109.5

N3—C13—C10	111.46 (18)	H21A—C21—H21C	109.5
C14—C13—C10	113.3 (2)	H21B—C21—H21C	109.5
N3—C13—H13	110.0	C14—C22—C9	104.4 (2)
C14—C13—H13	110.0	C14—C22—H22A	110.9
C10—C13—H13	110.0	C9—C22—H22A	110.9
C13—C14—C22	102.6 (2)	C14—C22—H22B	110.9
C13—C14—H14A	111.2	C9—C22—H22B	110.9
C22—C14—H14A	111.2	H22A—C22—H22B	108.9
C13—C14—H14B	111.2		

C8—N6—C7—C11	−66.5 (3)	C8—O1—C12—C16
C19—N6—C7—C11	104.7 (2)	C8—O1—C12—C20
C8—N6—C7—C15	175.8 (2)	C11—N3—C13—C14
C19—N6—C7—C15	−13.0 (3)	C9—N3—C13—C14
C12—O1—C8—O17	9.8 (4)	C11—N3—C13—C10
C12—O1—C8—N6	−170.5 (2)	C9—N3—C13—C10
C7—N6—C8—O17	171.5 (2)	O5—C10—C13—N3
C19—N6—C8—O17	1.0 (4)	O2—C10—C13—N3
C7—N6—C8—O1	−8.1 (3)	O5—C10—C13—C14
C19—N6—C8—O1	−178.6 (2)	O2—C10—C13—C14
C11—N3—C9—C22	−165.3 (2)	N3—C13—C14—C22
C13—N3—C9—C22	4.1 (3)	C10—C13—C14—C22
C13—N3—C11—O4	6.7 (3)	N6—C7—C15—C18
C9—N3—C11—O4	175.1 (2)	C11—C7—C15—C18
C13—N3—C11—C7	−174.12 (18)	C7—C15—C18—C19
C9—N3—C11—C7	−5.7 (3)	C8—N6—C19—C18
N6—C7—C11—O4	−41.4 (3)	C7—N6—C19—C18
C15—C7—C11—O4	71.3 (3)	C15—C18—C19—N6
N6—C7—C11—N3	139.4 (2)	C13—C14—C22—C9
C15—C7—C11—N3	−107.9 (3)	N3—C9—C22—C14
C8—O1—C12—C21	170.0 (2)	

Appendix C. Complete data for Boc-Aib-Aib-OMe (2)

Fractional atomic coordinates and isotropic or equivalent isotropic displacement parameters (Å^2) of (2)

	x	*y*	*z*	U_{iso}*/U_{eq}
O1	0.2670 (2)	0.16039 (5)	0.41605 (19)	0.0516 (5)
O2	−0.1019 (3)	0.14870 (5)	0.4262 (2)	0.0604 (5)
O3	−0.4191 (3)	0.07826 (5)	0.23466 (19)	0.0541 (5)
O4	−0.7053 (3)	0.10380 (7)	−0.0755 (2)	0.0813 (6)
O5	−0.4248 (3)	0.06321 (6)	−0.1201 (2)	0.0744 (6)
N1	0.1338 (3)	0.10220 (6)	0.3412 (2)	0.0479 (6)
H1	0.269 (4)	0.0967 (7)	0.321 (3)	0.057*
N2	−0.1702 (3)	0.10786 (7)	0.0864 (2)	0.0491 (6)
H2	−0.031 (4)	0.1123 (7)	0.077 (3)	0.059*
C1	0.2528 (4)	0.20241 (7)	0.4585 (3)	0.0473 (6)
C2	0.1580 (5)	0.20702 (9)	0.6177 (3)	0.0774 (9)
H21	0.0030	0.1988	0.6131	0.116*
H22	0.1682	0.2348	0.6501	0.116*
H23	0.2413	0.1905	0.6931	0.116*
C3	0.4918 (4)	0.21536 (9)	0.4615 (3)	0.0638 (8)
H31	0.5750	0.2008	0.5431	0.096*
H32	0.5009	0.2438	0.4832	0.096*
H33	0.5541	0.2099	0.3601	0.096*
C4	0.1210 (5)	0.22449 (9)	0.3335 (4)	0.0768 (9)
H41	−0.0332	0.2159	0.3334	0.115*
H42	0.1815	0.2189	0.2316	0.115*
H43	0.1292	0.2530	0.3544	0.115*
C5	0.0831 (4)	0.13822 (8)	0.3984 (3)	0.0461 (6)
C6	−0.0347 (4)	0.07164 (7)	0.3184 (3)	0.0456 (6)
C7	−0.1250 (4)	0.05818 (9)	0.4738 (3)	0.0659 (8)
H71	−0.0033	0.0487	0.5423	0.099*
H72	−0.2317	0.0367	0.4551	0.099*
H73	−0.1977	0.0805	0.5234	0.099*
C8	0.0736 (4)	0.03673 (7)	0.2366 (3)	0.0652 (8)
H81	0.1967	0.0266	0.3025	0.098*
H82	0.1286	0.0456	0.1366	0.098*
H83	−0.0353	0.0156	0.2183	0.098*
C9	−0.2258 (4)	0.08686 (7)	0.2122 (3)	0.0428 (6)
C10	−0.3334 (4)	0.12650 (8)	−0.0190 (3)	0.0508 (7)
C11	−0.4388 (5)	0.16184 (8)	0.0611 (3)	0.0698 (8)
H111	−0.3237	0.1808	0.0944	0.105*
H112	−0.5164	0.1526	0.1522	0.105*
H113	−0.5437	0.1748	−0.0121	0.105*
C12	−0.2157 (5)	0.13999 (10)	−0.1642 (3)	0.0769 (9)
H121	−0.0990	0.1589	−0.1340	0.115*
H122	−0.3220	0.1528	−0.2370	0.115*
H123	−0.1506	0.1170	−0.2147	0.115*
C13	−0.5112 (4)	0.09716 (9)	−0.0703 (3)	0.0572 (7)

C14	−0.5805 (5)	0.03432 (11)	−0.1854 (5)	0.1104 (13)
H141	−0.5005	0.0107	−0.2180	0.166*
H142	−0.6606	0.0459	−0.2759	0.166*
H143	−0.6855	0.0270	−0.1065	0.166*

Atomic displacement parameters (Å^2) of (2)

	U^{11}	U^{22}	U^{33}	U^{12}	U^{13}	U^{23}
O1	0.0362 (9)	0.0482(11)	0.0705(11)	−0.0033 (8)	0.0018 (8)	−0.0078 (9)
O2	0.0363(10)	0.0641(12)	0.0813(13)	0.0005 (9)	0.0082 (9)	−0.0130(10)
O3	0.0340(10)	0.0661(12)	0.0627(11)	−0.0054 (8)	0.0069 (8)	0.0040 (9)
O4	0.0417 (12)	0.1106 (18)	0.0909 (15)	0.0075 (11)	−0.0046 (10)	−0.0054 (12)
O5	0.0531 (12)	0.0871 (15)	0.0827 (14)	−0.0007 (11)	−0.0002 (10)	−0.0313 (12)
N1	0.0323 (11)	0.0477 (14)	0.0639 (14)	−0.0018 (11)	0.0034 (10)	−0.0066 (11)
N2	0.0351 (11)	0.0659 (15)	0.0465 (12)	−0.0058 (11)	0.0034 (10)	0.0059 (11)
C1	0.0458 (15)	0.0449 (17)	0.0512 (15)	−0.0020 (12)	0.0031 (12)	−0.0063 (12)
C2	0.074 (2)	0.093 (2)	0.066 (2)	−0.0162 (18)	0.0191 (16)	−0.0227 (17)
C3	0.0527 (17)	0.065 (2)	0.0741 (19)	−0.0114 (14)	0.0033 (14)	−0.0091 (15)
C4	0.074 (2)	0.068 (2)	0.087 (2)	0.0009 (16)	−0.0112 (18)	0.0103 (17)
C5	0.0361 (15)	0.0530 (18)	0.0490 (15)	−0.0013 (13)	−0.0024 (12)	0.0001 (13)
C6	0.0360 (13)	0.0472 (16)	0.0538 (15)	−0.0017 (12)	0.0022 (12)	0.0003 (12)
C7	0.0590(17)	0.078 (2)	0.0602(18)	−0.0106(15)	−0.0016(14)	0.0176 (15)
C8	0.0521(16)	0.0479(17)	0.096 (2)	−0.0012(14)	0.0033 (15)	−0.0073(15)
C9	0.0364(14)	0.0429(15)	0.0492(15)	−0.0031(11)	0.0045 (12)	−0.0047(12)
C10	0.0427(15)	0.0653(19)	0.0448(15)	0.0023 (13)	0.0052 (12)	0.0053 (13)
C11	0.080 (2)	0.062 (2)	0.0686(19)	0.0120 (16)	0.0074 (16)	0.0050 (15)
C12	0.0661(19)	0.114 (3)	0.0514(17)	−0.0012(18)	0.0109 (15)	0.0208 (17)
C13	0.0397(16)	0.081 (2)	0.0504(16)	0.0049 (15)	−0.0010(12)	−0.0028(14)
C14	0.087 (2)	0.119 (3)	0.124 (3)	−0.022 (2)	−0.010 (2)	−0.060 (3)

Geometric parameters (Å °) of (2)

O1—C5	1.347 (3)	C4—H42	0.9800
O1—C1	1.467 (3)	C4—H43	0.9800
O2—C5	1.210 (3)	C6—C7	1.530 (3)
O3—C9	1.231 (3)	C6—C8	1.533 (3)
O4—C13	1.198 (3)	C6—C9	1.535 (3)
O5—C13	1.337 (3)	C7—H71	0.9800
O5—C14	1.455 (3)	C7—H72	0.9800
N1—C5	1.351 (3)	C7—H73	0.9800
N1—C6	1.460 (3)	C8—H81	0.9800
N1—H1	0.87 (2)	C8—H82	0.9800
N2—C9	1.346 (3)	C8—H83	0.9800

N2—C10	1.457 (3)	C10—C13	1.517 (4)
N2—H2	0.86 (2)	C10—C11	1.529 (4)
C1—C4	1.509 (3)	C10—C12	1.530 (3)
C1—C2	1.512 (3)	C11—H111	0.9800
C1—C3	1.514 (3)	C11—H112	0.9800
C2—H21	0.9800	C11—H113	0.9800
C2—H22	0.9800	C12—H121	0.9800
C2—H23	0.9800	C12—H122	0.9800
C3—H31	0.9800	C12—H123	0.9800
C3—H32	0.9800	C14—H141	0.9800
C3—H33	0.9800	C14—H142	0.9800
C4—H41	0.9800	C14—H143	0.9800

O1—C5	1.347 (3)	C4—H42	0.9800
O1—C1	1.467 (3)	C4—H43	0.9800
O2—C5	1.210 (3)	C6—C7	1.530 (3)
O3—C9	1.231 (3)	C6—C8	1.533 (3)
O4—C13	1.198 (3)	C6—C9	1.535 (3)
O5—C13	1.337 (3)	C7—H71	0.9800
O5—C14	1.455 (3)	C7—H72	0.9800
N1—C5	1.351 (3)	C7—H73	0.9800
N1—C6	1.460 (3)	C8—H81	0.9800
N1—H1	0.87 (2)	C8—H82	0.9800
N2—C9	1.346 (3)	C8—H83	0.9800
N2—C10	1.457 (3)	C10—C13	1.517 (4)
N2—H2	0.86 (2)	C10—C11	1.529 (4)
C1—C4	1.509 (3)	C10—C12	1.530 (3)
C1—C2	1.512 (3)	C11—H111	0.9800
C1—C3	1.514 (3)	C11—H112	0.9800
C2—H21	0.9800	C11—H113	0.9800
C2—H22	0.9800	C12—H121	0.9800
C2—H23	0.9800	C12—H122	0.9800
C3—H31	0.9800	C12—H123	0.9800
C3—H32	0.9800	C14—H141	0.9800
C3—H33	0.9800	C14—H142	0.9800
C4—H41	0.9800	C14—H143	0.9800

C5—O1—C1	120.53 (18)	C6—C7—H72	109.5
C13—O5—C14	116.1 (2)	H71—C7—H72	109.5
C5—N1—C6	121.1 (2)	C6—C7—H73	109.5
C5—N1—H1	119.7 (16)	H71—C7—H73	109.5
C6—N1—H1	119.2 (16)	H72—C7—H73	109.5
C9—N2—C10	122.7 (2)	C6—C8—H81	109.5
C9—N2—H2	116.1 (17)	C6—C8—H82	109.5
C10—N2—H2	120.8 (17)	H81—C8—H82	109.5
O1—C1—C4	109.6 (2)	C6—C8—H83	109.5
O1—C1—C2	110.6 (2)	H81—C8—H83	109.5
C4—C1—C2	112.4 (2)	H82—C8—H83	109.5

O1—C1—C3	102.57 (19)	O3—C9—N2	121.3 (2)
C4—C1—C3	110.5 (2)	O3—C9—C6	122.0 (2)
C2—C1—C3	110.7 (2)	N2—C9—C6	116.5 (2)
C1—C2—H21	109.5	N2—C10—C13	110.9 (2)
C1—C2—H22	109.5	N2—C10—C11	110.1 (2)
H21—C2—H22	109.5	C13—C10—C11	109.5 (2)
C1—C2—H23	109.5	N2—C10—C12	107.8 (2)
H21—C2—H23	109.5	C13—C10—C12	107.9 (2)
H22—C2—H23	109.5	C11—C10—C12	110.6 (2)
C1—C3—H31	109.5	C10—C11—H111	109.5
C1—C3—H32	109.5	C10—C11—H112	109.5
H31—C3—H32	109.5	H111—C11—H112	109.5
C1—C3—H33	109.5	C10—C11—H113	109.5
H31—C3—H33	109.5	H111—C11—H113	109.5
H32—C3—H33	109.5	H112—C11—H113	109.5
C1—C4—H41	109.5	C10—C12—H121	109.5
C1—C4—H42	109.5	C10—C12—H122	109.5
H41—C4—H42	109.5	H121—C12—H122	109.5
C1—C4—H43	109.5	C10—C12—H123	109.5
H41—C4—H43	109.5	H121—C12—H123	109.5
H42—C4—H43	109.5	H122—C12—H123	109.5
O2—C5—O1	125.9 (2)	O4—C13—O5	123.1 (3)
O2—C5—N1	124.1 (2)	O4—C13—C10	125.1 (3)
O1—C5—N1	109.9 (2)	O5—C13—C10	111.6 (2)
N1—C6—C7	111.5 (2)	O5—C14—H141	109.5
N1—C6—C8	107.08 (19)	O5—C14—H142	109.5
C7—C6—C8	110.3 (2)	H141—C14—H142	109.5
N1—C6—C9	110.58 (19)	O5—C14—H143	109.5
C7—C6—C9	109.19 (19)	H141—C14—H143	109.5
C8—C6—C9	108.2 (2)	H142—C14—H143	109.5
C6—C7—H71	109.5		

C1—O1—C5—N1	172.53 (19)	N1—C6—C9—O3	−142.1 (2)
O1—C5—N1—C6	176.89 (19)	C7—C6—C9—O3	−19.0 (3)
C5—N1—C6—C9	56.4 (3)	C8—C6—C9—O3	101.0 (3)
N1—C6—C9—N2	42.5 (3)	C7—C6—C9—N2	165.5 (2)
C6—C9—N2—C10	−175.7 (2)	C8—C6—C9—N2	−74.5 (3)
C9—N2—C10—C13	−50.4 (3)	C9—N2—C10—C11	71.0 (3)
N2—C10—C13—O5	−49.1 (3)	C9—N2—C10—C12	−168.3 (2)
C5—O1—C1—C4	−61.3 (3)	C14—O5—C13—O4	1.2 (4)
C5—O1—C1—C2	63.2 (3)	C14—O5—C13—C10	−174.6 (2)
C5—O1—C1—C3	−178.7 (2)	N2—C10—C13—O4	135.2 (3)
C5—N1—C6—C7	−65.3 (3)	C11—C10—C13—O4	13.4 (4)
C5—N1—C6—C8	174.1 (2)	C12—C10—C13—O4	−107.0 (3)
C1—O1—C5—O2	−6.2 (4)	C11—C10—C13—O5	−170.8 (2)
C6—N1—C5—O2	−4.4 (4)	C12—C10—C13—O5	68.8 (3)
C10—N2—C9—O3	8.9 (4)		

Appendix D. Complete data for Boc-Aib-Aib-OMe (3)

Fractional atomic coordinates and isotropic or equivalent isotropic displacement parameters (Å^2)

	x	*y*	*z*	U_{iso}*/U_{eq}
O1	0.09762 (19)	0.68882 (8)	0.36081 (7)	0.0269 (3)
O2	0.45547 (19)	0.71312 (8)	0.34527 (7)	0.0276 (3)
O3	0.72114 (18)	0.64846 (7)	0.19357 (7)	0.0219 (3)
O4	0.9903 (2)	0.47659 (8)	0.19011 (8)	0.0311 (3)
O5	0.6676 (2)	0.47866 (8)	0.11345 (7)	0.0284 (3)
N1	0.1922 (2)	0.68458 (9)	0.24668 (8)	0.0206 (3)
H1	0.0561	0.6713	0.2331	0.025*
N2	0.4834 (2)	0.55242 (9)	0.22883 (8)	0.0223 (3)
H2	0.3489	0.5416	0.2346	0.027*
C1	0.1352 (3)	0.69731 (13)	0.44300 (10)	0.0270 (4)
C2	0.2080 (4)	0.78694 (14)	0.46457 (11)	0.0379 (5)
H21	0.3515	0.7970	0.4503	0.057*
H22	0.2145	0.7940	0.5179	0.057*
H23	0.1046	0.8269	0.4392	0.057*
C3	−0.0916 (3)	0.67974 (15)	0.46397 (11)	0.0395 (5)
H31	−0.1351	0.6225	0.4496	0.059*
H32	−0.1956	0.7193	0.4383	0.059*
H33	−0.0881	0.6862	0.5173	0.059*
C4	0.2973 (3)	0.63063 (15)	0.47723 (12)	0.0408 (5)
H41	0.2436	0.5748	0.4620	0.061*
H42	0.3134	0.6348	0.5310	0.061*
H43	0.4378	0.6399	0.4604	0.061*
C5	0.2657 (3)	0.69746 (11)	0.32005 (10)	0.0219 (4)
C6	0.3401 (3)	0.69277 (10)	0.19011 (9)	0.0190 (4)
C7	0.4276 (3)	0.78325 (11)	0.18544 (10)	0.0235 (4)
H71	0.5090	0.7990	0.2330	0.035*
H72	0.3062	0.8219	0.1732	0.035*
H73	0.5228	0.7860	0.1472	0.035*
C8	0.2100 (3)	0.66722 (11)	0.11474 (10)	0.0246 (4)
H81	0.1549	0.6101	0.1181	0.037*
H82	0.3048	0.6697	0.0764	0.037*
H83	0.0885	0.7058	0.1024	0.037*
C9	0.5346 (3)	0.63031 (10)	0.20610 (9)	0.0185 (4)
C10	0.6492 (3)	0.48487 (11)	0.24417 (10)	0.0233 (4)
C11	0.7925 (3)	0.50089 (12)	0.31874 (11)	0.0306 (4)
H111	0.7015	0.5026	0.3582	0.046*
H112	0.8679	0.5544	0.3167	0.046*
H113	0.8988	0.4557	0.3285	0.046*
C12	0.5256 (3)	0.40034 (11)	0.24513 (12)	0.0317 (5)
H121	0.4354	0.4011	0.2848	0.047*
H122	0.6298	0.3543	0.2533	0.047*
H123	0.4338	0.3924	0.1979	0.047*
C13	0.7917 (3)	0.48166 (11)	0.18112 (11)	0.0237 (4)

C14	0.7893 (4)	0.47283 (15)	0.05059 (12)	0.0419 (5)
H141	0.6881	0.4710	0.0048	0.063*
H142	0.8773	0.4218	0.0550	0.063*
H143	0.8837	0.5217	0.0501	0.063*

Atomic displacement parameters (Å^2)

	U^{11}	U^{22}	U^{33}	U^{12}	U^{13}	U^{23}
O1	0.0178 (6)	0.0429 (8)	0.0205 (7)	−0.0050 (5)	0.0046 (5)	−0.0078 (6)
O2	0.0173 (6)	0.0403 (8)	0.0247 (7)	−0.0045 (5)	0.0014 (5)	−0.0007 (6)
O3	0.0158 (6)	0.0235 (6)	0.0272 (7)	−0.0027 (5)	0.0053 (5)	0.0011 (5)
O4	0.0193 (7)	0.0255 (7)	0.0498 (9)	0.0016 (5)	0.0093 (6)	−0.0006 (6)
O5	0.0247 (7)	0.0314 (7)	0.0302 (7)	−0.0022 (5)	0.0076 (5)	−0.0097 (6)
N1	0.0156 (7)	0.0263 (8)	0.0202 (8)	−0.0022 (6)	0.0038 (6)	−0.0039 (6)
N2	0.0161 (7)	0.0186 (7)	0.0340 (9)	−0.0004 (6)	0.0095 (6)	0.0005 (6)
C1	0.0224 (9)	0.0421 (11)	0.0168 (9)	−0.0027 (8)	0.0034 (7)	−0.0026 (8)
C2	0.0404 (12)	0.0459 (13)	0.0273 (11)	−0.0037 (10)	0.0042 (9)	−0.0079 (9)
C3	0.0257 (10)	0.0700 (16)	0.0244 (11)	−0.0075 (10)	0.0096 (8)	−0.0104 (10)
C4	0.0353 (12)	0.0523 (14)	0.0361 (12)	0.0063 (10)	0.0098 (9)	0.0117 (10)
C5	0.0199 (9)	0.0227 (9)	0.0236 (9)	−0.0006 (7)	0.0053 (7)	−0.0034 (7)
C6	0.0168 (8)	0.0194 (9)	0.0215 (9)	−0.0013 (7)	0.0049 (6)	−0.0012 (7)
C7	0.0246 (9)	0.0201 (9)	0.0269 (10)	0.0000 (7)	0.0068 (7)	−0.0001 (7)
C8	0.0219 (9)	0.0286 (10)	0.0236 (10)	−0.0030 (7)	0.0037 (7)	−0.0023 (8)
C9	0.0185 (8)	0.0193 (9)	0.0180 (9)	−0.0018 (7)	0.0032 (6)	−0.0033 (7)
C10	0.0197 (8)	0.0174 (8)	0.0335 (10)	0.0009 (7)	0.0065 (7)	0.0024 (7)
C11	0.0325 (11)	0.0266 (10)	0.0327 (11)	−0.0001 (8)	0.0048 (8)	0.0060 (8)
C12	0.0269 (10)	0.0200 (10)	0.0490 (13)	−0.0022 (8)	0.0088 (9)	0.0057 (8)
C13	0.0214 (9)	0.0153 (8)	0.0350 (11)	−0.0004 (7)	0.0056 (7)	−0.0021 (7)
C14	0.0386 (12)	0.0537 (14)	0.0362 (12)	−0.0051 (10)	0.0155 (9)	−0.0181 (10)

Geometric parameters (Å, °)

O1—C5	1.348 (2)	C4—H42	0.9600
O1—C1	1.469 (2)	C4—H43	0.9600
O2—C5	1.212 (2)	C6—C7	1.521 (2)
O3—C9	1.226 (2)	C6—C8	1.527 (2)
O4—C13	1.205 (2)	C6—C9	1.536 (2)
O5—C13	1.343 (2)	C7—H71	0.9600
O5—C14	1.438 (2)	C7—H72	0.9600
N1—C5	1.348 (2)	C7—H73	0.9600
N1—C6	1.456 (2)	C8—H81	0.9600
N1—H1	0.8600	C8—H82	0.9600
N2—C9	1.337 (2)	C8—H83	0.9600
N2—C10	1.466 (2)	C10—C11	1.518 (3)
N2—H2	0.8600	C10—C13	1.522 (3)
C1—C2	1.507 (3)	C10—C12	1.526 (2)

C1—C4	1.511 (3)	C11—H111	0.9600
C1—C3	1.512 (3)	C11—H112	0.9600
C2—H21	0.9600	C11—H113	0.9600
C2—H22	0.9600	C12—H121	0.9600
C2—H23	0.9600	C12—H122	0.9600
C3—H31	0.9600	C12—H123	0.9600
C3—H32	0.9600	C14—H141	0.9600
C3—H33	0.9600	C14—H142	0.9600
C4—H41	0.9600	C14—H143	0.9600

C5—O1—C1	120.73 (13)	C6—C7—H72	109.5
C13—O5—C14	115.09 (15)	H71—C7—H72	109.5
C5—N1—C6	120.90 (14)	C6—C7—H73	109.5
C5—N1—H1	119.6	H71—C7—H73	109.5
C6—N1—H1	119.6	H72—C7—H73	109.5
C9—N2—C10	122.07 (14)	C6—C8—H81	109.5
C9—N2—H2	119.0	C6—C8—H82	109.5
C10—N2—H2	119.0	H81—C8—H82	109.5
O1—C1—C2	110.04 (15)	C6—C8—H83	109.5
O1—C1—C4	110.49 (15)	H81—C8—H83	109.5
C2—C1—C4	112.63 (17)	H82—C8—H83	109.5
O1—C1—C3	102.20 (14)	O3—C9—N2	122.03 (15)
C2—C1—C3	110.76 (17)	O3—C9—C6	122.28 (15)
C4—C1—C3	110.23 (17)	N2—C9—C6	115.48 (14)
C1—C2—H21	109.5	N2—C10—C11	110.34 (14)
C1—C2—H22	109.5	N2—C10—C13	109.64 (14)
H21—C2—H22	109.5	C11—C10—C13	110.02 (16)
C1—C2—H23	109.5	N2—C10—C12	107.29 (15)
H21—C2—H23	109.5	C11—C10—C12	111.13 (15)
H22—C2—H23	109.5	C13—C10—C12	108.36 (15)
C1—C3—H31	109.5	C10—C11—H111	109.5
C1—C3—H32	109.5	C10—C11—H112	109.5
H31—C3—H32	109.5	H111—C11—H112	109.5
C1—C3—H33	109.5	C10—C11—H113	109.5
H31—C3—H33	109.5	H111—C11—H113	109.5
H32—C3—H33	109.5	H112—C11—H113	109.5
C1—C4—H41	109.5	C10—C12—H121	109.5
C1—C4—H42	109.5	C10—C12—H122	109.5
H41—C4—H42	109.5	H121—C12—H122	109.5
C1—C4—H43	109.5	C10—C12—H123	109.5
H41—C4—H43	109.5	H121—C12—H123	109.5
H42—C4—H43	109.5	H122—C12—H123	109.5
O2—C5—O1	125.43 (16)	O4—C13—O5	123.57 (17)
O2—C5—N1	124.73 (16)	O4—C13—C10	124.85 (17)
O1—C5—N1	109.83 (14)	O5—C13—C10	111.40 (15)
N1—C6—C7	112.18 (14)	O5—C14—H141	109.5
N1—C6—C8	107.34 (14)	O5—C14—H142	109.5
C7—C6—C8	109.86 (14)	H141—C14—H142	109.5
N1—C6—C9	110.65 (13)	O5—C14—H143	109.5

C7—C6—C9	109.52 (14)	H141—C14—H143	109.5
C8—C6—C9	107.15 (13)	H142—C14—H143	109.5
C6—C7—H7	109.5		

C1—O1—C5—N1	178.23 (14)	N1—C6—C9—O3	−144.36 (15)
O1—C5—N1—C6	178.14 (13)	C7—C6—C9—O3	−20.2 (2)
C5—N1—C6—C9	58.93 (19)	C8—C6—C9—O3	98.92 (18)
N1—C6—C9—N2	40.83 (19)	C7—C6—C9—N2	165.00 (14)
C6—C9—N2—C10	178.15 (14)	C8—C6—C9—N2	−75.88 (18)
C9—N2—C10—C13	−45.7 (2)	C9—N2—C10—C11	75.7 (2)
N2—C10—C13—O5	−50.44 (18)	C9—N2—C10—C12	−163.14 (16)
C5—O1—C1—C2	64.4 (2)	C14—O5—C13—O4	−2.8 (2)
C5—O1—C1—C4	−60.6 (2)	C14—O5—C13—C10	−178.16 (15)
C5—O1—C1—C3	−177.93 (16)	N2—C10—C13—O4	134.24 (17)
C1—O1—C5—O2	−0.7 (3)	C11—C10—C13—O4	12.7 (2)
C6—N1—C5—O2	−2.9 (3)	C12—C10—C13—O4	−108.96 (19)
C5—N1—C6—C7	−63.7 (2)	C11—C10—C13—O5	−171.97 (14)
C5—N1—C6—C8	175.53 (14)	C12—C10—C13—O5	66.35 (18)
C10—N2—C9—O3	3.3 (2)		

Appendix E. Complete data for Boc-Val-Val-OMe (4)

Fractional atomic coordinates and isotropic or equivalent isotropic displacement parameters (Å^2) of (4)

	x	*y*	*z*	U_{iso}*/U_{eq}	Occ. (<1)
O1A	0.49640 (19)	−0.09751 (11)	0.69331 (7)	0.0478 (5)	
O2A	0.57930 (19)	−0.06719 (11)	0.62027 (7)	0.0454 (5)	
O3A	0.85040 (17)	0.00666 (11)	0.70577 (6)	0.0422 (5)	
O4A	1.13948 (19)	0.00410 (13)	0.66892 (8)	0.0569 (6)	
O5A	1.0444 (2)	0.10669 (12)	0.65924 (8)	0.0563 (6)	
N1A	0.6074 (2)	−0.00280 (13)	0.68985 (8)	0.0346 (5)	
H1A	0.592 (2)	0.0003 (16)	0.7206 (7)	0.041*	
N2A	0.85771 (19)	0.02561 (12)	0.62425 (7)	0.0292 (5)	
H2A	0.823 (2)	0.0421 (14)	0.5983 (8)	0.035*	
C1A	0.4395 (3)	−0.16196 (17)	0.67449 (12)	0.0543 (9)	
C2A	0.3782 (4)	−0.1883 (2)	0.72026 (14)	0.0926 (16)	
H21A	0.4345	−0.2038	0.7449	0.139*	
H22A	0.3286	−0.2288	0.7115	0.139*	
H23A	0.3317	−0.1494	0.7340	0.139*	
C3A	0.3541 (3)	−0.14190 (19)	0.63514 (13)	0.0665 (10)	
H31A	0.3946	−0.1239	0.6060	0.100*	
H32A	0.3030	−0.1045	0.6478	0.100*	
H33A	0.3091	−0.1842	0.6260	0.100*	
C4A	0.5260 (4)	−0.2142 (2)	0.6559 (2)	0.0980 (16)	
H41A	0.5603	−0.1959	0.6254	0.147*	
H42A	0.4887	−0.2603	0.6493	0.147*	
H43A	0.5857	−0.2208	0.6809	0.147*	
C5A	0.5634 (2)	−0.05687 (14)	0.66395 (9)	0.0333 (6)	
C6A	0.6793 (2)	0.05132 (14)	0.66681 (9)	0.0301 (6)	
H61A	0.6549	0.0569	0.6316	0.036*	
C7A	0.6639 (2)	0.12366 (14)	0.69306 (9)	0.0324 (6)	
H71A	0.6783	0.1166	0.7292	0.039*	
C8A	0.5421 (3)	0.15018 (17)	0.68637 (12)	0.0503 (8)	
H81A	0.4887	0.1146	0.6998	0.075*	
H82A	0.5266	0.1573	0.6511	0.075*	
H83A	0.5324	0.1958	0.7039	0.075*	
C9A	0.7494 (3)	0.17798 (15)	0.67359 (10)	0.0436 (7)	
H91A	0.8272	0.1605	0.6795	0.065*	
H92A	0.7385	0.2238	0.6907	0.065*	
H93A	0.7376	0.1847	0.6380	0.065*	
C10A	0.8031 (2)	0.02623 (14)	0.66746 (9)	0.0301 (6)	
C11A	0.9737 (2)	−0.00139 (15)	0.62067 (9)	0.0307 (6)	
H10A	0.9748	−0.0512	0.6344	0.037*	
C12A	1.0111 (2)	−0.00523 (16)	0.56612 (9)	0.0361 (6)	
H11A	0.9509	−0.0329	0.5480	0.043*	
C13A	1.1228 (3)	−0.0468 (2)	0.56067 (11)	0.0536 (9)	
H12A	1.1156	−0.0934	0.5771	0.080*	
H13A	1.1852	−0.0195	0.5759	0.080*	

H14A	1.1394	−0.0540	0.5255	0.080*
C14A	1.0188 (3)	0.06776 (18)	0.54190 (11)	0.0506 (8)
H15A	1.0412	0.0621	0.5072	0.076*
H16A	1.0759	0.0969	0.5592	0.076*
H17A	0.9442	0.0916	0.5436	0.076*
C15A	1.0537 (3)	0.04445 (17)	0.65185 (10)	0.0384 (7)
C16A	1.2229 (3)	0.0428 (2)	0.69794 (16)	0.0899 (15)
H18A	1.2835	0.0098	0.7085	0.135*
H19A	1.1857	0.0634	0.7271	0.135*
H20A	1.2561	0.0813	0.6779	0.135*
O1B	0.78703 (19)	−0.14973 (9)	0.53897 (7)	0.0447 (5)
O2B	0.77226 (19)	−0.10896 (11)	0.46052 (7)	0.0477 (5)
O3B	0.72306 (16)	0.09860 (9)	0.55096 (6)	0.0303 (4)
O4B	0.76874 (16)	0.27789 (9)	0.53842 (6)	0.0353 (4)
O5B	0.60212 (16)	0.24088 (10)	0.50630 (7)	0.0364 (4)
N1B	0.69924 (19)	−0.04758 (11)	0.52536 (7)	0.0291 (5)
H1B	0.681 (2)	−0.0468 (14)	0.5560 (7)	0.035*
N2B	0.72894 (19)	0.12118 (11)	0.46954 (7)	0.0268 (5)
H2B	0.715 (2)	0.1070 (14)	0.4401 (7)	0.032*
C1B	0.8402 (3)	−0.21825 (14)	0.52547 (12)	0.0461 (8)
C2B	0.9501 (3)	−0.2066 (2)	0.4978 (2)	0.1004 (17)
H21B	1.0022	−0.1777	0.5180	0.151*
H22B	0.9342	−0.1814	0.4668	0.151*
H23B	0.9856	−0.2530	0.4906	0.151*
C3B	0.7592 (3)	−0.26276 (17)	0.49661 (16)	0.0694 (11)
H31B	0.6894	−0.2705	0.5159	0.104*
H32B	0.7946	−0.3091	0.4891	0.104*
H33B	0.7400	−0.2381	0.4657	0.104*
C4B	0.8639 (6)	−0.2512 (2)	0.57531 (16)	0.115 (2)
H41B	0.7915	−0.2588	0.5928	0.173*
H42B	0.9125	−0.2188	0.5946	0.173*
H43B	0.9029	−0.2972	0.5709	0.173*
C5B	0.7541 (2)	−0.10249 (13)	0.50405 (9)	0.0300 (6)
C6B	0.6445 (2)	0.00836 (12)	0.49649 (8)	0.0255 (5)
H61B	0.6556	−0.0026	0.4606	0.031*
C7B	0.5155 (2)	0.01176 (13)	0.50711 (9)	0.0303 (6)
H71B	0.5048	0.0237	0.5429	0.036*
C8B	0.4583 (3)	0.06980 (15)	0.47659 (11)	0.0404 (7)
H81B	0.4948	0.1160	0.4834	0.061*
H82B	0.3770	0.0725	0.4853	0.061*
H83B	0.4660	0.0584	0.4414	0.061*
C9B	0.4605 (3)	−0.06083 (15)	0.49744 (11)	0.0425 (7)
H91B	0.3784	−0.0580	0.5044	0.064*
H92B	0.4956	−0.0970	0.5189	0.064*
H93B	0.4722	−0.0743	0.4628	0.064*
C10B	0.7025 (2)	0.07975 (12)	0.50800 (8)	0.0242 (5)
C11B	0.7801 (2)	0.19143 (12)	0.47591 (8)	0.0261 (5)
H10B	0.8562	0.1857	0.4924	0.031*
C12B	0.7981 (2)	0.22597 (14)	0.42481 (9)	0.0324 (6)
H11B	0.7244	0.2231	0.4062	0.039*

C13B	0.8885 (3)	0.18444 (17)	0.39601 (10)	0.0438 (7)	
H12B	0.8656	0.1340	0.3935	0.066*	
H13B	0.9620	0.1878	0.4133	0.066*	
H14B	0.8960	0.2049	0.3628	0.066*	
C14B	0.8324 (3)	0.30448 (15)	0.42859 (11)	0.0471 (8)	
H15B	0.7726	0.3312	0.4460	0.071*	
H16B	0.8424	0.3243	0.3953	0.071*	
H17B	0.9045	0.3084	0.4469	0.071*	
C15B	0.7045 (2)	0.23771 (13)	0.50815 (9)	0.0294 (6)	
C16B	0.7076 (3)	0.32764 (15)	0.56933 (10)	0.0423 (7)	
H18B	0.7621	0.3546	0.5897	0.063*	
H19B	0.6549	0.3012	0.5908	0.063*	
H20B	0.6642	0.3610	0.5486	0.063*	
O1C	1.00074 (15)	−0.05171 (11)	0.37052 (6)	0.0386 (5)	
O2C	0.92916 (16)	−0.02679 (11)	0.29466 (6)	0.0416 (5)	
O3C	0.68130 (17)	0.05731 (10)	0.37772 (6)	0.0377 (5)	
O4C	0.55551 (17)	0.21872 (10)	0.35588 (7)	0.0377 (5)	
O5C	0.45338 (18)	0.12008 (11)	0.33855 (8)	0.0470 (5)	
N1C	0.81564 (19)	−0.06512 (13)	0.35680 (8)	0.0317 (5)	
H1C	0.815 (2)	−0.0730 (14)	0.3883 (7)	0.038*	
N2C	0.6565 (2)	0.06497 (12)	0.29594 (7)	0.0315 (5)	
H2C	0.657 (3)	0.0430 (14)	0.2681 (7)	0.038*	
C1C	1.1198 (2)	−0.03693 (17)	0.35642 (10)	0.0374 (7)	
C2C	1.1324 (3)	0.03910 (18)	0.33766 (13)	0.0583 (9)	
H21C	1.1073	0.0727	0.3633	0.087*	
H22C	1.0854	0.0455	0.3080	0.087*	
H23C	1.2128	0.0483	0.3296	0.087*	
C3C	1.1592 (3)	−0.09207 (18)	0.31974 (12)	0.0512 (8)	
H31C	1.1479	−0.1401	0.3335	0.077*	
H32C	1.2406	−0.0848	0.3126	0.077*	
H33C	1.1150	−0.0873	0.2891	0.077*	
C4C	1.1820 (3)	−0.0453 (2)	0.40566 (11)	0.0598 (10)	
H41C	1.1742	−0.0949	0.4173	0.090*	
H42C	1.1486	−0.0126	0.4301	0.090*	
H43C	1.2632	−0.0339	0.4012	0.090*	
C5C	0.9166 (2)	−0.04594 (15)	0.33699 (9)	0.0307 (6)	
C6C	0.7096 (2)	−0.05041 (13)	0.33120 (9)	0.0288 (6)	
H61C	0.7199	−0.0615	0.2953	0.035*	
C7C	0.6139 (2)	−0.09752 (15)	0.35164 (10)	0.0352 (6)	
H71C	0.6069	−0.0878	0.3879	0.042*	
C8C	0.6426 (3)	−0.17666 (15)	0.34486 (13)	0.0532 (8)	
H81C	0.5817	−0.2060	0.3593	0.080*	
H82C	0.7152	−0.1874	0.3614	0.080*	
H83C	0.6493	−0.1874	0.3095	0.080*	
C9C	0.5006 (3)	−0.07905 (17)	0.32738 (13)	0.0500 (8)	
H91C	0.4408	−0.1109	0.3401	0.075*	
H92C	0.5072	−0.0851	0.2915	0.075*	
H93C	0.4807	−0.0292	0.3349	0.075*	
C10C	0.6813 (2)	0.02898 (14)	0.33670 (9)	0.0279 (6)	
C11C	0.6353 (3)	0.14138 (14)	0.29801 (9)	0.0351 (6)	0.843 (7)

H10C	0.7051	0.1648	0.3119	0.042*	0.843 (7)
C12C	0.6148 (6)	0.1728 (4)	0.24571 (18)	0.0514 (12)	0.843 (7)
H11C	0.6724	0.1499	0.2234	0.062*	0.843 (7)
C13C	0.4977 (4)	0.1525 (2)	0.22559 (13)	0.0637 (15)	0.843 (7)
H12C	0.4919	0.1002	0.2233	0.096*	0.843 (7)
H13C	0.4877	0.1735	0.1927	0.096*	0.843 (7)
H14C	0.4382	0.1707	0.2478	0.096*	0.843 (7)
C14C	0.6382 (6)	0.2518 (2)	0.24456 (17)	0.0801 (19)	0.843 (7)
H15C	0.6347	0.2690	0.2104	0.120*	0.843 (7)
H16C	0.7145	0.2612	0.2581	0.120*	0.843 (7)
H17C	0.5808	0.2770	0.2645	0.120*	0.843 (7)
C11D	0.6353 (3)	0.14138 (14)	0.29801 (9)	0.0351 (6)	0.157 (7)
H10D	0.7055	0.1669	0.3096	0.042*	0.157 (7)
C12D	0.605 (3)	0.166 (2)	0.2450 (8)	0.0514 (12)	0.157 (7)
H11D	0.5547	0.1296	0.2286	0.062*	0.157 (7)
C13D	0.545 (3)	0.2383 (15)	0.2466 (11)	0.091 (8)*	0.157 (7)
H12D	0.5403	0.2583	0.2132	0.136*	0.157 (7)
H13D	0.5873	0.2711	0.2680	0.136*	0.157 (7)
H14D	0.4670	0.2320	0.2597	0.136*	0.157 (7)
C14D	0.714 (2)	0.1737 (16)	0.2170 (9)	0.091 (8)*	0.157 (7)
H15D	0.7554	0.1279	0.2173	0.136*	0.157 (7)
H16D	0.7616	0.2107	0.2327	0.136*	0.157 (7)
H17D	0.6978	0.1876	0.1828	0.136*	0.157 (7)
C15C	0.5361 (3)	0.15686 (14)	0.33294 (9)	0.0335 (6)	
C16C	0.4715 (3)	0.24052 (16)	0.39171 (11)	0.0459 (8)	
H18C	0.4955	0.2856	0.4072	0.069*	
H19C	0.4640	0.2033	0.4171	0.069*	
H20C	0.3976	0.2475	0.3753	0.069*	

Atomic displacement parameters (Å^2) of (4)

	U^{11}	U^{22}	U^{33}	U^{12}	U^{13}	U^{23}
O1A	0.0619 (14)	0.0496 (12)	0.0319 (10)	−0.0241 (11)	0.0005 (10)	0.0069 (9)
O2A	0.0624 (14)	0.0459 (11)	0.0280 (10)	−0.0115 (11)	0.0071 (10)	−0.0051 (9)
O3A	0.0489 (12)	0.0589 (13)	0.0188 (9)	0.0096 (11)	−0.0026 (9)	0.0105 (9)
O4A	0.0482 (13)	0.0712 (15)	0.0514 (13)	0.0159 (12)	−0.0251 (11)	−0.0163 (12)
O5A	0.0577 (15)	0.0483 (14)	0.0629 (14)	−0.0026 (12)	−0.0213 (12)	−0.0098 (11)
N1A	0.0448 (14)	0.0412 (13)	0.0177 (10)	−0.0118 (12)	0.0061 (10)	0.0001 (10)
N2A	0.0302 (12)	0.0407 (12)	0.0167 (10)	−0.0001 (10)	−0.0019 (9)	0.0055 (9)
C1A	0.069 (2)	0.0401 (17)	0.0534 (19)	−0.0208 (17)	−0.0127 (17)	0.0088 (15)
C2A	0.126 (4)	0.089 (3)	0.063 (2)	−0.067 (3)	−0.015 (2)	0.024 (2)
C3A	0.077 (3)	0.063 (2)	0.059 (2)	−0.024 (2)	−0.015 (2)	0.0046 (17)
C4A	0.102 (4)	0.043 (2)	0.150 (4)	0.001 (2)	−0.026 (3)	−0.007 (3)
C5A	0.0410 (16)	0.0341 (14)	0.0249 (14)	−0.0009 (13)	0.0026 (12)	0.0033 (12)
C6A	0.0373 (15)	0.0357 (15)	0.0174 (11)	−0.0019 (12)	0.0026 (11)	0.0031 (11)
C7A	0.0375 (16)	0.0361 (14)	0.0237 (13)	0.0001 (12)	−0.0018 (12)	0.0013 (11)
C8A	0.0438 (19)	0.0482 (18)	0.059 (2)	0.0069 (15)	−0.0021 (16)	−0.0039 (16)

C9A	0.055 (2)	0.0376 (16)	0.0385 (16)	−0.0027 (15)	0.0051 (14)	0.0033 (13)
C10A	0.0386 (16)	0.0317 (14)	0.0201 (13)	−0.0028 (12)	−0.0001 (12)	0.0043 (10)
C11A	0.0306 (15)	0.0391 (15)	0.0223 (12)	0.0024 (12)	−0.0023 (11)	0.0041 (11)
C12A	0.0293 (15)	0.0511 (17)	0.0280 (14)	−0.0016 (13)	−0.0008 (11)	−0.0069 (12)
C13A	0.0420 (19)	0.079 (2)	0.0402 (17)	0.0103 (18)	0.0009 (14)	−0.0137 (16)
C14A	0.0467 (19)	0.069 (2)	0.0359 (16)	−0.0063 (17)	0.0084 (14)	0.0126 (15)
C15A	0.0366 (17)	0.0485 (19)	0.0301 (15)	0.0008 (14)	−0.0065 (12)	−0.0037 (13)
C16A	0.065 (3)	0.114 (4)	0.091 (3)	0.017 (3)	−0.052 (2)	−0.035 (3)
O1B	0.0644 (14)	0.0313 (10)	0.0384 (11)	0.0196 (10)	−0.0086 (10)	0.0038 (8)
O2B	0.0648 (15)	0.0457 (12)	0.0326 (11)	0.0205 (11)	0.0169 (10)	0.0067 (9)
O3B	0.0437 (11)	0.0315 (9)	0.0158 (8)	−0.0008 (9)	−0.0034 (8)	−0.0001 (7)
O4B	0.0338 (11)	0.0351 (10)	0.0369 (10)	−0.0048 (9)	0.0019 (8)	−0.0133 (8)
O5B	0.0307 (12)	0.0406 (11)	0.0379 (11)	0.0000 (9)	−0.0012 (9)	−0.0020 (8)
N1B	0.0404 (13)	0.0266 (11)	0.0204 (10)	0.0058 (10)	−0.0006 (10)	0.0009 (9)
N2B	0.0359 (12)	0.0289 (11)	0.0155 (10)	−0.0038 (10)	−0.0020 (9)	−0.0019 (9)
C1B	0.0456 (19)	0.0273 (14)	0.065 (2)	0.0118 (14)	−0.0142 (16)	−0.0027 (14)
C2B	0.040 (2)	0.054 (2)	0.207 (5)	0.0153 (19)	0.009 (3)	−0.012 (3)
C3B	0.061 (2)	0.0375 (18)	0.109 (3)	0.0073 (17)	−0.025 (2)	−0.0124 (19)
C4B	0.200 (6)	0.060 (2)	0.086 (3)	0.065 (3)	−0.050 (4)	0.002 (2)
C5B	0.0282 (14)	0.0289 (13)	0.0329 (15)	0.0011 (12)	−0.0015 (12)	0.0032 (12)
C6B	0.0316 (14)	0.0263 (12)	0.0185 (11)	0.0038 (11)	−0.0010 (11)	0.0003 (10)
C7B	0.0347 (15)	0.0302 (14)	0.0259 (13)	0.0020 (12)	−0.0011 (11)	−0.0025 (11)
C8B	0.0372 (16)	0.0372 (15)	0.0468 (17)	0.0065 (13)	−0.0037 (14)	−0.0004 (13)
C9B	0.0393 (17)	0.0352 (15)	0.0531 (18)	−0.0033 (14)	−0.0029 (14)	0.0002 (14)
C10B	0.0255 (13)	0.0301 (13)	0.0170 (12)	0.0050 (11)	−0.0009 (10)	−0.0006 (10)
C11B	0.0268 (14)	0.0289 (12)	0.0227 (12)	−0.0015 (11)	−0.0042 (11)	−0.0001 (10)
C12B	0.0315 (15)	0.0397 (15)	0.0260 (13)	−0.0047 (13)	0.0001 (11)	0.0048 (11)
C13B	0.0399 (18)	0.0560 (19)	0.0354 (16)	−0.0057 (15)	0.0092 (13)	−0.0033 (14)
C14B	0.054 (2)	0.0401 (17)	0.0476 (17)	−0.0068 (15)	0.0058 (15)	0.0103 (14)
C15B	0.0354 (17)	0.0266 (13)	0.0262 (13)	−0.0037 (12)	−0.0022 (12)	0.0035 (10)
C16B	0.0470 (18)	0.0359 (15)	0.0439 (16)	0.0031 (14)	0.0057 (14)	−0.0142 (13)
O1C	0.0261 (10)	0.0674 (13)	0.0224 (9)	0.0006 (10)	−0.0015 (8)	0.0049 (9)
O2C	0.0383 (12)	0.0673 (13)	0.0190 (9)	−0.0094 (10)	−0.0025 (8)	0.0047 (9)
O3C	0.0543 (13)	0.0391 (10)	0.0198 (9)	−0.0008 (10)	−0.0045 (8)	−0.0075 (8)
O4C	0.0421 (12)	0.0361 (10)	0.0349 (10)	0.0076 (9)	−0.0008 (9)	−0.0089 (8)
O5C	0.0386 (12)	0.0453 (12)	0.0570 (13)	−0.0026 (10)	0.0021 (10)	−0.0084 (10)
N1C	0.0268 (12)	0.0482 (13)	0.0201 (10)	0.0034 (11)	0.0025 (9)	0.0042 (10)
N2C	0.0418 (13)	0.0349 (12)	0.0179 (10)	0.0048 (11)	−0.0021 (10)	−0.0045 (9)
C1C	0.0250 (15)	0.0574 (18)	0.0299 (14)	−0.0018 (13)	−0.0036 (11)	−0.0052 (13)
C2C	0.054 (2)	0.057 (2)	0.064 (2)	−0.0202 (18)	−0.0143 (18)	−0.0003 (17)
C3C	0.0354 (17)	0.068 (2)	0.0505 (19)	−0.0003 (16)	0.0093 (15)	−0.0118 (16)
C4C	0.0362 (18)	0.100 (3)	0.0432 (18)	0.0047 (19)	−0.0112 (15)	−0.0032 (18)
C5C	0.0303 (15)	0.0405 (15)	0.0211 (13)	0.0016 (12)	−0.0028 (11)	−0.0037 (11)
C6C	0.0276 (14)	0.0360 (14)	0.0229 (12)	0.0021 (12)	−0.0005 (11)	−0.0052 (11)
C7C	0.0301 (15)	0.0373 (15)	0.0381 (15)	0.0000 (13)	0.0029 (12)	−0.0046 (12)
C8C	0.049 (2)	0.0360 (16)	0.074 (2)	−0.0033 (15)	0.0020 (17)	−0.0019 (16)
C9C	0.0318 (17)	0.0495 (18)	0.069 (2)	−0.0042 (14)	−0.0043 (15)	−0.0050 (16)
C10C	0.0256 (14)	0.0378 (14)	0.0203 (12)	−0.0024 (11)	−0.0007 (11)	−0.0028 (11)
C11C	0.0458 (18)	0.0347 (15)	0.0247 (13)	0.0016 (13)	−0.0009 (12)	−0.0015 (11)
C12C	0.084 (3)	0.040 (2)	0.0304 (15)	0.010 (2)	0.0034 (17)	0.0041 (14)

C13C	0.096 (4)	0.063 (3)	0.032 (2)	0.033 (3)	−0.026 (2)	−0.0031 (18)
C14C	0.134 (5)	0.050 (3)	0.056 (3)	0.003 (3)	0.014 (3)	0.015 (2)
C11D	0.0458 (18)	0.0347 (15)	0.0247 (13)	0.0016 (13)	−0.0009 (12)	−0.0015 (11)
C12D	0.084 (3)	0.040 (2)	0.0304 (15)	0.010 (2)	0.0034 (17)	0.0041 (14)
C15C	0.0421 (17)	0.0342 (15)	0.0242 (13)	0.0093 (14)	−0.0092 (12)	−0.0021 (12)
C16C	0.056 (2)	0.0432 (17)	0.0384 (16)	0.0183 (16)	0.0050 (15)	−0.0041 (13)

Geometric parameters(Å °) of (4)

O1A—C5A	1.349 (3)	C8B—H81B	0.9800
O1A—C1A	1.465 (4)	C8B—H82B	0.9800
O2A—C5A	1.211 (3)	C8B—H83B	0.9800
O3A—C10A	1.230 (3)	C9B—H91B	0.9800
O4A—C15A	1.336 (4)	C9B—H92B	0.9800
O4A—C16A	1.445 (4)	C9B—H93B	0.9800
O5A—C15A	1.183 (3)	C11B—C15B	1.512 (4)
N1A—C5A	1.331 (3)	C11B—C12B	1.539 (3)
N1A—C6A	1.454 (3)	C11B—H10B	1.0000
N1A—H1A	0.851 (17)	C12B—C14B	1.522 (4)
N2A—C10A	1.332 (3)	C12B—C13B	1.525 (4)
N2A—C11A	1.451 (3)	C12B—H11B	1.0000
N2A—H2A	0.865 (17)	C13B—H12B	0.9800
C1A—C4A	1.491 (6)	C13B—H13B	0.9800
C1A—C3A	1.507 (5)	C13B—H14B	0.9800
C1A—C2A	1.512 (5)	C14B—H15B	0.9800
C2A—H21A	0.9800	C14B—H16B	0.9800
C2A—H22A	0.9800	C14B—H17B	0.9800
C2A—H23A	0.9800	C16B—H18B	0.9800
C3A—H31A	0.9800	C16B—H19B	0.9800
C3A—H32A	0.9800	C16B—H20B	0.9800
C3A—H33A	0.9800	O1C—C5C	1.343 (3)
C4A—H41A	0.9800	O1C—C1C	1.469 (3)
C4A—H42A	0.9800	O2C—C5C	1.208 (3)
C4A—H43A	0.9800	O3C—C10C	1.229 (3)
C6A—C10A	1.521 (4)	O4C—C15C	1.329 (3)
C6A—C7A	1.535 (4)	O4C—C16C	1.439 (3)
C6A—H61A	1.0000	O5C—C15C	1.196 (3)
C7A—C9A	1.517 (4)	N1C—C5C	1.345 (3)
C7A—C8A	1.519 (4)	N1C—C6C	1.447 (3)
C7A—H71A	1.0000	N1C—H1C	0.865 (17)
C8A—H81A	0.9800	N2C—C10C	1.323 (3)
C8A—H82A	0.9800	N2C—C11C	1.447 (3)
C8A—H83A	0.9800	N2C—H2C	0.859 (17)
C9A—H91A	0.9800	C1C—C3C	1.501 (4)
C9A—H92A	0.9800	C1C—C2C	1.513 (4)
C9A—H93A	0.9800	C1C—C4C	1.526 (4)

C11A—C15A	1.522 (4)	C2C—H21C	0.9800
C11A—C12A	1.540 (3)	C2C—H22C	0.9800
C11A—H10A	1.0000	C2C—H23C	0.9800
C12A—C14A	1.513 (4)	C3C—H31C	0.9800
C12A—C13A	1.526 (4)	C3C—H32C	0.9800
C12A—H11A	1.0000	C3C—H33C	0.9800
C13A—H12A	0.9800	C4C—H41C	0.9800
C13A—H13A	0.9800	C4C—H42C	0.9800
C13A—H14A	0.9800	C4C—H43C	0.9800
C14A—H15A	0.9800	C6C—C10C	1.524 (4)
C14A—H16A	0.9800	C6C—C7C	1.526 (4)
C14A—H17A	0.9800	C6C—H61C	1.0000
C16A—H18A	0.9800	C7C—C9C	1.518 (4)
C16A—H19A	0.9800	C7C—C8C	1.524 (4)
C16A—H20A	0.9800	C7C—H71C	1.0000
O1B—C5B	1.348 (3)	C8C—H81C	0.9800
O1B—C1B	1.467 (3)	C8C—H82C	0.9800
O2B—C5B	1.202 (3)	C8C—H83C	0.9800
O3B—C10B	1.237 (3)	C9C—H91C	0.9800
O4B—C15B	1.340 (3)	C9C—H92C	0.9800
O4B—C16B	1.439 (3)	C9C—H93C	0.9800
O5B—C15B	1.200 (3)	C11C—C15C	1.523 (4)
N1B—C5B	1.338 (3)	C11C—C12C	1.550 (5)
N1B—C6B	1.452 (3)	C11C—H10C	1.0000
N1B—H1B	0.854 (17)	C12C—C14C	1.498 (8)
N2B—C10B	1.332 (3)	C12C—C13C	1.521 (8)
N2B—C11B	1.450 (3)	C12C—H11C	1.0000
N2B—H2B	0.855 (17)	C13C—H12C	0.9800
C1B—C3B	1.481 (4)	C13C—H13C	0.9800
C1B—C2B	1.503 (5)	C13C—H14C	0.9800
C1B—C4B	1.507 (5)	C14C—H15C	0.9800
C2B—H21B	0.9800	C14C—H16C	0.9800
C2B—H22B	0.9800	C14C—H17C	0.9800
C2B—H23B	0.9800	C12D—C14D	1.49 (2)
C3B—H31B	0.9800	C12D—C13D	1.52 (2)
C3B—H32B	0.9800	C12D—H11D	1.0000
C3B—H33B	0.9800	C13D—H12D	0.9800
C4B—H41B	0.9800	C13D—H13D	0.9800
C4B—H42B	0.9800	C13D—H14D	0.9800
C4B—H43B	0.9800	C14D—H15D	0.9800
C6B—C10B	1.526 (3)	C14D—H16D	0.9800
C6B—C7B	1.537 (4)	C14D—H17D	0.9800
C6B—H61B	1.0000	C16C—H18C	0.9800
C7B—C8B	1.516 (4)	C16C—H19C	0.9800
C7B—C9B	1.521 (4)	C16C—H20C	0.9800
C7B—H71B	1.0000		

C5A—O1A—C1A	121.3 (2)	H91B—C9B—H92B	109.5
C15A—O4A—C16A	114.4 (3)	C7B—C9B—H93B	109.5

C5A—N1A—C6A	121.6 (2)	H91B—C9B—H93B	109.5
C5A—N1A—H1A	119 (2)	H92B—C9B—H93B	109.5
C6A—N1A—H1A	119 (2)	O3B—C10B—N2B	121.6 (2)
C10A—N2A—C11A	120.7 (2)	O3B—C10B—C6B	121.7 (2)
C10A—N2A—H2A	119.1 (19)	N2B—C10B—C6B	116.72 (19)
C11A—N2A—H2A	120.3 (19)	N2B—C11B—C15B	110.0 (2)
O1A—C1A—C4A	110.2 (3)	N2B—C11B—C12B	109.11 (19)
O1A—C1A—C3A	110.1 (3)	C15B—C11B—C12B	111.0 (2)
C4A—C1A—C3A	112.0 (3)	N2B—C11B—H10B	108.9
O1A—C1A—C2A	101.4 (3)	C15B—C11B—H10B	108.9
C4A—C1A—C2A	112.6 (3)	C12B—C11B—H10B	108.9
C3A—C1A—C2A	110.2 (3)	C14B—C12B—C13B	109.9 (2)
C1A—C2A—H21A	109.5	C14B—C12B—C11B	112.2 (2)
C1A—C2A—H22A	109.5	C13B—C12B—C11B	109.9 (2)
H21A—C2A—H22A	109.5	C14B—C12B—H11B	108.2
C1A—C2A—H23A	109.5	C13B—C12B—H11B	108.2
H21A—C2A—H23A	109.5	C11B—C12B—H11B	108.2
H22A—C2A—H23A	109.5	C12B—C13B—H12B	109.5
C1A—C3A—H31A	109.5	C12B—C13B—H13B	109.5
C1A—C3A—H32A	109.5	H12B—C13B—H13B	109.5
H31A—C3A—H32A	109.5	C12B—C13B—H14B	109.5
C1A—C3A—H33A	109.5	H12B—C13B—H14B	109.5
H31A—C3A—H33A	109.5	H13B—C13B—H14B	109.5
H32A—C3A—H33A	109.5	C12B—C14B—H15B	109.5
C1A—C4A—H41A	109.5	C12B—C14B—H16B	109.5
C1A—C4A—H42A	109.5	H15B—C14B—H16B	109.5
H41A—C4A—H42A	109.5	C12B—C14B—H17B	109.5
C1A—C4A—H43A	109.5	H15B—C14B—H17B	109.5
H41A—C4A—H43A	109.5	H16B—C14B—H17B	109.5
H42A—C4A—H43A	109.5	O5B—C15B—O4B	123.9 (2)
O2A—C5A—N1A	125.1 (2)	O5B—C15B—C11B	126.0 (2)
O2A—C5A—O1A	125.0 (3)	O4B—C15B—C11B	110.1 (2)
N1A—C5A—O1A	109.9 (2)	O4B—C16B—H18B	109.5
N1A—C6A—C10A	109.4 (2)	O4B—C16B—H19B	109.5
N1A—C6A—C7A	110.1 (2)	H18B—C16B—H19B	109.5
C10A—C6A—C7A	112.1 (2)	O4B—C16B—H20B	109.5
N1A—C6A—H61A	108.4	H18B—C16B—H20B	109.5
C10A—C6A—H61A	108.4	H19B—C16B—H20B	109.5
C7A—C6A—H61A	108.4	C5C—O1C—C1C	120.28 (19)
C9A—C7A—C8A	111.0 (2)	C15C—O4C—C16C	116.3 (2)
C9A—C7A—C6A	110.4 (2)	C5C—N1C—C6C	120.8 (2)
C8A—C7A—C6A	109.9 (2)	C5C—N1C—H1C	116.7 (19)
C9A—C7A—H71A	108.5	C6C—N1C—H1C	119.5 (19)
C8A—C7A—H71A	108.5	C10C—N2C—C11C	120.3 (2)
C6A—C7A—H71A	108.5	C10C—N2C—H2C	119.2 (19)
C7A—C8A—H81A	109.5	C11C—N2C—H2C	120.4 (19)
C7A—C8A—H82A	109.5	O1C—C1C—C3C	109.5 (2)
H81A—C8A—H82A	109.5	O1C—C1C—C2C	110.8 (2)
C7A—C8A—H83A	109.5	C3C—C1C—C2C	113.0 (3)
H81A—C8A—H83A	109.5	O1C—C1C—C4C	101.9 (2)

H82A—C8A—H83A	109.5		C3C—C1C—C4C	111.1	(3)
C7A—C9A—H91A	109.5		C2C—C1C—C4C	110.0	(3)
C7A—C9A—H92A	109.5		C1C—C2C—H21C	109.5	
H91A—C9A—H92A	109.5		C1C—C2C—H22C	109.5	
C7A—C9A—H93A	109.5		H21C—C2C—H22C	109.5	
H91A—C9A—H93A	109.5		C1C—C2C—H23C	109.5	
H92A—C9A—H93A	109.5		H21C—C2C—H23C	109.5	
O3A—C10A—N2A	121.4	(2)	H22C—C2C—H23C	109.5	
O3A—C10A—C6A	121.9	(2)	C1C—C3C—H31C	109.5	
N2A—C10A—C6A	116.7	(2)	C1C—C3C—H32C	109.5	
N2A—C11A—C15A	110.1	(2)	H31C—C3C—H32C	109.5	
N2A—C11A—C12A	110.2	(2)	C1C—C3C—H33C	109.5	
C15A—C11A—C12A	112.5	(2)	H31C—C3C—H33C	109.5	
N2A—C11A—H10A	108.0		H32C—C3C—H33C	109.5	
C15A—C11A—H10A	108.0		C1C—C4C—H41C	109.5	
C12A—C11A—H10A	108.0		C1C—C4C—H42C	109.5	
C14A—C12A—C13A	111.3	(3)	H41C—C4C—H42C	109.5	
C14A—C12A—C11A	112.9	(2)	C1C—C4C—H43C	109.5	
C13A—C12A—C11A	111.0	(2)	H41C—C4C—H43C	109.5	
C14A—C12A—H11A	107.1		H42C—C4C—H43C	109.5	
C13A—C12A—H11A	107.1		O2C—C5C—O1C	125.1	(2)
C11A—C12A—H11A	107.1		O2C—C5C—N1C	124.3	(2)
C12A—C13A—H12A	109.5		O1C—C5C—N1C	110.7	(2)
C12A—C13A—H13A	109.5		N1C—C6C—C10C	108.9	(2)
H12A—C13A—H13A	109.5		N1C—C6C—C7C	110.2	(2)
C12A—C13A—H14A	109.5		C10C—C6C—C7C	111.4	(2)
H12A—C13A—H14A	109.5		N1C—C6C—H61C	108.8	
H13A—C13A—H14A	109.5		C10C—C6C—H61C	108.8	
C12A—C14A—H15A	109.5		C7C—C6C—H61C	108.8	
C12A—C14A—H16A	109.5		C9C—C7C—C8C	111.1	(3)
H15A—C14A—H16A	109.5		C9C—C7C—C6C	110.6	(2)
C12A—C14A—H17A	109.5		C8C—C7C—C6C	110.6	(2)
H15A—C14A—H17A	109.5		C9C—C7C—H71C	108.1	
H16A—C14A—H17A	109.5		C8C—C7C—H71C	108.1	
O5A—C15A—O4A	124.3	(3)	C6C—C7C—H71C	108.1	
O5A—C15A—C11A	126.0	(3)	C7C—C8C—H81C	109.5	
O4A—C15A—C11A	109.7	(3)	C7C—C8C—H82C	109.5	
O4A—C16A—H18A	109.5		H81C—C8C—H82C	109.5	
O4A—C16A—H19A	109.5		C7C—C8C—H83C	109.5	
H18A—C16A—H19A	109.5		H81C—C8C—H83C	109.5	
O4A—C16A—H20A	109.5		H82C—C8C—H83C	109.5	
H18A—C16A—H20A	109.5		C7C—C9C—H91C	109.5	
H19A—C16A—H20A	109.5		C7C—C9C—H92C	109.5	
C5B—O1B—C1B	121.1	(2)	H91C—C9C—H92C	109.5	
C15B—O4B—C16B	115.9	(2)	C7C—C9C—H93C	109.5	
C5B—N1B—C6B	121.9	(2)	H91C—C9C—H93C	109.5	
C5B—N1B—H1B	123.2	(19)	H92C—C9C—H93C	109.5	
C6B—N1B—H1B	113.6	(19)	O3C—C10C—N2C	122.3	(2)
C10B—N2B—C11B	121.8	(2)	O3C—C10C—C6C	120.4	(2)
C10B—N2B—H2B	120.1	(18)	N2C—C10C—C6C	117.3	(2)

C11B—N2B—H2B	118.1	(18)	N2C—C11C—C15C	109.9	(2)
O1B—C1B—C3B	110.4	(2)	N2C—C11C—C12C	111.3	(3)
O1B—C1B—C2B	111.1	(3)	C15C—C11C—C12C	112.1	(3)
C3B—C1B—C2B	111.4	(4)	N2C—C11C—H10C	107.7	
O1B—C1B—C4B	102.1	(3)	C15C—C11C—H10C	107.7	
C3B—C1B—C4B	111.2	(3)	C12C—C11C—H10C	107.7	
C2B—C1B—C4B	110.3	(4)	C14C—C12C—C13C	113.7	(5)
C1B—C2B—H21B	109.5		C14C—C12C—C11C	111.3	(5)
C1B—C2B—H22B	109.5		C13C—C12C—C11C	111.8	(4)
H21B—C2B—H22B	109.5		C14C—C12C—H11C	106.5	
C1B—C2B—H23B	109.5		C13C—C12C—H11C	106.5	
H21B—C2B—H23B	109.5		C11C—C12C—H11C	106.5	
H22B—C2B—H23B	109.5		C12C—C13C—H12C	109.5	
C1B—C3B—H31B	109.5		C12C—C13C—H13C	109.5	
C1B—C3B—H32B	109.5		H12C—C13C—H13C	109.5	
H31B—C3B—H32B	109.5		C12C—C13C—H14C	109.5	
C1B—C3B—H33B	109.5		H12C—C13C—H14C	109.5	
H31B—C3B—H33B	109.5		H13C—C13C—H14C	109.5	
H32B—C3B—H33B	109.5		C12C—C14C—H15C	109.5	
C1B—C4B—H41B	109.5		C12C—C14C—H16C	109.5	
C1B—C4B—H42B	109.5		H15C—C14C—H16C	109.5	
H41B—C4B—H42B	109.5		C12C—C14C—H17C	109.5	
C1B—C4B—H43B	109.5		H15C—C14C—H17C	109.5	
H41B—C4B—H43B	109.5		H16C—C14C—H17C	109.5	
H42B—C4B—H43B	109.5		C14D—C12D—C13D	109	(2)
O2B—C5B—N1B	125.7	(2)	C14D—C12D—H11D	110.1	
O2B—C5B—O1B	124.7	(2)	C13D—C12D—H11D	110.1	
N1B—C5B—O1B	109.6	(2)	C12D—C13D—H12D	109.5	
N1B—C6B—C10B	108.70	(19)	C12D—C13D—H13D	109.5	
N1B—C6B—C7B	111.2	(2)	H12D—C13D—H13D	109.5	
C10B—C6B—C7B	111.3	(2)	C12D—C13D—H14D	109.5	
N1B—C6B—H61B	108.5		H12D—C13D—H14D	109.5	
C10B—C6B—H61B	108.5		H13D—C13D—H14D	109.5	
C7B—C6B—H61B	108.5		C12D—C14D—H15D	109.5	
C8B—C7B—C9B	110.8	(2)	C12D—C14D—H16D	109.5	
C8B—C7B—C6B	111.1	(2)	H15D—C14D—H16D	109.5	
C9B—C7B—C6B	110.2	(2)	C12D—C14D—H17D	109.5	
C8B—C7B—H71B	108.2		H15D—C14D—H17D	109.5	
C9B—C7B—H71B	108.2		H16D—C14D—H17D	109.5	
C6B—C7B—H71B	108.2		O5C—C15C—O4C	125.2	(3)
C7B—C8B—H81B	109.5		O5C—C15C—C11C	125.9	(2)
C7B—C8B—H82B	109.5		O4C—C15C—C11C	108.9	(2)
H81B—C8B—H82B	109.5		O4C—C16C—H18C	109.5	
C7B—C8B—H83B	109.5		O4C—C16C—H19C	109.5	
H81B—C8B—H83B	109.5		H18C—C16C—H19C	109.5	
H82B—C8B—H83B	109.5		O4C—C16C—H20C	109.5	
C7B—C9B—H91B	109.5		H18C—C16C—H20C	109.5	
C7B—C9B—H92B	109.5		H19C—C16C—H20C	109.5	

C1A—O1A—C5A—N1A	−178.4 (3)	C6B—N1B—C5B—O2B	6.3 (4)
O1A—C5A—N1A—C6A	−177.4 (2)	C5B—N1B—C6B—C7B	119.6 (3)
C5A—N1A—C6A—C10A	−87.6 (3)	C10B—C6B—C7B—C8B	59.1 (3)
N1A—C6A—C10A—N2A	126.2 (2)	C10B—C6B—C7B—C9B	−177.6 (2)
C6A—C10A—N2A—C11A	−176.4 (2)	C11B—N2B—C10B—O3B	−1.8 (4)
C10A—N2A—C11A—C15A	−62.6 (3)	N1B—C6B—C10B—O3B	−46.5 (3)
N2A—C11A—C15A—O4A	149.1 (2)	C7B—C6B—C10B—O3B	76.3 (3)
C11A—C15A—O4A—C16A	178.2 (3)	C7B—C6B—C10B—N2B	−102.9 (3)
N1A—C6A—C7A—C8A	−64.3 (3)	C10B—N2B—C11B—C12B	−179.0 (2)
N1A—C6A—C7A—C9A	172.9 (2)	C15B—C11B—C12B—C14B	48.8 (3)
N2A—C11A—C12A—C13A	−168.9 (2)	C15B—C11B—C12B—C13B	171.4 (2)
N2A—C11A—C12A—C14A	65.2 (3)	C16B—O4B—C15B—O5B	−0.9 (4)
C5A—O1A—C1A—C4A	59.7 (4)	N2B—C11B—C15B—O5B	−41.0 (3)
C5A—O1A—C1A—C3A	−64.2 (4)	C12B—C11B—C15B—O5B	79.9 (3)
C5A—O1A—C1A—C2A	179.2 (3)	C12B—C11B—C15B—O4B	−97.5 (2)
C1A—O1A—C5A—O2A	3.0 (4)	C1C—O1C—C5C—N1C	177.0 (2)
O2A—C5A—N1A—C6A	1.2 (4)	O1C—C5C—N1C—C6C	168.0 (2)
C5A—N1A—C6A—C7A	148.7 (3)	C5C—N1C—C6C—C10C	−76.2 (3)
C10A—C6A—C7A—C9A	50.8 (3)	N1C—C6C—C10C—N2C	129.5 (2)
C10A—C6A—C7A—C8A	173.7 (2)	C6C—C10C—N2C—C11C	−176.4 (2)
C11A—N2A—C10A—O3A	2.8 (4)	C10C—N2C—C11C—C15C	−58.3 (3)
N1A—C6A—C10A—O3A	−52.9 (3)	N2C—C11C—C15C—O4C	145.5 (2)
C7A—C6A—C10A—O3A	69.5 (3)	C11C—C15C—O4C—C16C	−178.0 (2)
C7A—C6A—C10A—N2A	−111.3 (3)	N1C—C6C—C7C—C8C	−60.2 (3)
C10A—N2A—C11A—C12A	172.7 (2)	N1C—C6C—C7C—C9C	176.3 (2)
C15A—C11A—C12A—C14A	−58.0 (3)	N2C—C11C—C12C—C13C	73.9 (5)
C15A—C11A—C12A—C13A	67.9 (3)	N2C—C11C—C12C—C14C	−157.8 (4)
C16A—O4A—C15A—O5A	0.0 (5)	C5C—O1C—C1C—C3C	−65.7 (3)
N2A—C11A—C15A—O5A	−32.7 (4)	C5C—O1C—C1C—C2C	59.5 (3)
C12A—C11A—C15A—O5A	90.6 (4)	C5C—O1C—C1C—C4C	176.6 (3)
C12A—C11A—C15A—O4A	−87.6 (3)	C1C—O1C—C5C—O2C	−2.4 (4)
C1B—O1B—C5B—N1B	174.5 (2)	C6C—N1C—C5C—O2C	−12.6 (4)
O1B—C5B—N1B—C6B	−174.1 (2)	C5C—N1C—C6C—C7C	161.4 (2)
C5B—N1B—C6B—C10B	−117.6 (2)	C10C—C6C—C7C—C9C	55.3 (3)
N1B—C6B—C10B—N2B	134.3 (2)	C10C—C6C—C7C—C8C	178.8 (2)
C6B—C10B—N2B—C11B	177.5 (2)	C11C—N2C—C10C—O3C	4.0 (4)
C10B—N2B—C11B—C15B	−57.0 (3)	N1C—C6C—C10C—O3C	−50.9 (3)
N2B—C11B—C15B—O4B	141.6 (2)	C7C—C6C—C10C—O3C	70.9 (3)
C11B—C15B—O4B—C16B	176.6 (2)	C7C—C6C—C10C—N2C	−108.8 (3)
N1B—C6B—C7B—C8B	−179.5 (2)	C10C—N2C—C11C—C12C	176.8 (3)
N1B—C6B—C7B—C9B	−56.3 (3)	C15C—C11C—C12C—C14C	78.6 (5)
N2B—C11B—C12B—C13B	−67.2 (3)	C15C—C11C—C12C—C13C	−49.8 (6)
N2B—C11B—C12B—C14B	170.2 (2)	C16C—O4C—C15C—O5C	2.8 (4)
C5B—O1B—C1B—C3B	−62.9 (4)	C16C—O4C—C15C—C11C	−178.0 (2)
C5B—O1B—C1B—C2B	61.2 (4)	N2C—C11C—C15C—O5C	−35.4 (4)
C5B—O1B—C1B—C4B	178.8 (3)	C12C—C11C—C15C—O5C	89.0 (4)
C1B—O1B—C5B—O2B	−5.9 (4)	C12C—C11C—C15C—O4C	−90.1 (4)

Appendix F. Complete data for Boc-allylSer-Aib-Val-OMe (5)

Fractional atomic coordinates and isotropic or equivalent isotropic displacement parameters (Å^2) of (5)

	x	*y*	*z*	U_{iso}*/U_{eq}
O1	0.33515 (9)	0.5968 (3)	0.85730 (8)	0.0337 (5)
O2	0.44156 (10)	0.4977 (4)	0.83791 (10)	0.0395 (5)
O3	0.28563 (10)	0.4215 (4)	0.63403 (11)	0.0446 (6)
O4	0.39443 (10)	0.7422 (3)	0.70272 (9)	0.0340 (5)
O5	0.52381 (10)	1.0590 (3)	0.64884 (9)	0.0351 (5)
O6	0.65078 (10)	1.3162 (3)	0.76240 (9)	0.0306 (5)
O7	0.68520 (10)	0.9709 (3)	0.73899 (9)	0.0331 (5)
N1	0.34191 (12)	0.4086 (4)	0.76929 (11)	0.0308 (6)
H1	0.2972	0.3867	0.7650	0.037*
N2	0.46615 (11)	0.4990 (4)	0.66589 (10)	0.0264 (5)
H2	0.4832	0.3616	0.6687	0.032*
N3	0.54917 (12)	0.8266 (4)	0.73301 (11)	0.0293 (5)
H3	0.5500	0.6883	0.7479	0.035*
C1	0.36279 (15)	0.7218 (6)	0.91622 (14)	0.0366 (7)
C2	0.4060 (2)	0.9198 (7)	0.9024 (2)	0.0645 (12)
H2A	0.3784	1.0154	0.8696	0.097*
H2B	0.4466	0.8644	0.8871	0.097*
H2C	0.4209	1.0077	0.9415	0.097*
C3	0.40084 (19)	0.5632 (8)	0.96601 (16)	0.0595 (11)
H3A	0.3701	0.4399	0.9728	0.089*
H3B	0.4161	0.6449	1.0062	0.089*
H3C	0.4411	0.5015	0.9514	0.089*
C4	0.29713 (16)	0.8059 (6)	0.93621 (15)	0.0444 (8)
H4A	0.2725	0.9081	0.9035	0.067*
H4B	0.3093	0.8863	0.9770	0.067*
H4C	0.2674	0.6774	0.9410	0.067*
C5	0.37886 (15)	0.5027 (5)	0.82263 (13)	0.0328 (7)
C6	0.37846 (15)	0.3444 (5)	0.71909 (13)	0.0298 (7)
H6	0.4144	0.2300	0.7364	0.036*
C7	0.32875 (15)	0.2429 (6)	0.66322 (14)	0.0369 (7)
H7A	0.3543	0.1757	0.6323	0.044*
H7B	0.3006	0.1238	0.6782	0.044*
C8	0.22470 (19)	0.3493 (6)	0.59443 (18)	0.0558 (10)
H8A	0.1949	0.2747	0.6205	0.067*
H8B	0.2357	0.2381	0.5633	0.067*
C9	0.1870 (2)	0.5446 (7)	0.55938 (19)	0.0645 (11)
H9	0.1410	0.5184	0.5375	0.077*
C10	0.2108 (2)	0.7424 (8)	0.5561 (2)	0.0709 (12)
H10A	0.2566	0.7766	0.5772	0.085*
H10B	0.1829	0.8558	0.5326	0.085*
C11	0.41346 (14)	0.5491 (5)	0.69609 (13)	0.0286 (6)
C12	0.49492 (14)	0.6675 (5)	0.62898 (12)	0.0273 (6)
C13	0.44074 (15)	0.7462 (6)	0.57207 (13)	0.0355 (7)

H13A	0.4234	0.6163	0.5454	0.053*
H13B	0.4616	0.8544	0.5468	0.053*
H13C	0.4025	0.8183	0.5875	0.053*
C14	0.55606 (14)	0.5607 (5)	0.60574 (13)	0.0313 (6)
H14A	0.5400	0.4309	0.5785	0.047*
H14B	0.5906	0.5112	0.6426	0.047*
H14C	0.5768	0.6718	0.5812	0.047*
C15	0.52225 (14)	0.8678 (5)	0.67123 (13)	0.0279 (6)
C16	0.57704 (14)	1.0118 (5)	0.77526 (13)	0.0303 (6)
H16	0.5429	1.1383	0.7686	0.036*
C17	0.58822 (15)	0.9382 (5)	0.84572 (13)	0.0309 (7)
H17	0.5462	0.8516	0.8508	0.037*
C18	0.59262 (16)	1.1423 (5)	0.88989 (14)	0.0371 (7)
H18A	0.5523	1.2391	0.8760	0.056*
H18B	0.6348	1.2274	0.8883	0.056*
H18C	0.5936	1.0915	0.9337	0.056*
C19	0.64990 (17)	0.7807 (5)	0.86558 (14)	0.0386 (7)
H19A	0.6454	0.6516	0.8365	0.058*
H19B	0.6513	0.7275	0.9093	0.058*
H19C	0.6926	0.8621	0.8637	0.058*
C20	0.64353 (14)	1.0934 (5)	0.75652 (12)	0.0277 (6)
C21	0.71269 (15)	1.4071 (5)	0.74440 (15)	0.0361 (7)
H21A	0.7138	1.5709	0.7503	0.054*
H21B	0.7123	1.3719	0.6995	0.054*
H21C	0.7536	1.3398	0.7713	0.054*

Atomic displacement parameters (Å^2) of (5)

	U^{11}	U^{22}	U^{33}	U^{12}	U^{13}	U^{23}
O1	0.0296 (10)	0.0422 (13)	0.0295 (10)	0.0029 (9)	0.0064 (9)	−0.0031 (10)
O2	0.0288 (11)	0.0454 (14)	0.0435 (12)	0.0029 (10)	0.0052 (9)	−0.0062 (11)
O3	0.0345 (12)	0.0491 (14)	0.0477 (13)	−0.0058 (11)	0.0015 (10)	−0.0104 (11)
O4	0.0337 (11)	0.0307 (12)	0.0395 (11)	0.0009 (10)	0.0113 (9)	−0.0020 (10)
O5	0.0432 (12)	0.0264 (11)	0.0371 (11)	0.0025 (9)	0.0112 (9)	0.0036 (10)
O6	0.0306 (10)	0.0222 (10)	0.0410 (11)	−0.0031 (8)	0.0121 (9)	−0.0008 (9)
O7	0.0322 (10)	0.0260 (11)	0.0424 (12)	−0.0012 (9)	0.0105 (9)	−0.0014 (10)
N1	0.0245 (12)	0.0369 (14)	0.0331 (13)	−0.0045 (11)	0.0106 (11)	−0.0015 (12)
N2	0.0294 (12)	0.0202 (12)	0.0308 (12)	−0.0007 (10)	0.0087 (10)	−0.0002 (10)
N3	0.0310 (12)	0.0220 (12)	0.0329 (13)	−0.0049 (10)	0.0012 (10)	0.0032 (11)
C1	0.0343 (16)	0.0406 (19)	0.0344 (16)	0.0000 (14)	0.0055 (13)	−0.0048 (15)
C2	0.062 (2)	0.057 (2)	0.084 (3)	−0.020 (2)	0.038 (2)	−0.032 (2)
C3	0.061 (2)	0.074 (3)	0.0364 (18)	0.026 (2)	−0.0059 (17)	−0.007 (2)
C4	0.0401 (18)	0.056 (2)	0.0369 (17)	0.0090 (16)	0.0072 (14)	−0.0054 (17)
C5	0.0350 (16)	0.0294 (17)	0.0354 (16)	0.0016 (14)	0.0107 (14)	0.0043 (14)
C6	0.0298 (15)	0.0263 (16)	0.0351 (16)	−0.0013 (12)	0.0111 (13)	−0.0024 (13)
C7	0.0355 (16)	0.0358 (17)	0.0424 (17)	−0.0030 (14)	0.0151 (14)	−0.0049 (15)
C8	0.058 (2)	0.052 (2)	0.053 (2)	−0.0150 (19)	0.0003 (18)	−0.0004 (19)
C9	0.059 (2)	0.058 (2)	0.068 (3)	−0.020 (2)	−0.009 (2)	−0.002 (2)

C10	0.061 (3)	0.067 (3)	0.081 (3)	0.006 (2)	0.006 (2)	−0.011 (3)
C11	0.0280 (14)	0.0280 (17)	0.0291 (14)	0.0012 (13)	0.0036 (12)	−0.0042 (13)
C12	0.0277 (15)	0.0287 (16)	0.0255 (14)	0.0017 (12)	0.0054 (12)	0.0015 (12)
C13	0.0361 (16)	0.0390 (18)	0.0299 (15)	0.0020 (14)	0.0026 (13)	−0.0024 (14)
C14	0.0340 (15)	0.0302 (16)	0.0316 (15)	0.0017 (13)	0.0111 (13)	0.0026 (13)
C15	0.0272 (14)	0.0264 (16)	0.0310 (15)	0.0006 (12)	0.0082 (12)	0.0033 (13)
C16	0.0283 (14)	0.0266 (16)	0.0356 (15)	0.0000 (12)	0.0053 (13)	0.0008 (13)
C17	0.0304 (14)	0.0304 (16)	0.0321 (16)	−0.0049 (13)	0.0069 (12)	0.0002 (13)
C18	0.0396 (18)	0.0359 (17)	0.0355 (16)	−0.0012 (14)	0.0061 (14)	−0.0023 (14)
C19	0.0504 (19)	0.0335 (18)	0.0303 (15)	0.0051 (15)	0.0041 (14)	0.0036 (14)
C20	0.0310 (15)	0.0233 (16)	0.0269 (15)	−0.0018 (13)	0.0010 (12)	−0.0001 (12)
C21	0.0367 (16)	0.0289 (16)	0.0445 (18)	−0.0044 (13)	0.0126 (14)	0.0014 (14)

Geometric parameters (Å °) of (5)

O1—C5	1.362 (3)	C7—H7A	0.9900
O1—C1	1.470 (3)	C7—H7B	0.9900
O2—C5	1.218 (3)	C8—C9	1.497 (6)
O3—C8	1.396 (4)	C8—H8A	0.9900
O3—C7	1.425 (4)	C8—H8B	0.9900
O4—C11	1.223 (3)	C9—C10	1.272 (6)
O5—C15	1.234 (3)	C9—H9	0.9500
O6—C20	1.334 (3)	C10—H10A	0.9500
O6—C21	1.455 (3)	C10—H10B	0.9500
O7—C20	1.211 (3)	C12—C15	1.526 (4)
N1—C5	1.348 (4)	C12—C13	1.527 (4)
N1—C6	1.455 (4)	C12—C14	1.530 (4)
N1—H1	0.8800	C13—H13A	0.9800
N2—C11	1.360 (3)	C13—H13B	0.9800
N2—C12	1.456 (3)	C13—H13C	0.9800
N2—H2	0.8800	C14—H14A	0.9800
N3—C15	1.344 (4)	C14—H14B	0.9800
N3—C16	1.460 (4)	C14—H14C	0.9800
N3—H3	0.8800	C16—C20	1.525 (4)
C1—C3	1.507 (5)	C16—C17	1.540 (4)
C1—C2	1.515 (5)	C16—H16	1.0000
C1—C4	1.526 (4)	C17—C18	1.527 (4)
C2—H2A	0.9800	C17—C19	1.529 (4)
C2—H2B	0.9800	C17—H17	1.0000
C2—H2C	0.9800	C18—H18A	0.9800
C3—H3A	0.9800	C18—H18B	0.9800
C3—H3B	0.9800	C18—H18C	0.9800
C3—H3C	0.9800	C19—H19A	0.9800
C4—H4A	0.9800	C19—H19B	0.9800
C4—H4B	0.9800	C19—H19C	0.9800
C4—H4C	0.9800	C21—H21A	0.9800
C6—C7	1.514 (4)	C21—H21B	0.9800
C6—C11	1.526 (4)	C21—H21C	0.9800

C6—H6	1.0000				
C5—O1—C1	120.2	(2)	C9—C10—H10A	120.0	
C8—O3—C7	114.0	(3)	C9—C10—H10B	120.0	
C20—O6—C21	115.0	(2)	H10A—C10—H10B	120.0	
C5—N1—C6	117.8	(2)	O4—C11—N2	122.7	(3)
C5—N1—H1	121.1		O4—C11—C6	122.7	(2)
C6—N1—H1	121.1		N2—C11—C6	114.5	(2)
C11—N2—C12	121.5	(2)	N2—C12—C15	110.3	(2)
C11—N2—H2	119.3		N2—C12—C13	110.7	(2)
C12—N2—H2	119.3		C15—C12—C13	110.1	(2)
C15—N3—C16	119.9	(2)	N2—C12—C14	107.9	(2)
C15—N3—H3	120.1		C15—C12—C14	107.7	(2)
C16—N3—H3	120.1		C13—C12—C14	110.1	(2)
O1—C1—C3	109.8	(3)	C12—C13—H13A	109.5	
O1—C1—C2	110.7	(2)	C12—C13—H13B	109.5	
C3—C1—C2	113.6	(3)	H13A—C13—H13B	109.5	
O1—C1—C4	102.2	(2)	C12—C13—H13C	109.5	
C3—C1—C4	110.0	(3)	H13A—C13—H13C	109.5	
C2—C1—C4	110.0	(3)	H13B—C13—H13C	109.5	
C1—C2—H2A	109.5		C12—C14—H14A	109.5	
C1—C2—H2B	109.5		C12—C14—H14B	109.5	
H2A—C2—H2B	109.5		H14A—C14—H14B	109.5	
C1—C2—H2C	109.5		C12—C14—H14C	109.5	
H2A—C2—H2C	109.5		H14A—C14—H14C	109.5	
H2B—C2—H2C	109.5		H14B—C14—H14C	109.5	
C1—C3—H3A	109.5		O5—C15—N3	120.8	(3)
C1—C3—H3B	109.5		O5—C15—C12	121.4	(2)
H3A—C3—H3B	109.5		N3—C15—C12	117.7	(2)
C1—C3—H3C	109.5		N3—C16—C20	108.5	(2)
H3A—C3—H3C	109.5		N3—C16—C17	110.7	(2)
H3B—C3—H3C	109.5		C20—C16—C17	112.3	(2)
C1—C4—H4A	109.5		N3—C16—H16	108.4	
C1—C4—H4B	109.5		C20—C16—H16	108.4	
H4A—C4—H4B	109.5		C17—C16—H16	108.4	
C1—C4—H4C	109.5		C18—C17—C19	111.6	(2)
H4A—C4—H4C	109.5		C18—C17—C16	110.9	(2)
H4B—C4—H4C	109.5		C19—C17—C16	113.5	(2)
O2—C5—N1	124.8	(3)	C18—C17—H17	106.8	
O2—C5—O1	125.7	(3)	C19—C17—H17	106.8	
N1—C5—O1	109.4	(2)	C16—C17—H17	106.8	
N1—C6—C7	110.2	(2)	C17—C18—H18A	109.5	
N1—C6—C11	110.4	(2)	C17—C18—H18B	109.5	
C7—C6—C11	109.2	(2)	H18A—C18—H18B	109.5	
N1—C6—H6	109.0		C17—C18—H18C	109.5	
C7—C6—H6	109.0		H18A—C18—H18C	109.5	
C11—C6—H6	109.0		H18B—C18—H18C	109.5	
O3—C7—C6	106.8	(2)	C17—C19—H19A	109.5	
O3—C7—H7A	110.4		C17—C19—H19B	109.5	

C6—C7—H7A	110.4	H19A—C19—H19B	109.5
O3—C7—H7B	110.4	C17—C19—H19C	109.5
C6—C7—H7B	110.4	H19A—C19—H19C	109.5
H7A—C7—H7B	108.6	H19B—C19—H19C	109.5
O3—C8—C9	110.5 (3)	O7—C20—O6	123.9 (3)
O3—C8—H8A	109.5	O7—C20—C16	124.3 (3)
C9—C8—H8A	109.5	O6—C20—C16	111.9 (2)
O3—C8—H8B	109.5	O6—C21—H21A	109.5
C9—C8—H8B	109.5	O6—C21—H21B	109.5
H8A—C8—H8B	108.1	H21A—C21—H21B	109.5
C10—C9—C8	126.1 (4)	O6—C21—H21C	109.5
C10—C9—H9	117.0	H21A—C21—H21C	109.5
C8—C9—H9	117.0	H21B—C21—H21C	109.5

O1—C5—N1—C6	166.4 (2)	N1—C6—C11—O4	−22.7 (4)
C5—N1—C6—C11	−59.1 (3)	C7—C6—C11—O4	98.7 (3)
N1—C6—C11—N2	159.3 (2)	C7—C6—C11—N2	−79.4 (3)
C6—C11—N2—C12	166.3 (2)	C11—N2—C12—C13	−63.4 (3)
C11—N2—C12—C15	58.7 (3)	C11—N2—C12—C14	176.0 (2)
N2—C12—C15—N3	33.2 (3)	C16—N3—C15—O5	3.6 (4)
C12—C15—N3—C16	179.0 (2)	N2—C12—C15—O5	−151.4 (2)
C15—N3—C16—C20	−70.3 (3)	C13—C12—C15—O5	−28.9 (3)
N3—C16—C20—O6	143.5 (2)	C14—C12—C15—O5	91.2 (3)
C5—O1—C1—C3	−66.4 (3)	C13—C12—C15—N3	155.7 (2)
C5—O1—C1—C2	59.8 (4)	C14—C12—C15—N3	−84.3 (3)
C5—O1—C1—C4	176.9 (2)	C15—N3—C16—C17	166.0 (2)
C6—N1—C5—O2	−15.5 (4)	N3—C16—C17—C18	−160.1 (2)
C1—O1—C5—O2	5.3 (4)	C20—C16—C17—C18	78.4 (3)
C1—O1—C5—N1	−176.6 (2)	N3—C16—C17—C19	73.3 (3)
C5—N1—C6—C7	−179.8 (3)	C20—C16—C17—C19	−48.2 (3)
C8—O3—C7—C6	−161.9 (3)	C21—O6—C20—O7	1.6 (4)
N1—C6—C7—O3	69.6 (3)	C21—O6—C20—C16	−179.1 (2)
C11—C6—C7—O3	−51.9 (3)	N3—C16—C20—O7	−37.2 (3)
C7—O3—C8—C9	−172.8 (3)	C17—C16—C20—O7	85.6 (3)
O3—C8—C9—C10	11.7 (6)	C17—C16—C20—O6	−93.7 (3)
C12—N2—C11—O4	−11.7 (4)		